

A GENERAL FRAMEWORK ON ADAPTIVE HYBRID BEAMFORMING AND
CHANNEL ACQUISITION FOR WIDEBAND MM-WAVE MASSIVE MIMO
SYSTEMS

A THESIS SUBMITTED TO
THE GRADUATE SCHOOL OF NATURAL AND APPLIED SCIENCES
OF
MIDDLE EAST TECHNICAL UNIVERSITY

BY

ANIL KURT

IN PARTIAL FULFILLMENT OF THE REQUIREMENTS
FOR
THE DEGREE OF MASTER OF SCIENCE
IN
ELECTRICAL AND ELECTRONICS ENGINEERING

AUGUST 2019

Approval of the thesis:

**A GENERAL FRAMEWORK ON ADAPTIVE HYBRID BEAMFORMING
AND CHANNEL ACQUISITION FOR WIDEBAND MM-WAVE MASSIVE
MIMO SYSTEMS**

submitted by **ANIL KURT** in partial fulfillment of the requirements for the degree
of **Master of Science in Electrical and Electronics Engineering Department,**
Middle East Technical University by,

Prof. Dr. Halil Kalipçılar
Dean, Graduate School of **Natural and Applied Sciences** _____

Prof. Dr. İlkey Ulusoy
Head of Department, **Electrical and Electronics Engineering** _____

Assist. Prof. Dr. Gökhan Muzaffer Güvensen
Supervisor, **Electrical and Electronics Engineering, METU** _____

Examining Committee Members:

Prof. Dr. Yalçın Tanık
Electrical and Electronics Engineering, METU _____

Assist. Prof. Dr. Gökhan Muzaffer Güvensen
Electrical and Electronics Engineering, METU _____

Prof. Dr. Tolga Mete Duman
Electrical and Electronics Engineering, Bilkent University _____

Assoc. Prof. Dr. Cenk Toker
Computer Engineering, Hacettepe University _____

Assist. Prof. Dr. Barış Nakiboğlu
Electrical and Electronics Engineering, METU _____

Date:

I hereby declare that all information in this document has been obtained and presented in accordance with academic rules and ethical conduct. I also declare that, as required by these rules and conduct, I have fully cited and referenced all material and results that are not original to this work.

Name, Surname: Anıl Kurt

Signature :

ABSTRACT

A GENERAL FRAMEWORK ON ADAPTIVE HYBRID BEAMFORMING AND CHANNEL ACQUISITION FOR WIDEBAND MM-WAVE MASSIVE MIMO SYSTEMS

Kurt, Anıl

M.S., Department of Electrical and Electronics Engineering

Supervisor: Assist. Prof. Dr. Gökhan Muzaffer Güvensen

August 2019, 132 pages

In this thesis, an efficient hybrid beamforming architecture together with a novel spatio-temporal receiver processing is proposed for single-carrier (SC) mm-wave wideband massive MIMO channels in time-domain duplex (TDD) mode. The design of two-stage beamformer is realized by using a virtual sectorization via second-order channel statistics based user grouping. The novel feature of the proposed architecture is that the effect of both inter-group-interference (due to non-orthogonality of virtual angular sectors) and the inter-symbol-interference (due to SC wideband transmission) are taken into account. While designing the analog beamformer, the dimension reduction and proper subspace (beamspace) construction problems are examined (by exploiting the joint angle-delay sparsity map and power profile of the multi-user channel) based on which a highly efficient spatio-temporal digital receiver processing is proposed. Furthermore, a least square type channel estimator, based on a proper subspace projection via radio frequency (RF) processing, is proposed. It is shown to achieve a remarkable robustness to pilot contamination with a significant reduction in pilot length. Moreover, the effect of utilizing inaccurate estimates for central an-

gle, the angular spread (AS) and channel covariance matrices (CCMs) on achievable information rate (AIR) is analyzed. Finally, adaptive methods for the reconstruction of the analog beamformer are proposed for a mobile channel where estimates are erroneous. Proposed methods are shown to decrease the computational complexity significantly, while decreasing the performance slightly.

Keywords: adaptive hybrid beamforming, massive MIMO, millimeter wave, channel acquisition, single-carrier, wideband communication

ÖZ

GENİŞBANT MİLİMETRE DALGA MASİF MIMO SİSTEMLER İÇİN ADAPTİF MELEZ HÜZME ŞEKİLENDİRME VE KANAL KESTİRİMİ ÜZERİNE GENEL BİR ÇERÇEVE

Kurt, Anıl

Yüksek Lisans, Elektrik ve Elektronik Mühendisliği Bölümü

Tez Yöneticisi: Dr. Öğr. Üyesi. Gökhan Muzaffer Güvensen

Ağustos 2019 , 132 sayfa

Bu tezde; zaman bölgesinde çift yönlü moddaki tek taşıyıcılı, milimetre-dalga, geniş bant, masif MIMO kanallar için yenilikçi bir uzamsal-zamansal alıcı işlemesi ile birlikte verimli bir melez hüzme şekillendirme yapısı önerilmektedir. İki aşamalı hüzme şekillendiricilerin tasarımı, ikinci derece kanal istatistiklerini baz alan bir kullanıcı gruplandırma işlemi yoluyla sanal bir bölümlere ayırma işlemi kullanılarak gerçekleştirilmiştir. Önerilen mimarinin yenilikçi tarafı; hem kullanıcı grupları arası girişimin etkisinin, hem de semboller arası girişimin etkisinin hesaba katılmış olmasıdır. Analog hüzme şekillendirici tasarımında, boyut düşürme problemi ve üzerine yüksek verimlilikte uzamsal-zamansal sayısal alıcı işleme tasarımı önerilecek olan uygun alt-uzay yapılandırma işlemi ele alınmıştır. Dahası, RF işleme yardımıyla uygun bir altuzay izdüşümüne dayanan en küçük kare tipinde bir kanal kestiricisi önerilmiştir. Bu kestiricinin pilot kirliliğine karşı dikkat çekici bir gürbüzlüğe ve pilot uzunluğunda önemli bir düşüşe ulaştığı gösterilmiştir. Ayrıca; merkez açısı, açılabilir yayılma ve kanal kovaryans matrisleri için hatalı kestirimlerin kullanılmasının ulaşılabılır veri

hızına etkisi incelenmiştir. Son olarak, kestirimlerin hatalı olduğu hareketli bir senaryoda analog hüzme şekillendiricisi için adaptive yeniden hesaplama yöntemleri önerilmiştir. Önerilen metodların performansta küçük bir düşüş karşılığında işlemsel karmaşıklığı önemli derecede azalttığı gösterilmiştir.

Anahtar Kelimeler: adaptif melez hüzme şekillendirme, masif MIMO, milimetre dalga, kanal kestirimi, tek taşıyıcı, genişbant haberleşme

To my loved ones

ACKNOWLEDGMENTS

I want to thank my supervisor Gökhan Muzaffer Güvensen, for his endless support and guidance. He always provided me with his time and interest. He encouraged me in my attempts on the topic, even if they looked hopeless in the first sight. I did see him trying to help me when I needed, even in the situations that are out of his responsibilities. I am grateful, and very glad to have him as the supervisor of my thesis.

I thank my teacher Ali Özgür Yılmaz. He always supported me, provided me with valuable opportunities and helped me to improve as an engineer.

I would like to thank my teacher Yalçın Tanık. I learnt the fundamentals of the field of telecommunications from him, which almost all my engineering knowledge is built upon.

I want to thank TÜBİTAK for the financial support they provided through 2210-A National Scholarship Programme for MSc Students. I also thank "Bilgi Teknolojileri ve İletişim Kurumu", BTK, for the opportunities they provided.

Finally, I want to thank my family for always listening, helping and supporting me. They have the greatest role in all the success I have.

TABLE OF CONTENTS

ABSTRACT	v
ÖZ	vii
ACKNOWLEDGMENTS	x
TABLE OF CONTENTS	xi
LIST OF TABLES	xv
LIST OF FIGURES	xvi
LIST OF ABBREVIATIONS	xx
NOMENCLATURE	xxii
CHAPTERS	
1 INTRODUCTION	1
1.1 Motivation	1
1.2 Brief Problem Definition	2
1.3 Literature Survey	3
1.4 Contributions	4
1.5 The Outline of the Thesis	5
2 SYSTEM MODEL FOR HYBRID BEAMFORMING BASED MASSIVE MIMO CHANNELS	7
2.1 Channel Model	7

2.1.1	Sparsity in Millimeter-Wave Channels	9
2.1.2	User Grouping Based JSDM Framework	10
2.2	Hybrid Beamformer Architecture	13
2.3	Proposed Architecture for Single Carrier Wideband Massive MIMO Channels	17
2.3.1	Joint Angle-Delay Power Profile and Sparsity Map	17
2.3.2	Analog Beamformer	18
2.3.3	Instantaneous Channel Estimator in Reduced Dimension	20
2.3.4	Digital Beamformer	20
3	HYBRID BEAMFORMER DESIGN	21
3.1	Analog Beamformer Design	21
3.1.1	Nearly Optimal Generalized Eigen-Beamformer	22
3.1.1.1	Optimality Criteria for Generalized Eigen-Beamformer	23
3.1.2	Conventional DFT Beamformer	25
3.2	Digital Beamformer Design	25
3.2.1	Channel Matched Filter (CMF)	28
3.2.2	Regularized Spatial Zero Forcing (SZF)	30
4	SUBSPACE-AWARE CSI ACQUISITION TECHNIQUES	33
4.1	Minimum Mean Square Error Estimator	35
4.2	Conventional Least Square Estimator	35
4.3	Beamspace-Aware Least Square Estimator (BA-LS)	36
5	PERFORMANCE ANALYSIS FOR THE PROPOSED ARCHITECTURE	37
5.1	Hybrid Beamforming Based Massive MIMO Performance in Terms of AIR for Several Intra-Group Multiplexing Techniques	37

5.1.1	CMF and SZF	37
5.1.2	CMF without TDMA	40
5.1.3	CMF with TDMA	41
5.1.4	Analytical Expressions for Signal Powers at the Output of CMF	41
5.1.5	Analytically Calculated Approximation for Achievable Infor- mation Rate	42
5.2	Sensitivity to Estimation Error for Long-Term Channel Parameters . .	44
5.3	Numerical Results	44
6	ADAPTIVE CONSTRUCTION OF ANALOG BEAMFORMER	55
6.1	Slow-Time Adaptation	55
6.2	Mobile Channel Model	56
6.3	Recursive Filtering of Matrices and Vectors	57
6.4	Modifications on Channel Covariance Matrices	58
6.4.1	Azimuth Angle - Phase Transformation	58
6.4.2	Hadamard Factorization of Channel Covariance Matrices	61
6.4.3	Patching in Angular Domain	62
6.4.4	Quantization of Patch Power Levels	64
6.4.5	Update of Inverse of a Matrix with Patched Structure	66
6.4.6	Summary of Blocks	70
6.5	Modifications on Generalized Eigen-Beamformer	71
6.6	Proposed Adaptive Construction Methods for Analog Beamformer . .	75
6.6.1	GEB with Recursively Filtered Channel Covariance Matrices .	75
6.6.1.1	Asymptotic Analysis for the Recursive Filtering Output	76

6.6.2	Wiener Filter Type Analog Beamformer	79
6.6.3	Whitening Filter Type Analog Beamformer	80
6.6.4	LMS Type Analog Beamformer	81
6.7	Complexity Analysis	83
6.8	Numerical Results	84
7	CONCLUSIONS	101
	REFERENCES	103
A	GENERALIZED HERMITIAN EIGENDECOMPOSITION	107
A.1	A Congruence Related with Generalized Eigen-pairs	108
A.2	The Relation with Rayleigh Quotient	109
B	DERIVATION OF ANALYTICAL EXPRESSIONS FOR SIGNAL POW- ERS AT THE OUTPUT OF THE CHANNEL MATCHED FILTER	111
B.1	Components in the Channel Matched Filter Output	111
B.2	Expression of the Power of Components in Terms of Effective Chan- nel Matrices	113
B.2.1	Summary	119
B.3	Derivation of Analytical Results for Probabilistic Terms	120
B.3.1	Expectation Type 1	120
B.3.2	Expectation Type 2	121
B.4	Implementation of Analytical Results	123
B.4.1	Summary	128
B.5	Perfect Channel Estimation	129
B.5.1	Summary	131
B.6	Estimated Channel	132

LIST OF TABLES

TABLES

Table 5.1	Angular sectors of multipath components	45
Table 6.1	Average number of changes in the quantized patch power levels for quantization parameter 1	100
Table 6.2	Average number of changes in the quantized patch power levels for quantization parameter 2	100
Table 6.3	Average number of changes in the quantized patch power levels for quantization parameter 4	100

LIST OF FIGURES

FIGURES

Figure 2.1	Antenna array with 4 antenna elements	8
Figure 2.2	Sparsity Map	10
Figure 2.3	User grouping and MPCs ($G = 2, K_1 = 3, K_2 = 2, M^{(1)} = 2$ and $M^{(2)} = 2$)	11
Figure 2.4	Analog beamformer architecture for an antenna array consisting of $N = 4$ antennas (transmitter is on the left and receiver is on the right)	15
Figure 2.5	Digital beamformer architecture for an antenna array consisting of $N = 4$ antennas (transmitter is on the left and receiver is on the right)	15
Figure 2.6	Hybrid beamformer architecture with 2 RF chains and 4 antenna elements ($D = 2, N = 4$, transmitter is on the left and receiver is on the right)	16
Figure 2.7	Equivalent Receiver Processing	17
Figure 3.1	Power pattern of GEB. (a) $\mathbf{S}_1^{(g)}$. (b) $\mathbf{S}_2^{(g)}$. (c) $\mathbf{S}_3^{(g)}$. (d) $\mathbf{S}^{(g)}$. (e) Placement in the angular domain $\rho_{\phi,t}(\phi)$	24
Figure 3.2	Design of DFT beamformer	25
Figure 3.3	Power pattern of DFT beamformer. (a) $\mathbf{S}_1^{(g)}$. (b) $\mathbf{S}_2^{(g)}$. (c) $\mathbf{S}_3^{(g)}$. (d) $\mathbf{S}^{(g)}$. (e) Placement in the angular domain $\rho_{\phi,t}(\phi)$	26
Figure 3.4	Comparison of Power Patterns of GEB and DFT Beamformers. (a) $\mathbf{S}^{(g)}$. (b) Placement in the angular domain $\rho_{\phi,t}(\phi)$	27

Figure 3.5	Digital beamformer	27
Figure 3.6	Equivalent receiver processing for only the intended group . . .	28
Figure 4.1	Training and data transmission scheme	33
Figure 5.1	Comparison of analytically calculated approximation for AIR and AIR obtained through Monte Carlo method. (Group 1, GEB, CMF, perfect instantaneous channel estimation, perfect angular estimation) . .	43
Figure 5.2	Performance of GEB and comparison of intra-group multiplexing techniques. (a) Group 1. (b) Group 2. (c) Group 3. (d) Group 4. (Perfect instantaneous channel estimation, perfect angular estimation) .	48
Figure 5.3	Performance of DFT beamformer and comparison of intra-group multiplexing techniques. (a) Group 1. (b) Group 2. (c) Group 3. (d) Group 4. (Perfect instantaneous channel estimation, perfect angular estimation)	49
Figure 5.4	Comparison of instantaneous channel estimation techniques when GEB is used. (a) Group 1. (b) Group 2. (c) Group 3. (d) Group 4. (CMF with SZF, training length $T = 4$, perfect angular estimation)	50
Figure 5.5	Performances of instantaneous channel estimation techniques versus training length when GEB is used. (a) Group 1. (b) Group 2. (c) Group 3. (d) Group 4. (CMF with SZF, 30 dB SNR, perfect angular estimation)	51
Figure 5.6	Performance of GEB and DFT-BF against number of RF chains D_g for the group 1. All the groups have equal signal powers. (30 dB SNR, CMF, training length $T = 4$, perfect angular estimation)	52
Figure 5.7	Performance of GEB and DFT-BF against near-far effect for the group 1. All inter-groups have equal signal powers, signal power of the intended group depends on SIR. (30 dB SNR, CMF, training length $T = 4$, perfect angular estimation)	52

Figure 5.8	Performance of GEB and DFT-BF against number of antennas for the group 1. All the groups have equal signal powers. Number of RF chains is 3 and remains the same. (30 dB SNR, CMF, training length $T = 4$, perfect angular estimation)	53
Figure 5.9	Performance of GEB and DFT-BF against number of antennas for the group 1. All the groups have equal signal powers. Number of RF chains is proportional to the number of antennas with ratio 3/100, ceiled if needed. (30 dB SNR, CMF, training length $T = 4$, perfect angular estimation)	53
Figure 5.10	Performance against bias in angular estimation for the group 1. All the groups have equal signal powers. (30 dB SNR, 6 RF Chains, CMF, training length $T = 4$, no error in the estimate of angular spread) .	54
Figure 5.11	Performance against error in angular spread for the group 1. All the groups have equal signal powers. (30 dB SNR, 6 RF Chains, CMF, training length $T = 4$, unbiased angular estimates)	54
Figure 6.1	Recursive filtering block	58
Figure 6.2	Comparison of exact and approximated angular transformations .	60
Figure 6.3	Angular transformation block	60
Figure 6.4	Patching and CCM Construction	63
Figure 6.5	Separate quantization of MPC patch power levels	66
Figure 6.6	Woodbury inverter block	70
Figure 6.7	Map of Variables	72
Figure 6.8	The spreading effect of recursive filtering with erroneous estimates	78
Figure 6.9	Adaptive analog beamformer construction	80
Figure 6.10	Angular Movement of the MPCs. (a) $\alpha = 0.9$. (b) $\alpha = 0.99$. (c) $\alpha = 0.999$. (d) $\alpha = 0.9999$	89

Figure 6.11	Estimated Angular positions of the MPCs for $\alpha = 0.999$. (a) $\sigma_{est} = 0.1$. (b) $\sigma_{est} = 0.5$. (c) $\sigma_{est} = 1$. (d) $\sigma_{est} = 2$	90
Figure 6.12	The performance of the recursive filtering combined with GEB for the mobile channel with $\alpha = 0.999$. (a) $\sigma_{est} = 0.1$. (b) $\sigma_{est} = 0.5$. (c) $\sigma_{est} = 1$. (d) $\sigma_{est} = 2$	91
Figure 6.13	Performance against channel mobility index α . (a) $\sigma_{est} = 0.1$. (b) $\sigma_{est} = 0.5$. (c) $\sigma_{est} = 1$. (d) $\sigma_{est} = 2$	92
Figure 6.14	Performance against recursive filtering parameter β . (a) $\alpha = 0.9$. (b) $\alpha = 0.99$. (c) $\alpha = 0.999$. (d) $\alpha = 0.9999$	93
Figure 6.15	Performance against standard deviation of the channel estimation error σ_{est} . (a) $\alpha = 0.9$. (b) $\alpha = 0.99$. (c) $\alpha = 0.999$. (d) $\alpha = 0.9999$	94
Figure 6.16	Change of probability of outage with recursive filtering parameter β . (a) $\alpha = 0.9$. (b) $\alpha = 0.99$. (c) $\alpha = 0.999$. (d) $\alpha = 0.9999$	95
Figure 6.17	Change of probability of outage with recursive filtering parameter β . (a) $\sigma_{est} = 0.1$. (b) $\sigma_{est} = 0.5$. (c) $\sigma_{est} = 1$. (d) $\sigma_{est} = 2$	96
Figure 6.18	Comparison of complexity and performance of different methods for $\beta = 0.9$ and $\sigma_{est} = 0.5$. (a) $\alpha = 0.9$. (b) $\alpha = 0.99$. (c) $\alpha = 0.999$	97
Figure 6.19	Comparison of complexity and performance of different methods for $\alpha = 0.99$ and $\sigma_{est} = 0.5$. (a) $\beta = 0$. (b) $\beta = 0.5$. (c) $\beta = 0.9$	98
Figure 6.20	Comparison of complexity and performance of different methods for $\alpha = 0.99$ and $\beta = 0.9$. (a) $\sigma_{est} = 0.1$. (b) $\sigma_{est} = 0.5$. (c) $\sigma_{est} = 2$	99

LIST OF ABBREVIATIONS

AIR	Achievable information rate
AoA	Angle of arrival
AS	Angular spread
AWGN	Additive white Gaussian noise
BA-LS	Beam-aware least squares
BF	Beamformer
BS	Base station
CCM	Channel covariance matrix
CMF	Channel matched filter
DFT	Discrete Fourier transform
FDMA	Frequency-division multiple access
GEB	Generalized eigen-beamformer
IG	Intended group
IGI	Inter-group interference
ISI	Inter-symbol interference
IU	Intended user
JSDM	Joint spatial division and multiplexing
LMS	Least mean squares
LS	Least squares
MIMO	Multiple-input multiple-output
MMSE	Minimum mean square error
MPC	Multipath component
MUI	Multi-user interference
OFDM	Orthogonal frequency-division multiplexing

RF	Radio frequency
SC	Single carrier
SDMA	Spatial division multiple access
SICEE	Self interference due to channel estimation error
SINR	Signal to interference-and-noise ratio
SIR	Signal to interference ratio
SNR	Signal to noise ratio
SZF	Spatial zero forcing
TDMA	Time-division multiple access
UT	User terminal
ZF	Zero forcing

NOMENCLATURE

Scalars

α	Correlation parameter of the mobile channel model
β	Recursive filtering parameter
$\mu_{\phi,l}^{(g)}$	Mean AoA of the MPC of the group g with delay l , in azimuth domain
$\mu_{\theta,l}^{(g)}$	Mean AoA of the MPC of the group g with delay l , in phase domain
ϕ	Azimuth angle
$\rho_{\phi,l}^{(g)}(\phi)$	Angular power profile of the MPC of the group g with delay l , in azimuth domain
$\rho_{\theta,l}^{(g)}(\theta)$	Angular power profile of the MPC of the group g with delay l , in phase domain
$\sigma_{\phi,l}^{(g)}$	Angular spread of the MPC of the group g with delay l , in azimuth domain
$\sigma_{\theta,l}^{(g)}$	Angular spread profile of the MPC of the group g with delay l , in phase domain
σ_{est}	Standard deviation of the error in the mean AoA estimates for the mobile channel
σ_v	Asymptotic variance of the mobile channel model
θ	Phase-domain equivalent of azimuth angle ϕ , through $\theta = \sin(\phi)\pi$
\tilde{g}	Intended group
D_g	Total number of RF chains allocated for the group g
$d_m^{(g)}$	Number of RF chains allocated for m^{th} MPC of the group g
$E_s^{(g)}$	Signal power of the users in the group g
G	Number of groups
g	Group index
g_k	The k^{th} user of the g^{th} group
K_g	Number of users in the group g

L	Maximum delay
$M^{(g)}$	Number of MPCs of the group g
N	Number of antennas
N_0	Noise power
$r_n^{(g_k)}$	CMF output for the k^{th} user of the g^{th} group in n^{th} time instance
$x_n^{(g_k)}$	Transmitted symbol by the k^{th} user of the g^{th} group in n^{th} time instance
$z_n^{(g_k)}$	SZF output for the k^{th} user of the g^{th} group in n^{th} time instance

Vectors

$\boldsymbol{\eta}_n^{(g)}$	Interference-and-noise for the g^{th} group in n^{th} time instance
$\boldsymbol{\eta}_{eff,n}^{(g)}$	Effective interference-and-noise for the g^{th} group in n^{th} time instance, at the output of analog beamformer
$\mathbf{e}_{K,k}$	The selection vector of length K , whose all the entries are zero but the k^{th} one is 1
$\mathbf{h}_l^{(g_k)}$	Channel vector of the MPC of k^{th} user of the g^{th} group with delay l
$\mathbf{h}_{eff,l}^{(g',g_k)}$	Effective channel vector of the MPC of k^{th} user of the g^{th} group with delay l , at the output of the beamformer constructed for the group g'
$\mathbf{h}_{eff,l}^{(g_k)}$	Effective channel vector of the MPC of k^{th} user of the g^{th} group with delay l , at the output of the beamformer constructed for the intended group \tilde{g}
\mathbf{n}_n	Received noise in n^{th} time instance
$\mathbf{q}(\theta)$	Antenna array response to an incidence from azimuth angle ϕ , correspondent to θ through $\theta = \sin(\phi)\pi$
$\mathbf{r}_n^{(g)}$	Output of CMF for g^{th} group, in n^{th} time instance
$\mathbf{s}_n^{(g)}$	Output of the analog beamformer constructed for g^{th} group, in n^{th} time instance
$\mathbf{u}(\phi)$	Antenna array response to an incidence from azimuth angle ϕ
$\mathbf{x}_n^{(g)}$	Transmitted symbol by k^{th} user of the g^{th} group in n^{th} time instance
\mathbf{y}_n	Received signal in n^{th} time instance
$\mathbf{z}_n^{(g)}$	Output of the regularized spatial zero forcing filter constructed for g^{th} group, in n^{th} time instance

Matrices

- $\mathbf{H}_l^{(g)}$ Channel matrix of the MPC of the g^{th} group with delay l
- $\mathbf{H}_{eff,l}^{(g',g)}$ Effective channel matrix of the MPC of the g^{th} group with delay l , at the output of the beamformer constructed for the group g'
- $\mathbf{H}_{eff,l}^{(g)}$ Effective channel matrix of the MPC of the g^{th} group with delay l , at the output of the beamformer constructed for the intended group \tilde{g}
- \mathbf{I}_N Identity matrix of size N
- $\mathbf{R}_l^{(g)}$ The CCM of the MPC of the group g with delay l
- \mathbf{R}_y The covariance matrix of the received signal
- $\mathbf{R}_{\eta,l}^{(g)}$ Covariance matrix of the MPC-specific interference-and-noise term for MPC of the group g with delay l
- $\mathbf{R}_{\eta}^{(g)}$ Covariance matrix of the interference-and-noise term for the group g
- $\mathbf{R}_{eff,\eta}^{(g)}$ Effective Covariance matrix of the interference-and-noise term for the group g , at the output of the beamformer constructed for the group g
- $\mathbf{R}_{eff,l}^{(g)}$ The effective CCM of the MPC of the group g with delay l , at the output of the beamformer constructed for the intended group \tilde{g}
- $\mathbf{S}^{(g)}$ Analog beamformer matrix constructed for the group g
- $\mathbf{S}_m^{(g)}$ Analog beamformer matrix constructed for the m^{th} MPC of the group g
- $\mathbf{W}_l^{(g)}$ Digital beamformer matrix constructed for the MPC of the group g with delay l
- $\mathbf{Y}^{(g)}$ Regularized spatial zero forcing filter matrix constructed for the group g
- $\mathbf{Z}^{(g)}$ Instantaneous channel estimator matrix constructed for the group g

CHAPTER 1

INTRODUCTION

1.1 Motivation

5G beyond systems are expected to utilize millimeter-wave (mm-wave) frequency range, which possesses wide frequency bands to satisfy the need of much larger data rates than the currently deployed standards [1]. Properties of propagation in mm-wave range differ such that scattering decreases and path loss increases. As a result, the number of multipath components (MPCs) that survive to arrive the receiving end is limited and angular spreads of MPCs are narrow. Therefore, a sparsity in the angular domain is experienced [2], [3]. Moreover, the increase in the carrier frequency results in smaller antenna sizes and narrower beamwidths. These properties of the channel make massive MIMO technology more practical, with its benefits through beamforming.

On the other hand, the availability of wide frequency band urges the use of single-carrier (SC) wideband communication for higher data rates. In such a case, the disadvantage would be the difficulty of user multiplexing and channel equalization, because it would be abandoning the strengths of widely used frequency division schemes in these operations, such as OFDM. However, the sparsity in the angular domain and spatial diversity of the MPCs bring an opportunity to realize these objectives in spatial domain by using beamforming capacity of the massive MIMO technology. As a result of wideband communication, a sparsity is encountered also in the temporal domain.

The biggest hesitation for the use of massive MIMO with fully digital beamformer and large number of antenna elements is the inherent constraints of cost and energy

which make it impractical to build a complete radio frequency (RF) chain for each antenna element. A promising solution is to use two-stage hybrid beamformer structure which consists of analog and digital beamformer stages. In this structure, a combination of analog beamformers in the RF domain feeds a reduced number of RF chains [4], [5]. The two-stage beamforming under the name of Joint Spatial Division and Multiplexing (JSDM), which is naturally fitting the hybrid beamformer structure, was proposed to reduce the dimension of the massive MIMO channel effectively, and to enable massive MIMO gains and simplified system operations [2], [6], [7], [8]. When the beamformer is designed such that the long-term parameters of the channel are governed by the analog beamformer stage, it is possible to reduce the dimensionality of the received signal in analog domain, considering the mm-wave conditions [9]. Then, the digital beamformer governs instantaneous properties of the channel, which requires more frequent channel state information (CSI) updates, in a reduced-dimension subspace. The key idea lies in proper acquisition of the long-term channel parameters and user-grouping, i.e., partitioning the user population supported by the serving base station (BS) into multiple groups each of which consists of users with approximately same channel covariance eigenspaces [6], [8], [10].

The motivation of this thesis is to demonstrate that it is possible to benefit from available wide bandwidths in the mm-wave range to achieve larger data rates by using wideband single-carrier communication, without suffering from problems in user multiplexing, channel equalization, physical construction of the beamformer circuitry, and the computational complexity of updating the beamformer in a mobile scenario.

1.2 Brief Problem Definition

The thesis considers a scenario where BS communicates with a number of users in uplink data mode. In the scenario, users are clustered into separate groups in the angular domain, where all the users are transmitting at the same time with different signal powers, allowing to observe a near-far effect. Users have MPCs with different AoA and delays, therefore the inter-symbol interference (ISI) is also a factor to be solved. Long-term angular estimates are assumed to be given with different error lev-

els. In such a scenario, it is aimed to propose methods to design the analog and digital stages of the hybrid beamforming and a reduced-dimension estimator to perform instantaneous channel acquisition. The mobility of the channel and reconstruction of the analog beamformer is also a concern of the thesis. In such a scenario where all the users are actively transmitting, performance is demonstrated in terms of output signal to interference-and-noise ratio (SINR) and an upper bound for the achievable information rate (AIR) per user. There is no equalization process or a division in the frequency or time to multiplex different groups in the proposed scheme because the analog beamformer is designed such that ISI and interference between the user groups are taken care of. However, for the multiplexing of the users in the same group, time-division multiple access (TDMA) will be assessed as a choice. As a secondary case, a number of efficient methods are proposed for adaptive reconstruction of the beamformer where the aforementioned scenario experiences a mobility.

1.3 Literature Survey

The expectancy of the usage of massive MIMO technology in mm-wave frequency bands in the context of 5G beyond communication systems is expressed in a lot of studies such as [1], [3], [4], [11]. Properties of the propagation in mm-wave region and their effects on the communication systems are investigated in [1], [12], [13], [14]. [15] and [16] address the benefits of using the massive MIMO technology particularly in mm-wave ranges. [17] elaborates the advantages of single-carrier transmission in large-scale antenna systems in terms of communication rate. Channel sparsity is investigated by [2], [12], [13], [14]. Effects of path loss in mm-wave frequency bands are addressed by [2] and [3]. Channel estimation is elaborated in [18], [19], [20]. In these studies, abilities of the analog beamformer cannot be exploited enough. As a result, pilot reuse leads to a pilot interference, and orthogonal pilot use leads to pilot contamination. [21] and [22] investigate channel estimation algorithms based on compressed sensing, which exploit the channel sparsity.

In such channel conditions, two-stage beamforming concept is offered by a number of studies [6], [8], [7], [23]. In [8] and [23], massive MIMO gains and simplified system operations are investigated. In [6] and [7], a concept called Joint Spatial Division

Multiplexing (JSDM) is proposed for effective reduction of the channel dimension. For these two stages, the combination of analog and digital beamformer stages is offered as hybrid beamformer in [19], [24], [25], [26]; for its competitive cost, size, and energy consumption properties. In hybrid beamformer, the analog stage acts as the statistical pre-beamformer operating with long-term channel parameters, and the digital beamformer implements the multi-user MIMO precoding and decoding.

For mobile channels, [27] investigates the AoA tracking problem. For beam-tracking purposes, [28] and [29] offer iterative methods based on instantaneous channel and using extended Kalman filter. [30] proposes a matrix perturbation based iterative approach which uses the instantaneous channel. In this thesis, the analog beamformer is constructed based on the second-order channel statistics.

1.4 Contributions

This thesis provides a novel hybrid beamforming design for massive MIMO systems operating in millimeter-wave frequency bands where

- Wideband single-carrier communication is used,
- ISI is mitigated and inter-group user multiplexing is handled in spatial domain by the analog beamformer,
- Multipath components are combined efficiently and intra-group user multiplexing is handled by the digital beamformer,
- Efficient instantaneous channel estimators are offered, which decrease the pilot contamination by shortening the training length and operating in reduced-dimension subspace,
- Low-complexity adaptive reconstruction methods are offered for a mobile scenario.

The proposed statistical analog beamformer, inspired from the previous work [31] and the work in [9], takes both inter-group interference and inter-symbol interference (ISI)

into account. It is constructed by using the strongest generalized eigenbeams of intra-group and inter-group signal correlation matrices. These eigenbeams are combined to construct the analog beamformer while guaranteeing the orthogonality of effective MPCs in reduced-dimensional subspace. Then, a highly efficient spatio-temporal channel matched filtering (CMF) type digital processing, that eliminates ISI completely, is proposed. This reduces the complexity in digital domain considerably. In addition to that, a subspace aware reduced rank channel estimator, taking the sparsity of the mm-wave channel both in angle and delay domain into account, is suggested. The robustness of the proposed schemes against angular spread (AS) and central AoA estimation errors is analyzed. The performances are shown to achieve the genie-aided matched filter bound (when inter-group interference and ISI are completely removed after fully digital CMF). In addition, generalized eigen-beamformer is modified for efficient reconstruction in a mobile channel. Efficiency comparison is made between modified adaptive beamformer structures and generalized eigen-beamformer in an analysis where performance and complexity are jointly assessed.

1.5 The Outline of the Thesis

A system model is given in Chapter 2 where the channel model, beamformer architectures and the processing blocks of the proposed architecture are briefly introduced. Hybrid beamformer design methods are shown in Chapter 3. In Chapter 4, design methods for the instantaneous channel estimator are discussed. In Chapter 5, several analytical derivations are made and some numerical results are shown for a scenario where users are not mobile. Mobility of the channel is modeled in Chapter 6. Then, in the light of numerical results about the performances of the design methods in Chapter 5, some modifications and analyses for the mobile scenario are given, leading to classes of low-complexity adaptive construction methods for the analog beamformer.

Throughout the thesis, scalars, column vectors, and matrices will be shown as x , \mathbf{x} , and \mathbf{X} , respectively. Also, $(\mathbf{X})_{ij}$ will be used to indicate the entry in the i^{th} row and j^{th} column.

CHAPTER 2

SYSTEM MODEL FOR HYBRID BEAMFORMING BASED MASSIVE MIMO CHANNELS

2.1 Channel Model

In the thesis, a wideband massive MIMO system is considered which is operating in millimeter-wave bands and employing single carrier transmission. Throughout the thesis, uplink data mode, in which user terminals (UTs) transmit and the base station (BS) receives signals, will be addressed. The BS has N antenna elements and serves U single-antenna UTs in time-domain duplex (TDD) mode. In this frame, the observation vector \mathbf{y}_n of size N , consisting of samples from signals received by antenna elements in uplink data mode, is modeled as shown in (2.1). Although signals are analog from antenna elements until the digital circuitry in such a system, their equivalent digital forms according to Nyquist theorem are expressed, assuming the sampling rate after pulse matched filtering is not less than the bandwidth.

$$\mathbf{y}_n = \sum_{u=1}^U \sum_{l=0}^{L-1} \mathbf{h}_l^{(u)} x_{n-l}^{(u)} + \mathbf{n}_n \quad (2.1)$$

In (2.1), $\mathbf{h}_l^{(u)}$ of size N is the channel vector of the MPC of the u^{th} user in l^{th} delay, $x_n^{(u)}$ is the transmitted symbol by u^{th} user in n^{th} time instance, and \mathbf{n}_n is the additive white Gaussian noise (AWGN) vector in n^{th} time. The delays of MPCs are counted until L , although existence of an MPC for each delay l is not necessary. There might be empty delays for which $\mathbf{h}_l^{(u)}$ is simply a zero vector.

Each user has statistically independent channels with independent MPCs where chan-

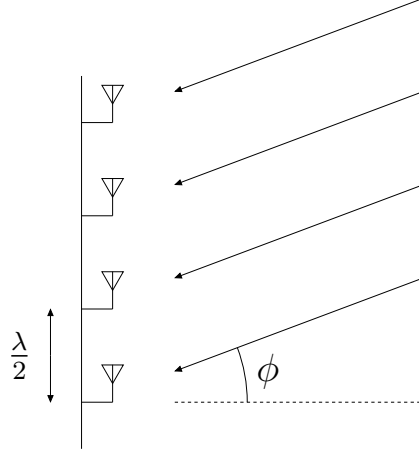


Figure 2.1: Antenna array with 4 antenna elements

nel vector $\mathbf{h}_l^{(u)} \sim \mathcal{CN}(\mathbf{0}, \mathbf{R}_l^{(u)})$; that is,

$$E \left\{ \mathbf{h}_l^{(u)} \left[\mathbf{h}_{l'}^{(u')} \right]^H \right\} = \mathbf{R}_l^{(u)} \delta_{uu'} \delta_{ll'}. \quad (2.2)$$

The channel covariance matrix (CCM) $\mathbf{R}_l^{(u)}$ depends on the angular power profile of the related MPC of the related user and can be obtained as

$$\mathbf{R}_l^{(u)} = \int_{-\frac{\pi}{2}}^{+\frac{\pi}{2}} \rho_{\phi,l}^{(u)}(\phi) \mathbf{u}(\phi) \mathbf{u}(\phi)^H d\phi, \quad (2.3)$$

where

$$\mathbf{u}(\phi) \triangleq \frac{1}{\sqrt{N}} \left[1 \quad e^{j\pi \sin(\phi)} \quad e^{j2\pi \sin(\phi)} \quad \dots \quad e^{j(N-1)\pi \sin(\phi)} \right]^T \quad (2.4)$$

is the array response vector to an incidence from angle ϕ with respect to the perpendicular to the array, for a uniform linear array with half wavelength distance between antenna elements, as shown in Figure 2.1. $\rho_{\phi,l}^{(u)}(\phi)$ is the angular power profile of the MPC of the user u in l^{th} delay and assumed to be nonzero in a very narrow angular interval considering mm-wave conditions. Also, $\rho_{\phi,l}^{(u)}(\phi)$ adjusts the power distribution among MPCs of a user in such a way that $\sum_{l=0}^{L-1} \text{tr}(\mathbf{R}_l^{(u)}) = 1$ for $u = 1, \dots, U$.

The AWGN vector \mathbf{n}_n is independent and identically distributed (i.i.d.) for different time instances and $\mathbf{n}_n \sim \mathcal{CN}(\mathbf{0}, N_0 \mathbf{I}_N)$ where N_0 is the noise power and \mathbf{I}_N is the identity matrix of size $N \times N$. Transmitted symbols are assumed to be complex, zero mean, and uncorrelated as shown in (2.5).

$$E \left\{ x_n^{(u)} \left[x_{n'}^{(u')} \right]^* \right\} = E_s^{(u)} \delta_{uu'} \delta_{nn'} \quad (2.5)$$

$E_s^{(u)}$ in (2.5) is the symbol energy of u^{th} user and it is used to control the relative power distances among users and introduce the near-far effect. The signal-to-noise ratio (SNR) $\gamma^{(u)}$ for the user u can be written as

$$\gamma^{(u)} = E_s^{(u)} / N_0. \quad (2.6)$$

2.1.1 Sparsity in Millimeter-Wave Channels

In millimeter-wave bands, it is known that electromagnetic waves do not scatter much, resulting in a limited number of resolvable and angularly narrow multipath components which reside sparsely in the angular domain. Moreover, wideband transmission, which is equivalent to use short time intervals for each symbol, prevents differences between arrival times of MPCs from being negligible. In fact, the difference of arrival times between MPCs from the same source can be larger than one symbol interval. Therefore, a picture of sparsity in both angular and temporal domains is encountered. An example of joint angle-delay sparsity map and power profile is shown in Figure 2.2.

In order to justify the sparsity in temporal domain shown in Figure 2.2, a numerical case study can be given as follows. Considering 30 GHz carrier frequency and 100 MHz bandwidth, one delay tap corresponds to 10 nanoseconds of delay and 3 meters of distance. The maximum delay considered in Figure 2.2 corresponds to 90 meters of extra distance travelled by the multipath component. For a user 100 meters away from the base station, it means that the multipath component travels a distance nearly twice of that of LOS component. In addition, for 30 GHz carrier frequency, wavelength is 1 centimetres. Therefore, a uniform linear antenna array with $N = 100$ antenna elements has a length of 50 centimetres, given that it has half-wavelength distance between successive antennas.

It is seen in Figure 2.2 that both angular and temporal domains are sparsely occupied. In angular domain, it is also seen that MPCs are on very narrow supports. This fact results in low-rank CCMs of MPCs $\mathbf{R}_l^{(u)}$, meaning that they have limited number of nonzero eigenvalues and most probably some of them (one or two) are very dominant

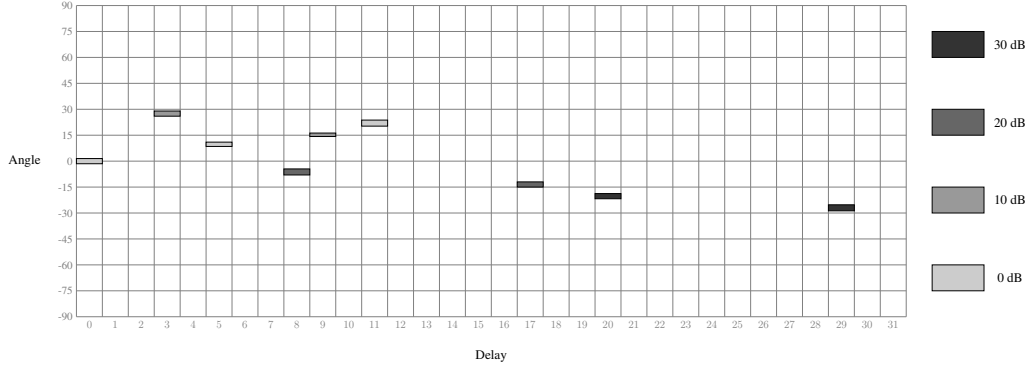


Figure 2.2: Sparsity Map

(e.g., larger in magnitude) against others. Therefore, they can be approximated as

$$\mathbf{R}_l^{(u)} \approx \sum_{p=1}^P \lambda_p \mathbf{v}_p \mathbf{v}_p^H \quad (2.7)$$

where λ_p and \mathbf{v}_p are p^{th} eigenvalue and eigenvector of $\mathbf{R}_l^{(u)}$ and λ_p is in descending order as p increases. In addition, P is a very small integer which is greater than or equal to 1.

On the other hand, it is seen that MPCs occupy a few delay taps in the delay axis. In other words, there are a lot of empty delays. Because of this, it is appropriate to make a definition which will be helpful in the next chapters of the thesis. Let $M^{(u)}$ be the total number of MPCs of the user u . If the m^{th} MPC of the user u is in l^{th} delay where $1 \leq m \leq M^{(u)}$, m and l are dependent on each other through $\mathcal{L}^{(u)}(\cdot)$ as

$$l = \mathcal{L}^{(u)}(m). \quad (2.8)$$

2.1.2 User Grouping Based JSDM Framework

The sparsity in the angular domain, small angular spreads, the availability of small antenna sizes in mm-wave conditions, therefore the availability of large antenna arrays are all opportunities to benefit from beamforming and angular selectivity. Users can be divided and multiplexed in angular domain without dividing time and bandwidth resources between users, which is the case in TDMA and FDMA. This idea takes place in the literature with various names, such as Joint Spatial Division and Multiplexing (JSDM) [2], [6], [7]. However, despite the angular sparsity assumption,

the possibility of angle of arrivals (AoA) of different users being close to each other is not ignored and users are subject to a grouping process before transmission. Angularly adjacent users, or MPCs of users, are clustered into a group and group-specific beams are attained for that group. The multiplexing procedure between the users in the same group (e.g., intra-group users) is left for a later stage. This thesis does not study the user grouping algorithms, but related work can be found in the literature [10].

User grouping is a transformation from the set of users to set of pairs consisting of group number g and intra-group user index k . It is considered that UTs are partitioned into G groups such that angularly adjacent UTs are in the same group. The g^{th} group consists of K_g users. Each group has $M^{(g)}$ MPCs arriving at BS with different AoA and delays. The delay of m^{th} MPC of g^{th} group is

$$l = \mathcal{L}^{(g)}(m). \quad (2.9)$$

UTs in the same group share properties of these MPCs. User grouping idea and MPCs are illustrated in Figure 2.3 for a simple scenario.

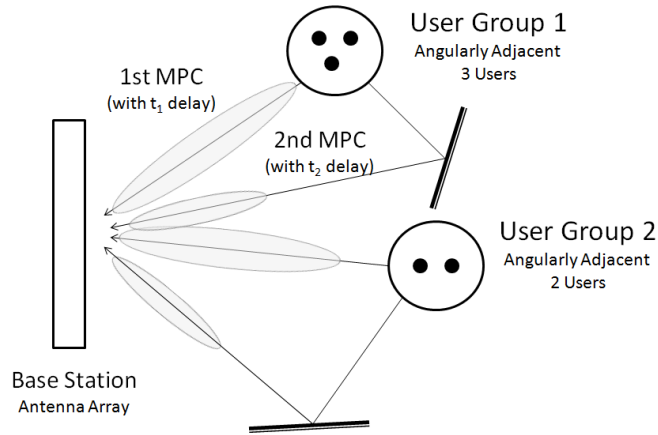


Figure 2.3: User grouping and MPCs ($G = 2$, $K_1 = 3$, $K_2 = 2$, $M^{(1)} = 2$ and $M^{(2)} = 2$)

After user grouping, the channel model in (2.1) can be rewritten as

$$\mathbf{y}_n = \sum_{g=1}^G \sum_{k=1}^{K_g} \sum_{l=0}^{L-1} \mathbf{h}_l^{(gk)} x_{n-l}^{(gk)} + \mathbf{n}_n, \quad (2.10)$$

or equivalently

$$\mathbf{y}_n = \sum_{g=1}^G \sum_{l=0}^{L-1} \mathbf{H}_l^{(g)} \mathbf{x}_{n-l}^{(g)} + \mathbf{n}_n, \quad (2.11)$$

where

$$\mathbf{H}_l^{(g)} \triangleq [\mathbf{h}_l^{(g_1)}, \mathbf{h}_l^{(g_2)}, \dots, \mathbf{h}_l^{(g_{K_g})}] \quad (2.12)$$

is a channel matrix of size $N \times K_g$,

$$\mathbf{x}_n^{(g)} \triangleq [x_n^{(g_1)}, x_n^{(g_2)}, \dots, x_n^{(g_{K_g})}]^T \quad (2.13)$$

is a symbol vector of size K_g , and \mathbf{n}_n is the additive white Gaussian noise (AWGN) vector. In addition, $\mathbf{h}_l^{(g_k)}$ is a channel vector and $x_n^{(g_k)}$ is a transmitted symbol. Subscripts and superscripts $(\cdot)^{(g)}$, $(\cdot)^{(g_k)}$, $(\cdot)_l$ and $(\cdot)_n$ indicate affiliations to the group g , k^{th} user of the group g , the l^{th} delay and the n^{th} time instance, respectively. Interference for group g can be defined as

$$\boldsymbol{\xi}_n^{(g)} \triangleq \sum_{\substack{g'=1 \\ g' \neq g}}^G \sum_{l=0}^{L-1} \mathbf{H}_l^{(g')} \mathbf{x}_{n-l}^{(g')}. \quad (2.14)$$

Then, (2.11) can be written as

$$\mathbf{y}_n = \sum_{l=0}^{L-1} \mathbf{H}_l^{(g)} \mathbf{x}_{n-l}^{(g)} + \boldsymbol{\xi}_n^{(g)} + \mathbf{n}_n. \quad (2.15)$$

The interference-and-noise term is

$$\boldsymbol{\eta}_n^{(g)} \triangleq \boldsymbol{\xi}_n^{(g)} + \mathbf{n}_n. \quad (2.16)$$

Intra-group users (the users in the same group) are assumed to share some properties such as angular power profile, CCMs, power distribution among MPCs, symbol energy and SNR. However, their probabilistic variables remain independent and uncorrelated. After user grouping, (2.2),(2.3), (2.5) and (2.6) can be rewritten as

$$E \left\{ \mathbf{h}_l^{(g_k)} [\mathbf{h}_{l'}^{(g_{k'})}]^H \right\} = \mathbf{R}_l^{(g)} \delta_{gg'} \delta_{kk'} \delta_{ll'}, \quad (2.17)$$

$$\mathbf{R}_l^{(g)} = \int_{-\frac{\pi}{2}}^{\frac{\pi}{2}} \rho_{\phi,l}^{(g)}(\phi) \mathbf{u}(\phi) \mathbf{u}(\phi)^H d\phi, \quad (2.18)$$

$$E \left\{ x_n^{(gk)} \left[x_{n'}^{(g'k')} \right]^* \right\} = E_s^{(g)} \delta_{gg'} \delta_{kk'} \delta_{nn'} \quad (2.19)$$

$$\gamma^{(gk)} = E_s^{(g)} / N_0. \quad (2.20)$$

Also, it will be useful in the next chapters to define observation covariance matrix $\mathbf{R}_y \triangleq E [\mathbf{y}_n \mathbf{y}_n^H]$, group-specific interference covariance matrix $\mathbf{R}_\eta^{(g)}$, MPC-specific interference covariance matrix $\mathbf{R}_{\eta,l}^{(g)}$ and the total angular power profile of users $\rho_{\phi,t}(\phi)$ as

$$\mathbf{R}_y \triangleq \sum_{g=1}^G K_g E_s^{(g)} \sum_{l=0}^{L-1} \mathbf{R}_l^{(g)} + N_0 \mathbf{I}_N, \quad (2.21)$$

$$\mathbf{R}_\eta^{(g)} \triangleq \sum_{\substack{g'=1 \\ g' \neq g}}^G K_{g'} E_s^{(g')} \sum_{l=0}^{L-1} \mathbf{R}_l^{(g')} + N_0 \mathbf{I}_N, \quad (2.22)$$

$$\mathbf{R}_{\eta,l}^{(g)} \triangleq \sum_{\substack{g'=1 \\ g' \neq g}}^G K_{g'} E_s^{(g')} \sum_{l'=0}^{L-1} \mathbf{R}_{l'}^{(g')} + K_g E_s^{(g)} \sum_{\substack{l'=1 \\ l' \neq l}}^{L-1} \mathbf{R}_{l'}^{(g)} + N_0 \mathbf{I}_N, \quad (2.23)$$

$$\rho_{\phi,t}(\phi) \triangleq \sum_{g=1}^G K_g E_s^{(g)} \sum_{l=0}^{L-1} \rho_{\phi,l}^{(g)}(\phi). \quad (2.24)$$

Note that $\mathbf{R}_\eta^{(g)} = \mathbf{R}_y - K_g E_s^{(g)} \sum_{l=0}^{L-1} \mathbf{R}_l^{(g)}$, $\mathbf{R}_{\eta,l}^{(g)} = \mathbf{R}_y - K_g E_s^{(g)} \mathbf{R}_l^{(g)}$ and $\mathbf{R}_y = \int \rho_{\phi,t}(\phi) \mathbf{u}(\phi) \mathbf{u}(\phi)^H d\phi + N_0 \mathbf{I}_N$.

In the next parts of the thesis, g , k , and m will be used as indices for groups, users of groups, and multipath components; and they are from 1 to G , K , and M , respectively. The indexing variable l will be used for delay, which is from 0 to $L - 1$. Estimates will be shown as $\hat{\square}$, a chosen index will be indicated with $\tilde{\square}$, and $\bar{\square}$ will generally show the result of Kronecker product or concatenation.

2.2 Hybrid Beamformer Architecture

The sparsity in millimeter-wave channels and the user grouping idea make the usage of two-stage beamforming advantageous. Limited parts of the angular spectrum

experience an activity and the inactive region is relatively wider. In addition, the positioning of these regions is highly correlated in time and changes with a slow rate. In this case, a two-stage beamforming scheme becomes prominent where one stage is governing the slowly changing long term parameters of the channel. In this way, spectral sparsity in the angular domain enables efficient dimension reduction operation which will be performed by the first stage again. Therefore, the second stage will conduct the operations about short term parameters on a reduced number of coefficients; i.e., in a reduced-dimension subspace. In this section, the architectures of fully analog, fully digital, and hybrid beamformers will be elaborated.

Beamformer is basically a system used on multi-antenna systems, realizing a synthesis operation for transmitting and an analysis operation for receiving. They transform between intended baseband signals and baseband equivalents of the signals at antennas. Upon these operations, power pattern (or beam pattern) of the whole antenna array can be formed or steered so that it is directed to a specific direction. Therefore, the basis vectors for these synthesis and analysis operations are dependent on desired angular parameters. Moreover, these basis vectors can be formed in several ways, which are referred as beamformer design methods in this thesis.

Transmitter and receiver circuits generally consist of digital and analog parts, the analog part being at the antenna side. The mentioned beamformer objectives can be seen as matrix multiplication, which fundamentally consists of multiplying and summing operations. Beamformer can be named as analog beamformer or digital beamformer according to the place where multiplying and summing operations are performed. In analog beamformer, these operations can be done with controllable analog phase shifters, attenuators and summers, on analog RF signals. In digital beamformer, the operations are done with digital circuitry, on digitized baseband signals. Analog beamformer and digital beamformer architectures are illustrated for an antenna array with 4 antenna elements in Figures 2.4 and 2.5, respectively.

Analog beamformer consists of N controllable phase shifters, N controllable attenuators and one RF chain. Phase shifters adjust the phase of the signal, and attenuators adjust the magnitude of the signal. Attenuators might not be needed in some applications, such as phase-only beamforming. RF chain is the name given to the chain of

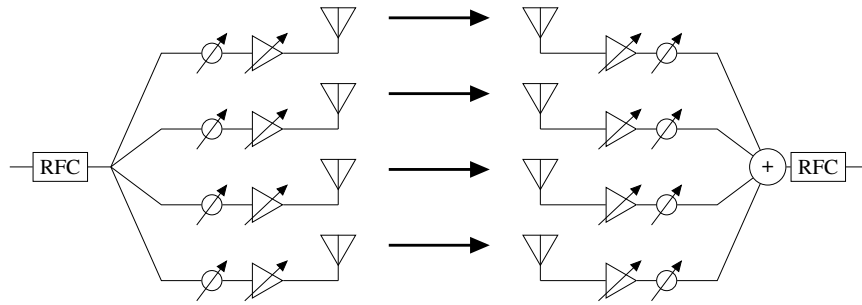


Figure 2.4: Analog beamformer architecture for an antenna array consisting of $N = 4$ antennas (transmitter is on the left and receiver is on the right)

circuitry responsible for the transformation of the baseband signal to the RF signal, or vice versa. It includes pieces of equipment such as local oscillator and DAC (or ADC).

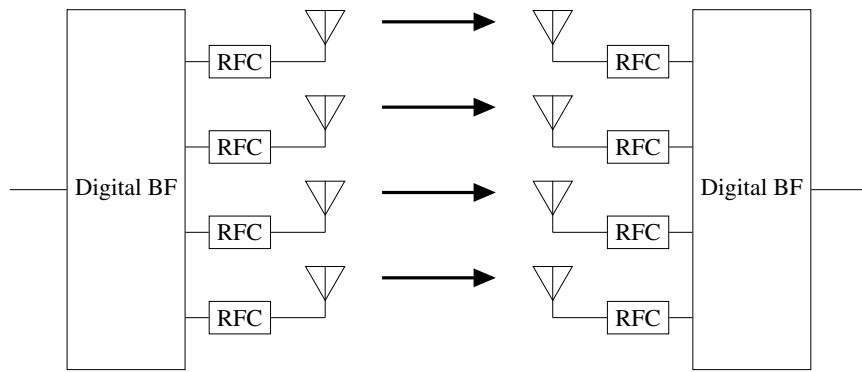


Figure 2.5: Digital beamformer architecture for an antenna array consisting of $N = 4$ antennas (transmitter is on the left and receiver is on the right)

Digital beamformer consists of a digital circuitry which is able to perform aforementioned beamforming operations in parallel. It has one RF chain for each of the antennas.

Analog beamformer uses phase shifters and attenuators which have constraints on resolution and update rate. Digital beamformer performs operations in digital domain, which is less constrained. Also, while analog beamformer equipped with one RF chain, which is considered to be more complex and expensive than the other parts; digital beamformer has one RF chain for each of the antennas. In conclusion, while analog beamformer is a cheaper, low-complexity and low-performance solution, digi-

tal beamformer is a more complex and expensive choice promising high-performance. For large antenna arrays, advantages and disadvantages of these architectures goes to extremities. Hybrid beamformer architecture is a solution compromising these advantages and disadvantages in order to make large antenna arrays practical, to benefit from the advantages of millimeter-wave conditions for antenna arrays and beamforming. Hybrid beamformer architecture is given in Figure 2.6.

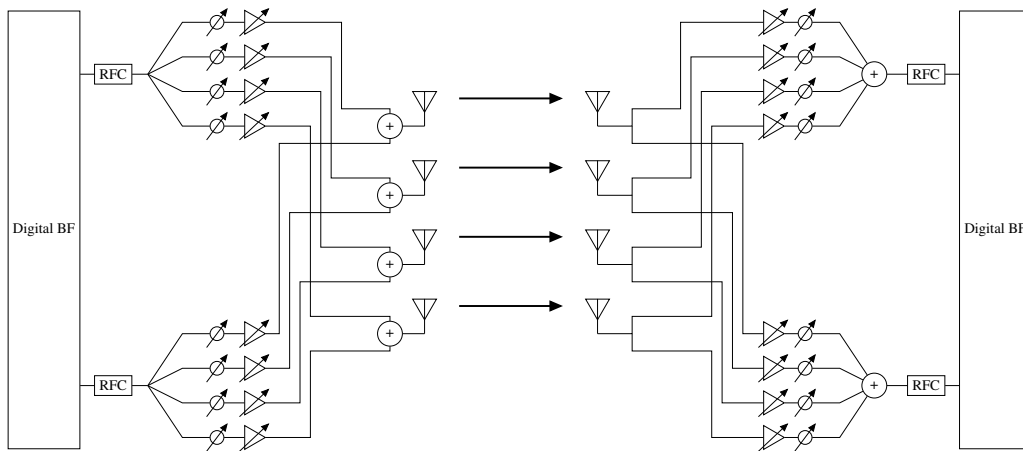


Figure 2.6: Hybrid beamformer architecture with 2 RF chains and 4 antenna elements ($D = 2$, $N = 4$, transmitter is on the left and receiver is on the right)

Hybrid beamformer has DN sets of phase shifters and attenuators, D RF chains which is less than N ($D < N$), where N is the number of antennas. This architecture moves the responsibility of high update rate from the analog beamformer to the digital beamformer, while decreasing the cost and complexity with a smaller number of RF chains. Hybrid beamformer enables the separation of beamforming operation into two parts. When the digital beamformer is matched to the instantaneous channel properties, and the analog beamformer is matched to the long term channel parameters, the number of parameters to be estimated for instantaneous channel acquisition also decreases to the number of RF chains D .

2.3 Proposed Architecture for Single Carrier Wideband Massive MIMO Channels

Proposed system consists of analog beamformer, digital beamformer, joint angle-delay sparsity map and power profile, instantaneous channel estimator in reduced dimension and demodulators. Baseband digital equivalent of the proposed receiver processing is shown in Figure 2.7.

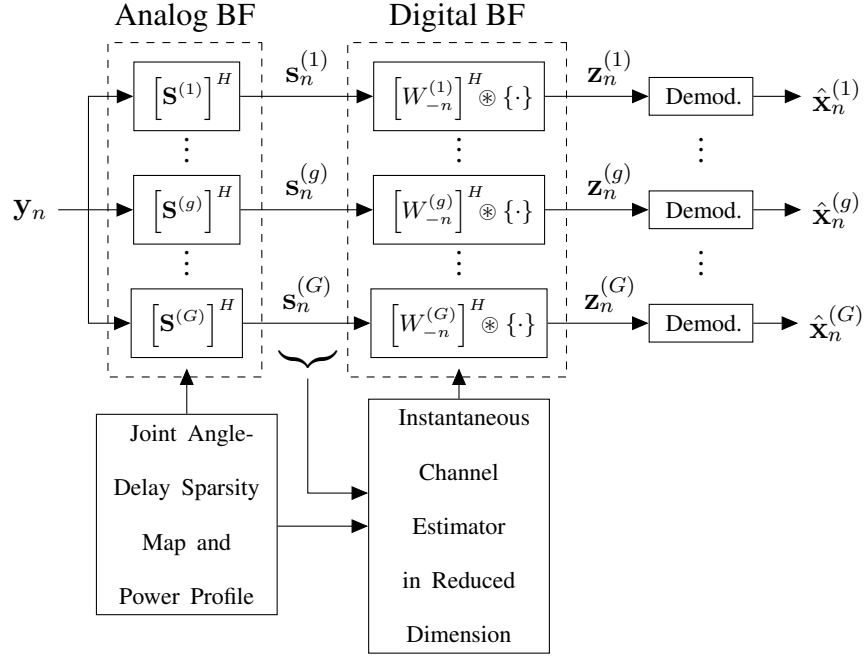


Figure 2.7: Equivalent Receiver Processing

Processing blocks in Figure 2.7 will be explained in following subsections in introductory level, where fundamental information, input-output relations and flow of signal expressions will be given. Design methods for these blocks will be addressed in the next chapters.

2.3.1 Joint Angle-Delay Power Profile and Sparsity Map

This block estimates angular properties of signals transmitted by users. Power distribution is estimated on angle-delay plane. It is assumed that the block outputs estimates for a center angle $\hat{\mu}_{\phi,l}^{(g)}$, angular spread $\hat{\sigma}_{\phi,l}^{(g)}$, and power profile $\hat{\rho}_{\phi,l}^{(g)}(\phi)$ for all

MPCs of all users. $\hat{\mu}_{\phi,l}^{(g)}$ and $\hat{\sigma}_{\phi,l}^{(g)}$ indicate the nonzero region of $\hat{\rho}_{\phi,l}^{(g)}(\phi)$, and they are implied by $\hat{\rho}_{\phi,l}^{(g)}(\phi)$. With this information, CCM estimate $\hat{\mathbf{R}}_l^{(g)}$ can be calculated parametrically as in (2.25). A computationally easier method for parametric CCM construction is derived in Section 6.4.2.

$$\hat{\mathbf{R}}_l^{(g)} = \int_{\hat{\mu}_{\phi,l}^{(g)} - \frac{\hat{\sigma}_{\phi,l}^{(g)}}{2}}^{\hat{\mu}_{\phi,l}^{(g)} + \frac{\hat{\sigma}_{\phi,l}^{(g)}}{2}} \hat{\rho}_{\phi,l}^{(g)}(\phi) \mathbf{u}(\phi) \mathbf{u}(\phi)^H d\phi. \quad (2.25)$$

Output estimates are used in the design of analog beamformer and instantaneous channel estimator. This work does not propose a design method for this block but questions the needed level of accuracy in $\hat{\mu}_{\phi,l}^{(g)}$ and $\hat{\sigma}_{\phi,l}^{(g)}$ by performing performance analysis against given errors in these estimates.

2.3.2 Analog Beamformer

Analog beamformer is a bank of filters each of which projects N -dimensional observation into group-specific D_g -dimensional subspaces where D_g is the number of RF chains allocated for the group g . This process aims to benefit from the low-rank property of CCMs in order to ease instantaneous channel estimation and further processing steps. Analog beamformer selects intended group signals, rejects interference due to other groups (i.e., inter-group interference, IGI) and separates MPCs in angular domain. The analog beamformer matrix $\mathbf{S}^{(g)}$ is of size $N \times D_g$ where $D_g < N$. Its output is

$$\mathbf{s}_n^{(g)} \triangleq [\mathbf{S}^{(g)}]^H \mathbf{y}_n. \quad (2.26)$$

Substituting \mathbf{y}_n using (2.11);

$$\mathbf{s}_n^{(g)} = \sum_{g'=1}^G \sum_{l=0}^{L-1} [\mathbf{S}^{(g)}]^H \mathbf{H}_l^{(g')} \mathbf{x}_{n-l}^{(g')} + [\mathbf{S}^{(g)}]^H \mathbf{n}_n \quad (2.27)$$

Defining effective channel matrix $\mathbf{H}_{eff,l}^{(g,g')}$ as

$$\mathbf{H}_{eff,l}^{(g,g')} \triangleq [\mathbf{S}^{(g)}]^H \mathbf{H}_l^{(g')}, \quad (2.28)$$

(2.27) can be rewritten as

$$\mathbf{s}_n^{(g)} = \sum_{l=0}^{L-1} \mathbf{H}_{eff,l}^{(g,g)} \mathbf{x}_{n-l}^{(g)} + \sum_{\substack{g'=1 \\ g' \neq g}}^G \sum_{l=0}^{L-1} \mathbf{H}_{eff,l}^{(g,g')} \mathbf{x}_{n-l}^{(g')} + [\mathbf{S}^{(g)}]^H \mathbf{n}_n. \quad (2.29)$$

The first term is intra-group signal, the second is inter-group signal and the last one is the noise term. Defining the interference $\boldsymbol{\eta}_{eff,n}^{(g)}$ as

$$\boldsymbol{\eta}_{eff,n}^{(g)} \triangleq \sum_{\substack{g'=1 \\ g' \neq g}}^G \sum_{l=0}^{L-1} \mathbf{H}_{eff,l}^{(g,g')} \mathbf{x}_{n-l}^{(g')} + [\mathbf{S}^{(g)}]^H \mathbf{n}_n, \quad (2.30)$$

the final expression is obtained as

$$\mathbf{s}_n^{(g)} = \sum_{l=0}^{L-1} \mathbf{H}_{eff,l}^{(g,g)} \mathbf{x}_{n-l}^{(g)} + \boldsymbol{\eta}_{eff,n}^{(g)}. \quad (2.31)$$

Note that $\mathbf{H}_{eff,l}^{(g,g')}$ is the effective channel matrix of the group g' projected on the subspace created for the group g . When $g \neq g'$, the channel is among the inter-group interference and expected to be suppressed; i.e., to have smaller entries compared to $\mathbf{H}_{eff,l}^{(g,g)}$. It is implied by above equations that

$$\mathbf{H}_{eff,l}^{(g,g')} = \begin{bmatrix} \mathbf{h}_{eff,l}^{(g,g'_1)} & \mathbf{h}_{eff,l}^{(g,g'_2)} & \dots & \mathbf{h}_{eff,l}^{(g,g'_{K_{g'}})} \end{bmatrix} \quad (2.32)$$

where

$$\mathbf{h}_{eff,l}^{(g,g'_k)} \triangleq [\mathbf{S}^{(g)}]^H \mathbf{h}_l^{(g'_k)} \quad (2.33)$$

is the effective channel of the k^{th} user of the group g' for l^{th} delay, in the subspace created for the group g .

At the output of the analog beamformer, the effective channel covariance matrix $\mathbf{R}_{eff,l}^{(g,g')} \triangleq E \left\{ \mathbf{h}_{eff,l}^{(g,g'_k)} \left(\mathbf{h}_{eff,l}^{(g,g'_k)} \right)^H \right\}$ and the interference covariance matrix $\mathbf{R}_{eff,\eta}^{(g)} \triangleq E \left\{ \boldsymbol{\eta}_{eff,n}^{(g)} \left[\boldsymbol{\eta}_{eff,n}^{(g)} \right]^H \right\}$ are given below.

$$\mathbf{R}_{eff,l}^{(g,g')} = [\mathbf{S}^{(g)}]^H \mathbf{R}_l^{(g')} \mathbf{S}^{(g)}, \quad \text{for } g, g' = 1, 2, \dots, G \quad (2.34)$$

$$\mathbf{R}_{eff,\eta}^{(g)} = \sum_{\substack{g'=1 \\ g' \neq g}}^G K_{g'} E_s^{(g')} \sum_{l=0}^{L-1} \mathbf{R}_{eff,l}^{(g,g')} + N_0 [\mathbf{S}^{(g)}]^H \mathbf{S}^{(g)}, \quad \text{for } g = 1, 2, \dots, G \quad (2.35)$$

It is also worth noting the independence among the channels of MPCs as

$$E \left\{ \mathbf{h}_{eff,l'}^{(g,g')} \left(\mathbf{h}_{eff,l''}^{(g,g'')} \right)^H \right\} = \mathbf{R}_{eff,l}^{(g,g')} \delta_{g'g''} \delta_{k'k''} \delta_{l'l''}. \quad (2.36)$$

$\hat{\mathbf{R}}_{eff,l}^{(g,g')}$ and $\hat{\mathbf{R}}_{eff,\eta}^{(g)}$ are estimates of these matrices and created using parametrically calculated $\hat{\mathbf{R}}_l^{(g)}$ instead of $\mathbf{R}_l^{(g)}$ in the equation system of (2.34) and (2.35).

The power pattern $p_\phi(\phi)$ that is created by an arbitrary analog beamformer \mathbf{S} can be calculated as

$$p_\phi(\phi) \triangleq \|\mathbf{S}^H \mathbf{u}(\phi)\|^2 \quad (2.37)$$

$$= \mathbf{u}^H(\phi) \mathbf{S} \mathbf{S}^H \mathbf{u}(\phi) \quad (2.38)$$

2.3.3 Instantaneous Channel Estimator in Reduced Dimension

This block produces effective channel estimates of intra-group users $\hat{\mathbf{H}}_{eff,l}^{(g,g)}$, appearing at the output of analog beamformer stage, through a training period of length T . Since it operates in reduced-dimension, its performance is dependent on former blocks. $\hat{\mathbf{H}}_{eff,l}^{(g,g)}$ produced in this block is used in the design of digital beamformer. Various design methods are given in Chapter 4.

2.3.4 Digital Beamformer

Digital beamformer is a space-time filter and processes the output of analog beamformer. It is constructed using the estimated channel $\hat{\mathbf{H}}_{eff,l}^{(g,g)}$ provided by the instantaneous channel estimator. Its first objective is effectively combining MPCs of the intended group. To be able to do that, a matrix convolution in the delay domain is utilized, where different MPCs in different delays are processed and combined. Its second objective is to separate the signals of intra-group users, the users in the intended group. Therefore, its output is a vector of length K_g expressed as

$$\mathbf{z}_n^{(g)} \triangleq \begin{bmatrix} z_n^{(g_1)} & z_n^{(g_2)} & \dots & z_n^{(g_{K_g})} \end{bmatrix}^T \quad (2.39)$$

whose each element belongs to one of the intra-group users. Construction methods can be found in Section 3.2.

CHAPTER 3

HYBRID BEAMFORMER DESIGN

3.1 Analog Beamformer Design

In the design of analog beamformer, the number of MPCs $M^{(g)}$, and angular estimates $\hat{\rho}_{\phi,l}^{(g)}$, $\hat{\mu}_{\phi,l}^{(g)}$ and $\hat{\sigma}_{\phi,l}^{(g)}(\phi)$ are assumed to be supplied by the block named Joint Angle-Delay Sparsity Map and Power Profile. Also, the total number of RF chains allocated for the g^{th} group D_g is assumed to be determined. With this information, D_g is distributed among MPCs such that $d_m^{(g)}$ RF chains are allocated for m^{th} MPC of g^{th} group which lies in the delay $l = \mathcal{L}^{(g)}(m)$ and $\sum_{m=1}^{M^{(g)}} d_m^{(g)} = D_g$. To do that, an optimization can be performed depending on power distribution of MPCs and inter-group occupancy in angular domain. However, power distribution among MPCs are uniform in the scenario used in this thesis. Therefore, the largest amount divisible by $M^{(g)}$ in D_g RF chains are distributed among MPCs uniformly and remaining RF chains are distributed randomly. Then, the analog beamformer matrix $\mathbf{S}^{(g)}$ of size $N \times D_g$ can be formed as

$$\mathbf{S}^{(g)} = \begin{bmatrix} \mathbf{S}_1^{(g)} & \mathbf{S}_2^{(g)} & \dots & \mathbf{S}_{M^{(g)}}^{(g)} \end{bmatrix} \quad (3.1)$$

for the group g , where $\mathbf{S}_m^{(g)}$ is the analog beamformer matrix designed for the m^{th} MPC of the g^{th} group and of size $N \times d_m^{(g)}$. Note that the configuration in (3.1) is important to separate MPCs in space, and to suppress ISI later. Following two methods are suggested to design $\mathbf{S}_m^{(g)}$.

3.1.1 Nearly Optimal Generalized Eigen-Beamformer

In this method, CCMs related to the l^{th} delay are used to construct the beamformer related to the m^{th} MPC $\mathbf{S}_m^{(g)}$, where the relation between m and l is constituted by the function $\mathcal{L}^{(g)}(\cdot)$ as $l = \mathcal{L}^{(g)}(m)$. Generalized eigenvectors \mathbf{v}_p of the matrix pair $(\hat{\mathbf{R}}_l^{(g)}, \hat{\mathbf{R}}_{\eta,l}^{(g)})$ which obey

$$\hat{\mathbf{R}}_l^{(g)} \mathbf{v}_p = \lambda_p \hat{\mathbf{R}}_{\eta,l}^{(g)} \mathbf{v}_p, \text{ for } p = 1, \dots, N \quad (3.2)$$

are found where λ_p is the p^{th} generalized eigenvalue which corresponds to \mathbf{v}_p . In addition, $\hat{\mathbf{R}}_l^{(g)}$ and $\hat{\mathbf{R}}_{\eta,l}^{(g)}$ are estimates of $\mathbf{R}_l^{(g)}$ and $\mathbf{R}_{\eta,l}^{(g)}$ which are defined in (2.18) and (2.23). If generalized eigenvalues are sorted in descending order as p increases (e.g., $\lambda_{p_1} \geq \lambda_{p_2}$ for $1 \leq p_1 < p_2 \leq N$), $\mathbf{S}_m^{(g)}$ is formed by horizontal concatenation of the most dominant $d_m^{(g)}$ generalized eigenvectors as

$$\mathbf{S}_m^{(g)} = \begin{bmatrix} \mathbf{v}_1 & \mathbf{v}_2 & \cdots & \mathbf{v}_{d_m^{(g)}} \end{bmatrix}. \quad (3.3)$$

Then, analog beamformer matrix $\mathbf{S}^{(g)}$ is constructed from $\mathbf{S}_m^{(g)}$ for $m = 1, \dots, M^{(g)}$ as shown in (3.1). Note that the estimated CCMs of each MPC, namely $\hat{\mathbf{R}}_l^{(g)}$, are constructed parametrically as in (2.25). Moreover, $\hat{\mathbf{R}}_{\eta,l}^{(g)}$ is found by replacing $\mathbf{R}_l^{(g)}$ with $\hat{\mathbf{R}}_l^{(g)}$ in (2.23).

The most dominant generalized eigenvectors of the matrix pair (\mathbf{A}, \mathbf{B}) selects the signals whose covariance matrix is \mathbf{A} and rejects the signals whose covariance matrix is \mathbf{B} , in the mean square sense, when used as a linear combiner. Let \mathbf{a} be the intended random signal and \mathbf{b} be the random interfering signal and $\mathbf{c} = \mathbf{a} + \mathbf{b}$ be the observation. When \mathbf{c} is linearly combined with \mathbf{w} by $\mathbf{w}^H \mathbf{c}$, the sum of the intended part $\mathbf{w}^H \mathbf{a}$ and the interference $\mathbf{w}^H \mathbf{b}$ is obtained. Expected powers of these are $E[\mathbf{w}^H \mathbf{a} \mathbf{a}^H \mathbf{w}] = \mathbf{w}^H \mathbf{A} \mathbf{w}$ and $E[\mathbf{w}^H \mathbf{b} \mathbf{b}^H \mathbf{w}] = \mathbf{w}^H \mathbf{B} \mathbf{w}$, respectively. Their ratio is Rayleigh Quotient

$$\mathcal{R}(\mathbf{w}) = \frac{\mathbf{w}^H \mathbf{A} \mathbf{w}}{\mathbf{w}^H \mathbf{B} \mathbf{w}} \quad (3.4)$$

and can be considered as output SNR. Generalized eigenvectors of the matrix pair (\mathbf{A}, \mathbf{B}) make the first derivative of the Rayleigh Quotient zero when used in the place of \mathbf{w} , as shown in Appendix A. Since the most dominant generalized eigenvectors of the matrix pair $(\hat{\mathbf{R}}_l^{(g)}, \hat{\mathbf{R}}_{\eta,l}^{(g)})$ are used in GEB, they select the related MPC and

reject all the others, including the other MPCs of the same group (or user). It can be observed in Figure (3.1) which consists of power patterns of $\mathbf{S}_1^{(g)}$, $\mathbf{S}_2^{(g)}$, $\mathbf{S}_3^{(g)}$, and $\mathbf{S}^{(g)}$. Total angular power profile $\rho_{\phi,t}(\phi)$ is also placed at the bottom to track the behavior of patterns according to the distribution of groups. In the exemplary scenario in Figure 3.1, the intended group consists of 3 MPCs and the first, second and third MPCs are centered about 0° , 10° and 20° azimuth, respectively.

Note that the interfering MPCs are stronger in power and suppressed by the GEB. It should also be noted that MPC-specific analog beamformer $\mathbf{S}_m^{(g)}$ suppresses the other MPCs of the same group. This fact is expected to be very helpful in ISI mitigation in angular domain, when combined with the channel matched filter (CMF) in the digital beamformer stage.

It is shown in Appendix A that the generalized eigenvectors of the matrix pair (\mathbf{A}, \mathbf{B}) and $(\mathbf{A}, \mathbf{B} + k\mathbf{A})$ are the same except a scalar multiplier. Since $\hat{\mathbf{R}}_y^{(g)} = \hat{\mathbf{R}}_{\eta,l}^{(g)} + K_g E_s^{(g)} \hat{\mathbf{R}}_l^{(g)}$, the generalized eigenvectors \mathbf{v}_p of the matrix pair $(\hat{\mathbf{R}}_l^{(g)}, \hat{\mathbf{R}}_y^{(g)})$ can also be used instead of the pair $(\hat{\mathbf{R}}_l^{(g)}, \hat{\mathbf{R}}_{\eta,l}^{(g)})$, satisfying

$$\hat{\mathbf{R}}_l^{(g)} \mathbf{v}_p = \lambda_p \hat{\mathbf{R}}_y \mathbf{v}_p. \quad (3.5)$$

Then $\mathbf{S}_m^{(g)}$ is constructed as shown in (3.3) and $\mathbf{S}^{(g)}$ is constructed as shown in (3.1). This way, construction might be easier since the second matrix of the pair is always the same for all MPCs of all groups.

3.1.1.1 Optimality Criteria for Generalized Eigen-Beamformer

The proposed analog beamformer is structured based on the pre-processing technique in [9], where the optimality was demonstrated for several different criteria. These are minimization of error volume and normalized mean square error between reduced-dimension effective channels and their estimates, at the output of the analog beamformer. Also, it is shown to maximize the mutual information between full-dimension and reduced-dimension channels (i.e., between input and output of the analog beamformer). In this thesis, the scheme in [9] is modified such that the orthogonality between the eigenspaces of different MPCs in reduced-dimension is guaranteed by taking both inter-group interference and ISI into account. Therefore, there is no need

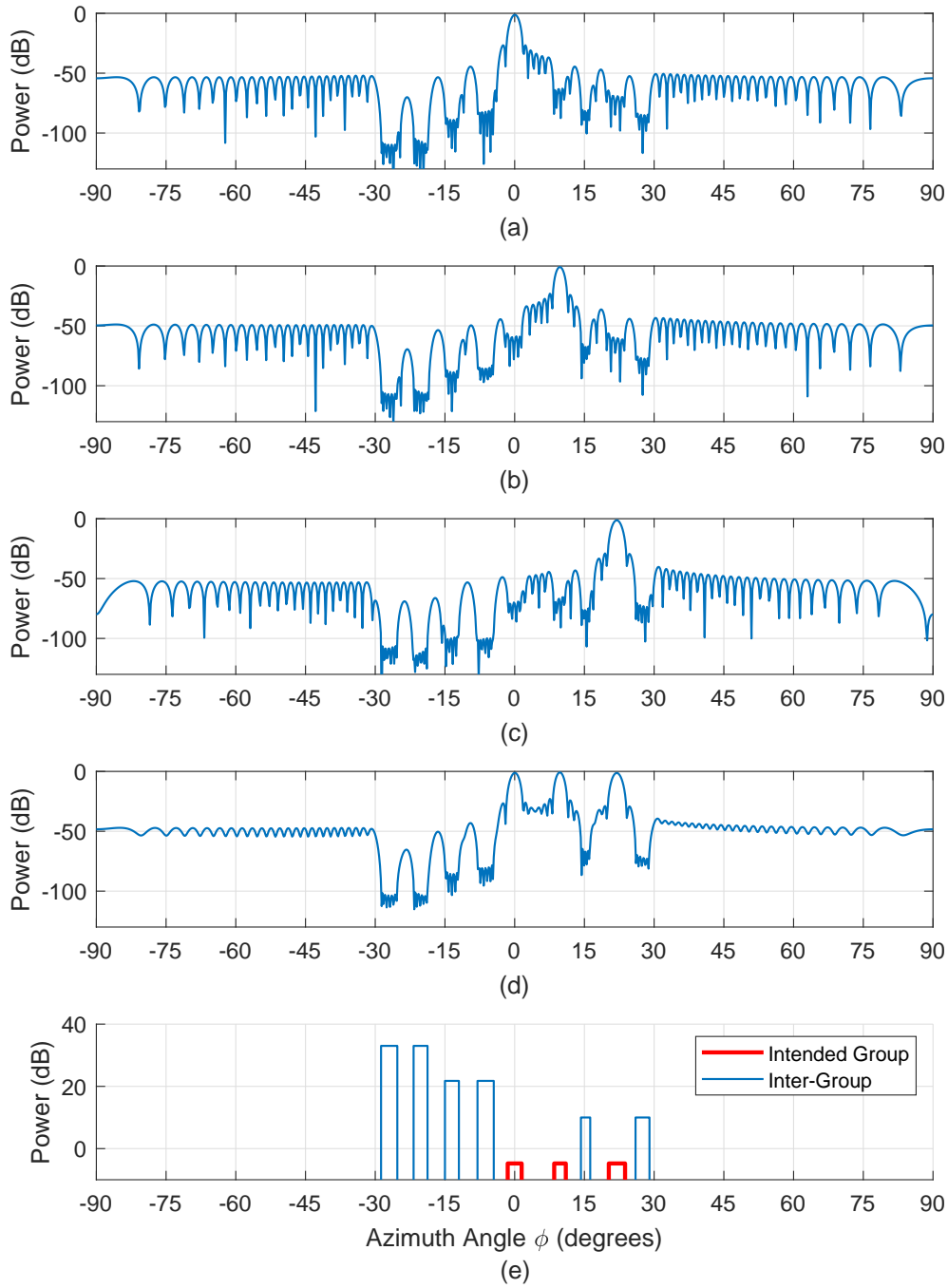


Figure 3.1: Power pattern of GEB. (a) $S_1^{(g)}$. (b) $S_2^{(g)}$. (c) $S_3^{(g)}$. (d) $S^{(g)}$. (e) Placement in the angular domain $\rho_{\phi,t}(\phi)$.

for equalization to mitigate ISI in digital domain (after analog beamforming); just channel matched filtering in reduced-dimension is sufficient to attain ISI-free samples (as an input to the demodulator in Figure 2.7) and full multipath diversity.

3.1.2 Conventional DFT Beamformer

The angular spread of m^{th} MPC of g^{th} group is divided into $d_m^{(g)}$ parts with equal lengths and the vector $\mathbf{u}(\cdot)$ in (2.4) is calculated for center angles of these parts. If these center angles are called $\beta_1, \beta_2, \dots, \beta_{d_m^{(g)}}$; $\mathbf{S}_m^{(g)}$ can be formed as

$$\mathbf{S}_m^{(g)} = \begin{bmatrix} \mathbf{u}(\beta_1) & \mathbf{u}(\beta_2) & \cdots & \mathbf{u}(\beta_{d_m^{(g)}}) \end{bmatrix}. \quad (3.6)$$

The process is illustrated in Figure 3.2 for an example where angular spread of the related MPC is from $\alpha_1 = \hat{\mu}_{\phi,l}^{(g)} - \frac{\hat{\sigma}_{\phi,l}^{(g)}}{2}$ to $\alpha_4 = \hat{\mu}_{\phi,l}^{(g)} + \frac{\hat{\sigma}_{\phi,l}^{(g)}}{2}$ and $d_m^{(g)} = 3$.

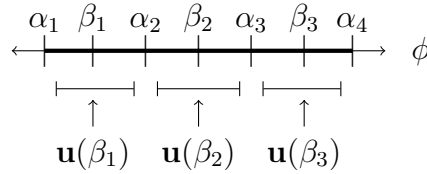


Figure 3.2: Design of DFT beamformer

The power pattern created by the DFT beamformer is given in Figure 3.3. The distribution of the MPC's are the same as in Figure 3.1, which was given for generalized eigen-beamformer. It is seen in Figure 3.3 that the conventional DFT beamformer selects the intended area and suppresses the remaining parts with a natural decrease. However, the pattern is unaware of the existence of the interfering area and there is no significant decrease in those areas as it is seen in the power pattern of GEB given in Figure 3.1. The two can be compared through Figure 3.4.

3.2 Digital Beamformer Design

The digital beamformer is proposed to consist of two stages: channel matched filter and regularized spatial zero forcing as shown in Figure 3.5.

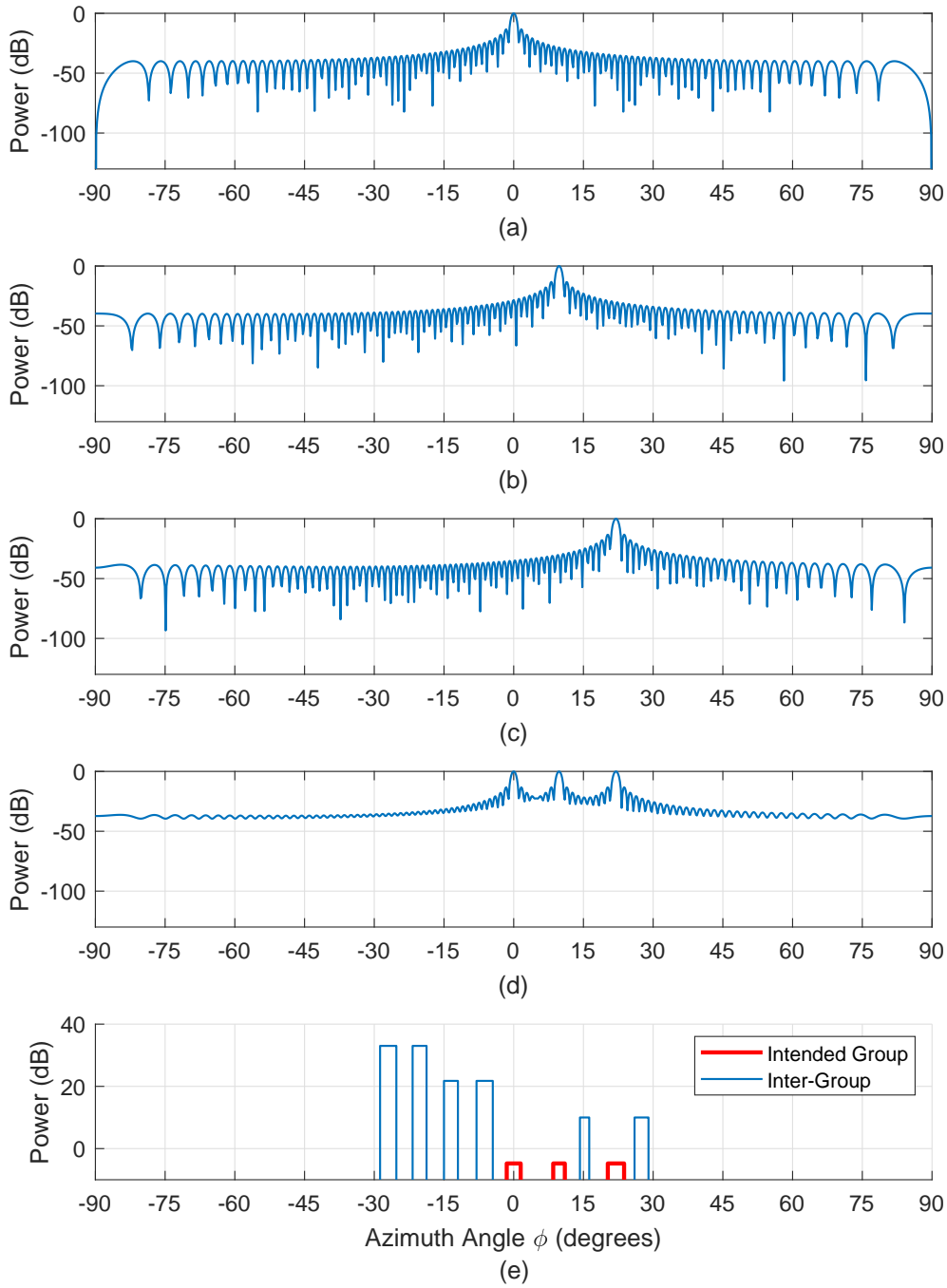


Figure 3.3: Power pattern of DFT beamformer. (a) $S_1^{(g)}$. (b) $S_2^{(g)}$. (c) $S_3^{(g)}$. (d) $S^{(g)}$. (e) Placement in the angular domain $\rho_{\phi,t}(\phi)$.

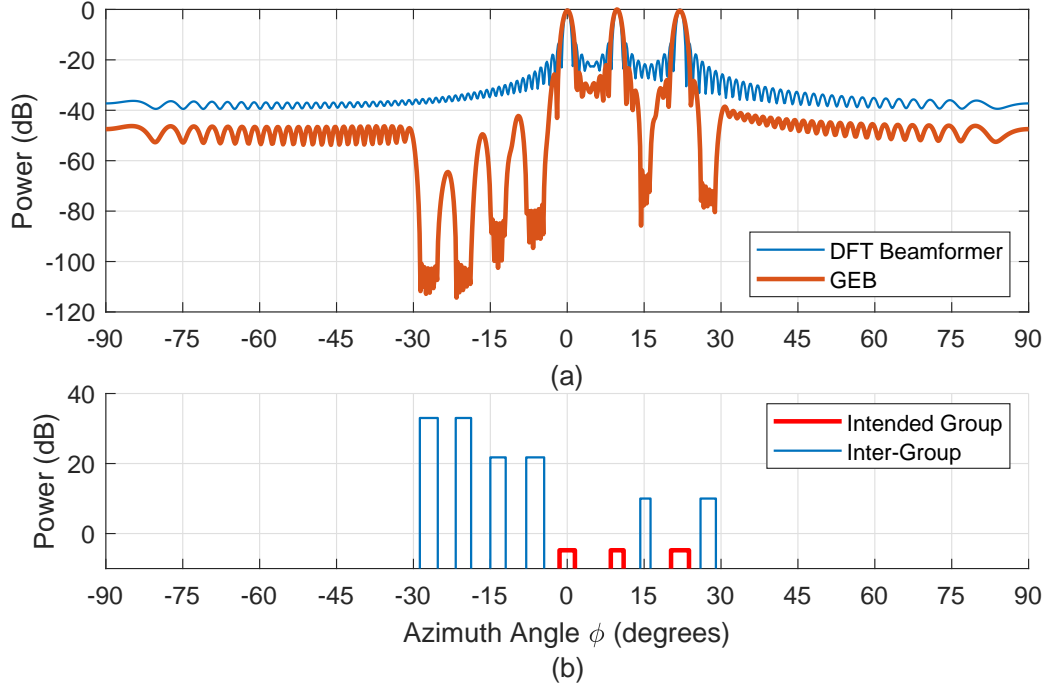


Figure 3.4: Comparison of Power Patterns of GEB and DFT Beamformers. (a) $\mathbf{S}^{(g)}$. (b) Placement in the angular domain $\rho_{\phi,t}(\phi)$.

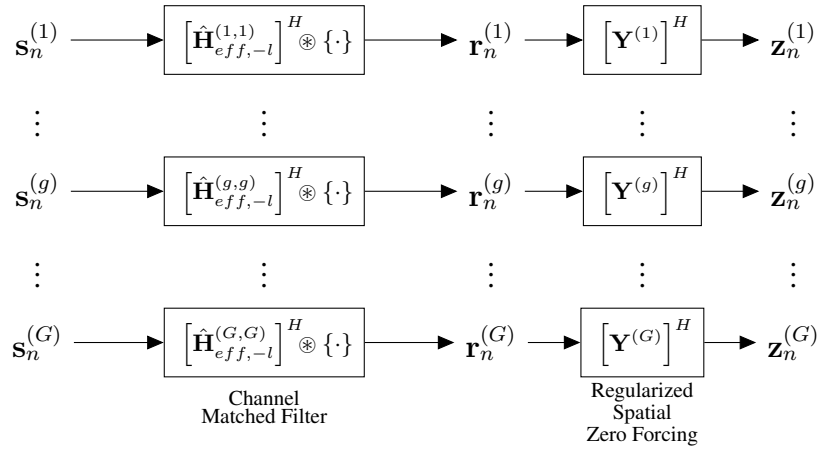


Figure 3.5: Digital beamformer

The digital beamformer operates in the subspace of the group specified by the analog beamformer. Channels of each group might be present in the subspace of the each group. This fact brings the need to denote these relations and a complexity in the notation of variables. In addition to these, the clarity of the concepts such as intended user, intra-group and inter-group are more important after this stage of the processing. Therefore, at this point, the group \tilde{g} is chosen, and only the related branch in Figure 2.7 is focused on, which is shown in Figure 3.6. In addition, the indicators of the subspace in the first place of the superscripts of $\mathbf{H}_{eff,l}^{(\tilde{g},g)}$, $\mathbf{h}_{eff,l}^{(\tilde{g},g_k)}$, $\mathbf{R}_{eff,l}^{(\tilde{g},g)}$ and their estimates are dropped for the sake of simplicity. They will be written as $\mathbf{H}_{eff,l}^{(g)}$, $\mathbf{h}_{eff,l}^{(g_k)}$ and $\mathbf{R}_{eff,l}^{(g)}$, which implies that they belong to the group g or the k^{th} user of the group g , projected on the subspace of the intended group \tilde{g} .

Users in the group \tilde{g} are called intra-group users, and users in groups $g \neq \tilde{g}$ are called inter-group users. Although following processing steps are explained for only the intended group \tilde{g} as shown in Figure 3.6, note that they are applied in parallel for other groups as well.

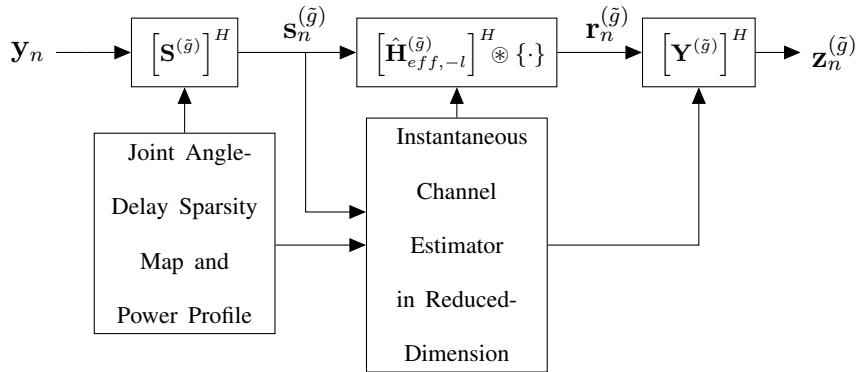


Figure 3.6: Equivalent receiver processing for only the intended group

3.2.1 Channel Matched Filter (CMF)

The output of the channel matched filter for the intended group is expressed as

$$\mathbf{r}_n^{(\tilde{g})} = \sum_{l=0}^{L-1} \left[\hat{\mathbf{H}}_{eff,l}^{(\tilde{g})} \right]^H \mathbf{s}_{n+l}^{(\tilde{g})}, \quad (3.7)$$

where $\hat{\mathbf{H}}_{eff,l}^{(\tilde{g})}$ is the estimated channel matrix for the MPC of the intended group \tilde{g} in the l^{th} delay and of size $D_{\tilde{g}} \times K_{\tilde{g}}$. As it is seen, (3.7) is a time convolution and \otimes in

Figures 2.7 and 3.6 indicates this operation. When $\mathbf{s}_{n+l}^{(\tilde{g})}$ is substituted using (2.31), the expression becomes

$$\mathbf{r}_n^{(\tilde{g})} = \sum_{l_1=0}^{L-1} \sum_{l_2=0}^{L-1} \left[\hat{\mathbf{H}}_{eff,l_1}^{(\tilde{g})} \right]^H \mathbf{H}_{eff,l_2}^{(\tilde{g})} \mathbf{x}_{n+l_1-l_2}^{(\tilde{g})} + \sum_{l=0}^{L-1} \left[\hat{\mathbf{H}}_{eff,l}^{(\tilde{g})} \right]^H \boldsymbol{\eta}_{eff,n+l}^{(\tilde{g})}. \quad (3.8)$$

Perform change of variables with $l_3 \triangleq l_2 - l_1$:

$$\begin{aligned} \mathbf{r}_n^{(\tilde{g})} &= \sum_{l_1=0}^{L-1} \sum_{l_3=-(L-1)}^{L-1} \left[\hat{\mathbf{H}}_{eff,l_1}^{(\tilde{g})} \right]^H \mathbf{H}_{eff,l_1+l_3}^{(\tilde{g})} \mathbf{x}_{n-l_3}^{(\tilde{g})} + \sum_{l=0}^{L-1} \left[\hat{\mathbf{H}}_{eff,l}^{(\tilde{g})} \right]^H \boldsymbol{\eta}_{eff,n+l}^{(\tilde{g})}, \quad (3.9) \\ &= \sum_{l_3=-(L-1)}^{L-1} \left(\sum_{l_1=0}^{L-1} \left[\hat{\mathbf{H}}_{eff,l_1}^{(\tilde{g})} \right]^H \mathbf{H}_{eff,l_3+l_1}^{(\tilde{g})} \right) \mathbf{x}_{n-l_3}^{(\tilde{g})} + \sum_{l=0}^{L-1} \left[\hat{\mathbf{H}}_{eff,l}^{(\tilde{g})} \right]^H \boldsymbol{\eta}_{eff,n+l}^{(\tilde{g})}. \end{aligned} \quad (3.10)$$

Defining $\mathbf{R}_l^{\hat{h}h}$ as

$$\mathbf{R}_l^{\hat{h}h} \triangleq \sum_{l_1=0}^{L-1} \left[\hat{\mathbf{H}}_{eff,l_1}^{(\tilde{g})} \right]^H \mathbf{H}_{eff,l+l_1}^{(\tilde{g})}, \quad (3.11)$$

a further simplification in (3.8) can be done as shown below.

$$\mathbf{r}_n^{(\tilde{g})} = \sum_{l=-(L-1)}^{L-1} \mathbf{R}_l^{\hat{h}h} \mathbf{x}_{n-l}^{(\tilde{g})} + \sum_{l=0}^{L-1} \left[\hat{\mathbf{H}}_{eff,l}^{(\tilde{g})} \right]^H \boldsymbol{\eta}_{eff,n+l}^{(\tilde{g})} \quad (3.12)$$

Channel matched filter combines MPC's of the related group which are in different delays. However, off-diagonal entries of matrices $\mathbf{R}_l^{\hat{h}h}$ for $l = -(L-1), \dots, L-1$ create intra-group multi-user interference, and diagonal entries of $\mathbf{R}_l^{\hat{h}h}$ for $l \neq 0$ create ISI.

Assume that the intended group \tilde{g} has three users and three active MPCs on delays $l = 0, l = 1$ and $l = 2$ (e.g., $\mathcal{L}^{(\tilde{g})}(m) = m - 1$), and one RF chain is attained to each of them (e.g., $\mathbf{S}_m^{(\tilde{g})}$ for $m = 1, 2, 3$ are column vectors). Assume also that the MPC-specific analog beamformer $\mathbf{S}_m^{(\tilde{g})}$ completely rejects all the interference coming from other MPCs of the same user or group, in addition to rejecting inter-group interference. When the entry in m^{th} row and k^{th} column of $\mathbf{H}_{eff,l}^{(\tilde{g})} = [\mathbf{S}^{(\tilde{g})}]^H \mathbf{H}_l^{(\tilde{g})}$ is denoted as $h_{l,mk}$, which is equal to $[\mathbf{S}_m^{(\tilde{g})}]^H \mathbf{h}_l^{(\tilde{g}_k)}$, $h_{l,mk} = 0$ for $l \neq \mathcal{L}^{(\tilde{g})}(m)$. Resulting

effective channel matrices are shown below.

$$\mathbf{H}_{eff,0}^{(\tilde{g})} = \begin{bmatrix} h_{0,11} & h_{0,12} & h_{0,13} \\ 0 & 0 & 0 \\ 0 & 0 & 0 \end{bmatrix} \quad (3.13)$$

$$\mathbf{H}_{eff,1}^{(\tilde{g})} = \begin{bmatrix} 0 & 0 & 0 \\ h_{1,21} & h_{1,22} & h_{1,23} \\ 0 & 0 & 0 \end{bmatrix} \quad (3.14)$$

$$\mathbf{H}_{eff,2}^{(\tilde{g})} = \begin{bmatrix} 0 & 0 & 0 \\ 0 & 0 & 0 \\ h_{2,31} & h_{2,32} & h_{2,33} \end{bmatrix} \quad (3.15)$$

Then assume that the channel is perfectly estimated (e.g., $\hat{\mathbf{H}}_{eff,l}^{(\tilde{g})} = \mathbf{H}_{eff,l}^{(\tilde{g})}$). With this information, calculating the matrices $\mathbf{R}_l^{\hat{h}h}$ for $l = -(L-1), \dots, L-1$, it is seen that they are all zero for $l \neq 0$, since the nonzero rows do not coincide. Therefore, ISI can be mitigated using such an analog beamformer. In Figure 3.1, it is shown that generalized eigen-beamformer operates in a similar way, therefore it promises ISI mitigation effect, when used with channel matched filtering.

On the other hand, multi-user interference (MUI) still exists, considering off-diagonal entries of $\mathbf{R}_0^{\hat{h}h}$. The equation (3.12) can be approximately rewritten in high SNR as

$$\mathbf{r}_n^{(\tilde{g})} \cong \mathbf{R}_0^{\hat{h}h} \mathbf{x}_n^{(\tilde{g})} \quad (3.16)$$

Therefore, MUI can be cleared with an attempt having a nature of matrix inversion. Considering that the matrix $\mathbf{R}_0^{\hat{h}h}$ might not be invertible, a pseudo-inverse with a diagonal loading can be used.

3.2.2 Regularized Spatial Zero Forcing (SZF)

This filter is denoted as $\mathbf{Y}^{(\tilde{g})}$ and its output is

$$\mathbf{z}_n^{(\tilde{g})} \triangleq [\mathbf{Y}^{(\tilde{g})}]^H \mathbf{r}_n^{(\tilde{g})} \quad (3.17)$$

It aims to suppress the interference between users in the same group (i.e., multi-user interference, MUI) and given in (3.18).

$$\mathbf{Y}^{(\tilde{g})} \triangleq \mathbf{R}_0^{\hat{h}\hat{h}} \left(\left[\mathbf{R}_0^{\hat{h}\hat{h}} \right]^H \mathbf{R}_0^{\hat{h}\hat{h}} + N_0 \mathbf{I}_{K_g} \right)^{-1} \quad (3.18)$$

In (3.18), $\mathbf{R}_0^{\hat{h}\hat{h}}$ is the estimate of \mathbf{R}_0^{hh} and it is obtained as

$$\mathbf{R}_l^{\hat{h}\hat{h}} \triangleq \sum_{l_1=0}^{L-1} \left[\hat{\mathbf{H}}_{eff,l_1}^{(\tilde{g})} \right]^H \hat{\mathbf{H}}_{eff,l+l_1}^{(\tilde{g})}. \quad (3.19)$$

The whole digital beamformer with CMF and SZF can be written as

$$\mathbf{W}_l^{(\tilde{g})} \triangleq \hat{\mathbf{H}}_{eff,l}^{(\tilde{g})} \mathbf{Y}^{(\tilde{g})}, \quad (3.20)$$

which operates on the output of the analog beamformer $\mathbf{s}_n^{(\tilde{g})}$ as

$$\mathbf{z}_n^{(\tilde{g})} = \sum_{l=0}^{L-1} \left[\mathbf{W}_l^{(\tilde{g})} \right]^H \mathbf{s}_{n+l}^{(\tilde{g})}. \quad (3.21)$$

The regularized spatial zero forcing matrix $\mathbf{Y}^{(\tilde{g})}$ is of size $K_{\tilde{g}} \times K_{\tilde{g}}$. When a single user exists in a group (e.g., $K_{\tilde{g}} = 1$), it is a scalar. In this case, it might be omitted as a whole block and the assumption where $\mathbf{z}_n^{(\tilde{g})} = \mathbf{r}_n^{(\tilde{g})}$ can be made. This is because a scalar multiplier does not change output SINR (signal to interference-and-noise ratio), hence the performance. In this case, the digital beamformer is simply

$$\mathbf{W}_l^{(\tilde{g})} = \hat{\mathbf{H}}_{eff,l}^{(\tilde{g})}. \quad (3.22)$$

CHAPTER 4

SUBSPACE-AWARE CSI ACQUISITION TECHNIQUES

Instantaneous channel estimator in reduced domain, shown in Figure 3.6, estimates effective channel matrix $\mathbf{H}_{eff,l}^{(\tilde{g}_k)}$, hence effective channel vectors $\mathbf{h}_{eff,l}^{(\tilde{g}_k)}$. To do this, users in the same group is subjected to a training phase where they are transmitting a predetermined training sequence consisting of T symbols. This training period does not need to be synchronized among groups, and other groups might be in data mode. Due to the wideband transmission and the sparsity in the delay domain, delay spread is large. This can cause a need for longer observation length than the actual training length, meaning no data transmission for that period. However, this issue can be dealt with the usage of received data symbols for the estimation of the delayed multipaths. Therefore, this approach can be used for frequent estimations, while a longer and proper estimation period is realized less frequently. The considered training and data transmission scheme is illustrated in Figure 4.1; where P, T and D denotes preamble, training and data transmission, respectively.



Figure 4.1: Training and data transmission scheme

It will be beneficial to express the variables to estimate as a single vector. Therefore, a new group channel vector notation is defined as

$$\bar{\mathbf{h}}_{eff}^{(g)} \triangleq \left[\left[\bar{\mathbf{h}}_{eff}^{(g_1)} \right]^H \quad \left[\bar{\mathbf{h}}_{eff}^{(g_2)} \right]^H \quad \dots \quad \left[\bar{\mathbf{h}}_{eff}^{(g_{K_g})} \right]^H \right]^H, \quad (4.1)$$

where

$$\bar{\mathbf{h}}_{eff}^{(g_k)} \triangleq \left[\left[\mathbf{h}_{eff,0}^{(g_k)} \right]^H \quad \left[\mathbf{h}_{eff,1}^{(g_k)} \right]^H \quad \dots \quad \left[\mathbf{h}_{eff,L-1}^{(g_k)} \right]^H \right]^H. \quad (4.2)$$

Using $\bar{\mathbf{h}}_{eff}^{(g)}$ and obeying general system definitions given in (2.11) and (2.31), the observation after the analog beamformer (i.e., in reduced-dimension) throughout one training period of T (i.e., for n from 0 to $T - 1$) is expressed as

$$\bar{\mathbf{s}}^{(\tilde{g})} = \sum_{g=1}^G (\mathbf{X}^{(g)} \otimes \mathbf{I}_{D_{\tilde{g}}}) \bar{\mathbf{h}}_{eff}^{(g)} + \left(\mathbf{I}_T \otimes [\mathbf{S}^{(\tilde{g})}]^H \right) \bar{\mathbf{n}}, \quad (4.3)$$

where \otimes is the Kronecker product operator. The reduced-dimension observation vector $\bar{\mathbf{s}}^{(\tilde{g})}$ of size $TD_{\tilde{g}}$ and the noise vector $\bar{\mathbf{n}}$ of size TN are vertically concatenated forms of reduced-dimension observation vector $\mathbf{s}_n^{(\tilde{g})}$ and full-dimension noise term \mathbf{n}_n for n from 0 to $T - 1$, respectively. The matrix $\mathbf{X}^{(g)}$ involves training sequences $x_n^{(g_k)}$ as

$$\mathbf{X}^{(g)} \triangleq \left[\mathbf{X}^{(g_1)} \quad \mathbf{X}^{(g_2)} \quad \dots \quad \mathbf{X}^{(g_{K_g})} \right]_{T \times K_g L}, \quad (4.4)$$

where $(\mathbf{X}^{(g_k)})_{ij} \triangleq x_{i-j}^{(g_k)}$ for $i = 1, \dots, T$ and $j = 1, \dots, L$ as

$$\mathbf{X}^{(g_k)} = \begin{bmatrix} x_0^{(g_k)} & x_{-1}^{(g_k)} & \dots & x_{-(L-1)}^{(g_k)} \\ x_1^{(g_k)} & x_0^{(g_k)} & \dots & x_{-(L-2)}^{(g_k)} \\ \vdots & \vdots & \ddots & \vdots \\ x_{T-1}^{(g_k)} & x_{T-2}^{(g_k)} & \dots & x_{-(T-L)}^{(g_k)} \end{bmatrix} \quad (4.5)$$

As it is seen, there is a need for training symbols with negative time indices, corresponding to a period before the training starts. If there is a preamble cycle before training, symbols from the preamble; otherwise decoded data symbols from the previous data transmission period are employed for these positions.

In the training period, only the intended group \tilde{g} trains and other groups are in the data mode. Therefore, $\mathbf{X}^{(\tilde{g})}$ is a deterministic matrix while $\mathbf{X}^{(g)}$ for $g \neq \tilde{g}$ are random matrices obeying symbol properties described in (2.19).

Estimated effective channel is found by

$$\hat{\mathbf{h}}_{eff}^{(\tilde{g})} = \mathbf{Z}^{(\tilde{g})} \bar{\mathbf{s}}^{(\tilde{g})}, \quad (4.6)$$

where $\mathbf{Z}^{(\tilde{g})}$ is the estimator matrix for the intended group \tilde{g} and of size $K_{\tilde{g}}LD_{\tilde{g}} \times TD_{\tilde{g}}$. Then, the long vector $\hat{\mathbf{h}}_{eff}^{(\tilde{g})}$ is partitioned to get needed effective channel estimates $\hat{\mathbf{h}}_{eff,l}^{(\tilde{g}_k)}$ according to the structure given in (4.1) and (4.2). Proposed estimator types are described in following subsections.

4.1 Minimum Mean Square Error Estimator

The following is a reduced-rank MMSE type estimator which is designed after analog beamforming [32]. It is an approximated MMSE estimator since the CCMs in reduced-dimension are assumed to be perfectly acquired. It is given as

$$\mathbf{Z}^{(\tilde{g})} = \hat{\mathbf{C}}^{(\tilde{g})} \left(\hat{\mathbf{R}}_s^{(\tilde{g})} \right)^{-1}, \quad (4.7)$$

where $\hat{\mathbf{R}}_s^{(\tilde{g})}$ is the estimate for $\bar{\mathbf{R}}_s^{(\tilde{g})} \triangleq E \left\{ \bar{\mathbf{s}}^{(\tilde{g})} [\bar{\mathbf{s}}^{(\tilde{g})}]^H \right\}$ and $\hat{\mathbf{C}}^{(\tilde{g})}$ is the estimate for $\bar{\mathbf{C}}^{(\tilde{g})} \triangleq E \left\{ \bar{\mathbf{h}}_{eff}^{(\tilde{g})} [\bar{\mathbf{s}}^{(\tilde{g})}]^H \right\}$. $\bar{\mathbf{R}}_s^{(\tilde{g})}$ and $\bar{\mathbf{C}}^{(\tilde{g})}$ are given in (4.8) and (4.9), respectively.

$$\bar{\mathbf{R}}_s^{(\tilde{g})} = (\mathbf{X}^{(\tilde{g})} \otimes \mathbf{I}_{D_{\tilde{g}}}) \bar{\mathbf{R}}_{eff}^{(\tilde{g})} (\mathbf{X}^{(\tilde{g})} \otimes \mathbf{I}_{D_{\tilde{g}}})^H + \mathbf{I}_T \otimes \mathbf{R}_{eff,\eta}^{(\tilde{g})} \quad (4.8)$$

$$\bar{\mathbf{C}}^{(\tilde{g})} = \bar{\mathbf{R}}_{eff}^{(\tilde{g})} (\mathbf{X}^{(\tilde{g})} \otimes \mathbf{I}_{D_{\tilde{g}}})^H \quad (4.9)$$

$\bar{\mathbf{R}}_{eff}^{(\tilde{g})} \triangleq E \left\{ \bar{\mathbf{h}}_{eff}^{(\tilde{g})} [\bar{\mathbf{h}}_{eff}^{(\tilde{g})}]^H \right\}$ in (4.8) and (4.9) can be found substituting $g = \tilde{g}$ in following expression.

$$\bar{\mathbf{R}}_{eff}^{(g)} \triangleq \mathbf{I}_{K_g} \otimes \left(\sum_{l=0}^{L-1} \mathbf{E}_{L,l+1} \otimes \mathbf{R}_{eff,l}^{(g)} \right) \quad (4.10)$$

In (4.10),

$$\mathbf{E}_{L,l+1} \triangleq \mathbf{e}_{L,l+1} (\mathbf{e}_{L,l+1})^H, \quad (4.11)$$

where $\mathbf{e}_{L,l+1}$ is the column vector of size L whose $(l+1)^{\text{st}}$ element is 1 and others are all zero. $\hat{\mathbf{R}}_s^{(\tilde{g})}$ and $\hat{\mathbf{C}}^{(\tilde{g})}$ are obtained using $\hat{\mathbf{R}}_{eff,l}^{(\tilde{g})}$ and $\hat{\mathbf{R}}_{eff,\eta}^{(\tilde{g})}$ (which are described at the end of Section 2.3.2) instead of $\mathbf{R}_{eff,l}^{(\tilde{g})}$ and $\mathbf{R}_{eff,\eta}^{(\tilde{g})}$ in (4.8) and (4.10).

4.2 Conventional Least Square Estimator

Least square (LS) estimator is a conventional and very simple estimator [32]. As it is seen, it does not need effective CCMs and only operates with the information of training sequence.

$$\mathbf{Z}^{(\tilde{g})} = \text{pinv} \left(\mathbf{X}^{(\tilde{g})} \otimes \mathbf{I}_{D_{\tilde{g}}} \right) \quad (4.12)$$

4.3 Beamspace-Aware Least Square Estimator (BA-LS)

This is a special form of reduced-rank LS estimator which is aware of the beam separation among MPCs in (3.1). When RF chains are designed specific to a multipath, so that each of them rejects the other MPCs of the same group, the rows of the channel matrices become specific to a delay l . The rows that are not specific for that delay are expected to be almost zero, when GEB is used. A level of suppression can still be expected from the DFT beamformer. This phenomenon is illustrated in (3.13), (3.14) and (3.15). The fact that nonzero rows of the channel matrices are non-overlapping for different delays is taken into account by this estimator, which is given as

$$\mathbf{Z}^{(\tilde{g})} = \sum_{l=0}^{L-1} \left[\text{pinv} \left(\mathbf{X}^{(\tilde{g})} [\mathbf{I}_{K_{\tilde{g}}} \otimes \mathbf{E}_{L,l+1}] \right) \otimes \sum_{n \in \mathcal{D}_l^{(\tilde{g})}} \mathbf{E}_{D_{\tilde{g}},n} \right] \quad (4.13)$$

In (4.13), $\mathcal{D}_l^{(\tilde{g})}$ is the set of indices of columns of $\mathbf{S}^{(\tilde{g})}$ which belong to the MPC of the group \tilde{g} in the l^{th} delay; or, the set of indices of rows of the channel matrix $\mathbf{H}_{eff,l}^{(\tilde{g})}$ that are expected to be nonzero when GEB is used.

CHAPTER 5

PERFORMANCE ANALYSIS FOR THE PROPOSED ARCHITECTURE

5.1 Hybrid Beamforming Based Massive MIMO Performance in Terms of AIR for Several Intra-Group Multiplexing Techniques

In this section, signal-to-interference-and-noise ratio (SINR) expression will be derived for \tilde{k}^{th} user of \tilde{g}^{th} group. Then, the achievable information rate (AIR) will be introduced. The availability of a metric in terms of information rate enables the comparison with TDMA utilization. Therefore, there will be variations in the digital beamformer for intra-group multiplexing. The first case will use CMF and SZF as explained in Chapter 4. The second case will omit the SZF stage and use TDMA instead. In this case, time is divided between intra group users and there is one active user at a time, therefore SZF is a scalar multiplication and unnecessary. In the third case, the SZF stage will be omitted again, but TDMA will not be utilized and all the intra-group users will be actively transmitting.

5.1.1 CMF and SZF

SZF outputs the vector $\mathbf{z}_n^{(\tilde{g})}$, whose k^{th} entry $z_n^{(\tilde{g}_k)}$ belongs to the k^{th} user of the intended group \tilde{g} . For the intended user \tilde{k} , the output $z_n^{(\tilde{g}_k)}$ involves symbols from all users in all groups, and they are not only from the current time index. Therefore, the content of the signal can be categorized as intended signal, inter-symbol interference (ISI), multi-user interference (MUI), inter-group interference (IGI) and noise. Since the output signal will be decoded according to the estimated channel, the intended signal should be the part whose scaling is known to the demodulator. Therefore, the remaining part which cannot be used by the demodulator is named as self-interference

due to channel estimation error (SICEE). This term will be counted as interference also. Expressions of these terms are found in Appendix B for the CMF output $r_n^{(\tilde{g}_k)}$. Since SZF is a matrix multiplication, it is straightforward to convert it for the SZF output $z_n^{(\tilde{g}_k)}$. The terms are expressed as

$$\begin{aligned}
z_n^{(\tilde{g}_k)} &= \underbrace{\mathbf{e}^H [\mathbf{Y}^{(g)}]^H \mathbf{R}_0^{\hat{h}h} \mathbf{e} x_n^{(\tilde{g}_k)}}_{\text{Intended Signal (S)}} + \underbrace{\mathbf{e}^H [\mathbf{Y}^{(g)}]^H \mathbf{R}_0^{\hat{h}e} \mathbf{e} x_n^{(\tilde{g}_k)}}_{\text{Self-Interference due to Ch. Est. Error (SICEE)}} \\
&+ \underbrace{\sum_{\substack{l=-(L-1) \\ l \neq 0}}^{L-1} \mathbf{e}^H [\mathbf{Y}^{(g)}]^H \mathbf{R}_l^{\hat{h}h} \mathbf{e} x_{n-l}^{(\tilde{g}_k)}}_{\text{Inter-Symbol Int. (ISI)}} + \underbrace{\sum_{l=-(L-1)}^{L-1} \sum_{\substack{k'=1 \\ k' \neq k}}^K \mathbf{e}^H [\mathbf{Y}^{(g)}]^H \mathbf{R}_l^{\hat{h}h} \mathbf{e}_{K_{\tilde{g},k'}} x_{n-l}^{(\tilde{g}_{k'})}}}_{\text{Multi-User Int. (MUI)}} \\
&+ \underbrace{\sum_{l=0}^{L-1} \mathbf{e}^H [\mathbf{Y}^{(g)}]^H [\hat{\mathbf{H}}_{eff,l}^{(\tilde{g})}]^H [\mathbf{S}^{(\tilde{g})}]^H \boldsymbol{\xi}_{n+l}}_{\text{Inter-Group Int. (IGI)}} \\
&+ \underbrace{\sum_{l=0}^{L-1} \mathbf{e}^H [\mathbf{Y}^{(g)}]^H [\hat{\mathbf{H}}_{eff,l}^{(\tilde{g})}]^H [\mathbf{S}^{(\tilde{g})}]^H \mathbf{n}_{n+l}}_{\text{Noise}}
\end{aligned} \tag{5.1}$$

where $\mathbf{e} \triangleq \mathbf{e}_{K_{\tilde{g},\tilde{k}}}$ for simplicity. In addition,

$$\mathbf{R}_0^{\hat{h}e} \triangleq \mathbf{R}_0^{\hat{h}h} - \mathbf{R}_0^{\hat{h}\hat{h}}. \tag{5.2}$$

The only correlated pair is the Intended Signal (S) and SICEE term in (5.1). The power of the intended signal term $P_S^{(\tilde{g}_k)}$ and the power of total interference (SICEE + ISI + MUI + IGI) and noise term $P_{IN}^{(\tilde{g}_k)}$ are given in (5.3) and (5.4), respectively.

$$\begin{aligned}
P_S^{(\tilde{g}_k)} &= E \left\{ \left| \mathbf{e}^H [\mathbf{Y}^{(g)}]^H \mathbf{R}_0^{\hat{h}h} \mathbf{e} x_n^{(\tilde{g}_k)} \right|^2 \right\} \\
&= E_s^{(\tilde{g})} \sum_{l_1=0}^{L-1} \sum_{l_2=0}^{L-1} \mathbf{e}^H E \left\{ \left[[\mathbf{Y}^{(g)}]^H \hat{\mathbf{H}}_{eff,l_1}^{(\tilde{g})} \right]^H \hat{\mathbf{H}}_{eff,l_1}^{(\tilde{g})} \mathbf{E}_{K_{\tilde{g},\tilde{k}}} \left[\hat{\mathbf{H}}_{eff,l_2}^{(\tilde{g})} \right]^H \hat{\mathbf{H}}_{eff,l_2}^{(\tilde{g})} \mathbf{Y}^{(g)} \right\} \mathbf{e}
\end{aligned} \tag{5.3}$$

$$\begin{aligned}
P_{IN}^{(\tilde{g}_k)} &= \sum_{g'=1}^G E_s^{(g')} \sum_{l=-(L-1)}^{L-1} \sum_{l_1=0}^{L-1} \sum_{l_2=0}^{L-1} \mathbf{e}^H E \left\{ [\mathbf{Y}^{(g)}]^H [\hat{\mathbf{H}}_{eff,l_1}^{(\tilde{g})}]^H \mathbf{H}_{eff,l+l_1}^{(g')} \right. \\
&\quad \left. [\mathbf{H}_{eff,l+l_2}^{(g')}]^H \hat{\mathbf{H}}_{eff,l_2}^{(\tilde{g})} \mathbf{Y}^{(g)} \right\} \mathbf{e} \\
&+ P_S - 2E_s^{(\tilde{g})} Re \left\{ \sum_{l_1=0}^{L-1} \sum_{l_2=0}^{L-1} \mathbf{e}^H E \left\{ [\mathbf{Y}^{(g)}]^H [\hat{\mathbf{H}}_{eff,l_1}^{(\tilde{g})}]^H \mathbf{H}_{eff,l_1}^{(\tilde{g})} \right. \right. \\
&\quad \left. \left. \mathbf{E}_{K_{\tilde{g},\tilde{k}}} [\hat{\mathbf{H}}_{eff,l_2}^{(\tilde{g})}]^H \hat{\mathbf{H}}_{eff,l_2}^{(\tilde{g})} \mathbf{Y}^{(g)} \right\} \mathbf{e} \right\} \\
&+ N_0 \sum_{l_1=0}^{L-1} \mathbf{e}^H E \left\{ [\mathbf{Y}^{(g)}]^H [\hat{\mathbf{H}}_{eff,l_1}^{(\tilde{g})}]^H [\mathbf{S}^{(\tilde{g})}]^H \mathbf{S}^{(\tilde{g})} \hat{\mathbf{H}}_{eff,l_1}^{(\tilde{g})} \mathbf{Y}^{(g)} \right\} \mathbf{e}
\end{aligned} \tag{5.4}$$

$P_S^{(\tilde{g}_k)}$ and $P_{IN}^{(\tilde{g}_k)}$ are instantaneous powers of signal and interference-plus-noise terms, respectively. Then, their ratio is the instantaneous output SINR as shown below.

$$SINR^{(\tilde{g}_k)} = \frac{P_S^{(\tilde{g}_k)}}{P_{IN}^{(\tilde{g}_k)}} \tag{5.5}$$

For different realizations of instantaneous channel, different output SINR values are obtained. Then, they are averaged to obtain the achievable information rate (AIR) per user, through Monte Carlo method.

$$AIR^{(\tilde{g})} = \frac{1}{K_{\tilde{g}}} \sum_{k=1}^{K_{\tilde{g}}} E [\log_2(1 + SINR^{(\tilde{g}_k)})] . \tag{5.6}$$

5.1.2 CMF without TDMA

The output of CMF $r_n^{(\tilde{g}_k)}$ is expressed as the sum of its components in Appendix B. It is given as

$$\begin{aligned}
r_n^{(\tilde{g}_k)} &= \underbrace{\mathbf{e}^H \mathbf{R}_0^{\hat{h}\hat{h}} \mathbf{e} x_n^{(\tilde{g}_k)}}_{\text{Intended Signal (S)}} + \underbrace{\mathbf{e}^H \mathbf{R}_0^{\hat{h}e} \mathbf{e} x_n^{(\tilde{g}_k)}}_{\text{Self-Interference due to Ch. Est. Error (SICEE)}} \\
&+ \underbrace{\sum_{\substack{l=-(L-1) \\ l \neq 0}}^{L-1} \mathbf{e}^H \mathbf{R}_l^{\hat{h}h} \mathbf{e} x_{n-l}^{(\tilde{g}_k)}}_{\text{Inter-Symbol Int. (ISI)}} + \underbrace{\sum_{l=-(L-1)}^{L-1} \sum_{\substack{k'=1 \\ k' \neq k}}^K \mathbf{e}^H \mathbf{R}_l^{\hat{h}h} \mathbf{e}_{K_{\tilde{g},k'}} x_{n-l}^{(\tilde{g}_{k'})}}}_{\text{Multi-User Int. (MUI)}} \\
&+ \underbrace{\sum_{l=0}^{L-1} \mathbf{e}^H \left[\hat{\mathbf{H}}_{eff,l}^{(\tilde{g})} \right]^H \left[\mathbf{S}^{(\tilde{g})} \right]^H \boldsymbol{\xi}_{n+l}}_{\text{Inter-Group Int. (IGI)}} + \underbrace{\sum_{l=0}^{L-1} \mathbf{e}^H \left[\hat{\mathbf{H}}_{eff,l}^{(\tilde{g})} \right]^H \left[\mathbf{S}^{(\tilde{g})} \right]^H \mathbf{n}_{n+l}}_{\text{Noise}}
\end{aligned} \tag{5.7}$$

Then,

$$\begin{aligned}
P_S^{(\tilde{g}_k)} &= E \left\{ \left| \mathbf{e}^H \mathbf{R}_0^{\hat{h}\hat{h}} \mathbf{e} x_n^{(\tilde{g}_k)} \right|^2 \right\} \\
&= E_s^{(\tilde{g})} \sum_{l_1=0}^{L-1} \sum_{l_2=0}^{L-1} \mathbf{e}^H E \left\{ \left[\hat{\mathbf{H}}_{eff,l_1}^{(\tilde{g})} \right]^H \hat{\mathbf{H}}_{eff,l_1}^{(\tilde{g})} \mathbf{E}_{K_{\tilde{g},\tilde{k}}} \left[\hat{\mathbf{H}}_{eff,l_2}^{(\tilde{g})} \right]^H \hat{\mathbf{H}}_{eff,l_2}^{(\tilde{g})} \right\} \mathbf{e}
\end{aligned} \tag{5.8}$$

$$\begin{aligned}
P_{IN}^{(\tilde{g}_k)} &= \sum_{g'=1}^G E_s^{(g')} \sum_{l=-(L-1)}^{L-1} \sum_{l_1=0}^{L-1} \sum_{l_2=0}^{L-1} \mathbf{e}^H E \left\{ \left[\hat{\mathbf{H}}_{eff,l_1}^{(\tilde{g})} \right]^H \mathbf{H}_{eff,l+l_1}^{(g')} \right. \\
&\quad \left. \left[\mathbf{H}_{eff,l+l_2}^{(g')} \right]^H \hat{\mathbf{H}}_{eff,l_2}^{(\tilde{g})} \right\} \mathbf{e} \\
&+ P_S - 2E_s^{(\tilde{g})} Re \left\{ \sum_{l_1=0}^{L-1} \sum_{l_2=0}^{L-1} \mathbf{e}^H E \left\{ \left[\hat{\mathbf{H}}_{eff,l_1}^{(\tilde{g})} \right]^H \mathbf{H}_{eff,l_1}^{(\tilde{g})} \right. \right. \\
&\quad \left. \left. \mathbf{E}_{K_{\tilde{g},\tilde{k}}} \left[\hat{\mathbf{H}}_{eff,l_2}^{(\tilde{g})} \right]^H \hat{\mathbf{H}}_{eff,l_2}^{(\tilde{g})} \right\} \mathbf{e} \right\} \\
&+ N_0 \sum_{l_1=0}^{L-1} \mathbf{e}^H E \left\{ \left[\hat{\mathbf{H}}_{eff,l_1}^{(\tilde{g})} \right]^H \left[\mathbf{S}^{(\tilde{g})} \right]^H \mathbf{S}^{(\tilde{g})} \hat{\mathbf{H}}_{eff,l_1}^{(\tilde{g})} \right\} \mathbf{e}
\end{aligned} \tag{5.9}$$

$P_S^{(\tilde{g}_k)}$ and $P_{IN}^{(\tilde{g}_k)}$ are used to obtain SINR and AIR as shown in (5.5) and (5.6).

5.1.3 CMF with TDMA

For this case, the number of users in the intended group is simply assumed as one and the calculations are done as explained for CMF without TDMA to find $SINR^{(\tilde{g})}$.

Then, the achievable information rate for TDMA is calculated as

$$AIR^{(\tilde{g}),\text{TDMA}} = \frac{1}{K_{\tilde{g}}} \log_2(1 + SINR^{(\tilde{g})}). \quad (5.10)$$

5.1.4 Analytical Expressions for Signal Powers at the Output of CMF

Analytical expressions for signal powers can be provided for the output of the CMF. It is due to the fact that channels are assumed to be circularly symmetric complex normal random vectors. Therefore, the output is only a sum of products of normally distributed random variables. To derive analytical solutions, some definitions should be made. Firstly,

$$E \left\{ \bar{\mathbf{h}}_{eff}^{(g)} \left[\bar{\mathbf{h}}_{eff}^{(g')} \right]^H \right\} = \delta_{gg'} \bar{\mathbf{R}}_{eff}^{(g)}, \quad (5.11)$$

where $\bar{\mathbf{R}}_{eff}^{(g)}$ is given in (4.10).

$\Phi \triangleq E \left\{ \hat{\mathbf{h}}_{eff}^{(\tilde{g})} \left[\hat{\mathbf{h}}_{eff}^{(\tilde{g})} \right]^H \right\}$ and $\Psi^{(g)} \triangleq E \left\{ \hat{\mathbf{h}}_{eff}^{(\tilde{g})} \left[\bar{\mathbf{h}}_{eff}^{(g)} \right]^H \right\}$ found to be as in (5.12) and (5.13), respectively; using (4.3), (4.6) and (5.11).

$$\Phi = \mathbf{Z}^{(\tilde{g})} \bar{\mathbf{R}}_s^{(\tilde{g})} \left[\mathbf{Z}^{(\tilde{g})} \right]^H \quad (5.12)$$

$$\Psi^{(g)} = \delta_{g\tilde{g}} \mathbf{Z}^{(\tilde{g})} \left(\mathbf{X}^{(g)} \otimes \mathbf{I}_{D_{\tilde{g}}} \right) \bar{\mathbf{R}}_{eff}^{(g)} \quad (5.13)$$

The matrices $\Phi_{l,l'} \triangleq E \left\{ \hat{\mathbf{h}}_{eff,l}^{(\tilde{g}_k)} \left[\hat{\mathbf{h}}_{eff,l'}^{(\tilde{g}_k)} \right]^H \right\}$ and $\Psi_{l,l'}^{(g_k)} \triangleq E \left\{ \hat{\mathbf{h}}_{eff,l}^{(\tilde{g}_k)} \left[\bar{\mathbf{h}}_{eff,l'}^{(g_k)} \right]^H \right\}$ are blocks residing somewhere in Φ and $\Psi^{(g)}$. They are retrieved from those large matrices as indicated with MATLAB notation below.

$$\Phi_{l,l'} = (\Phi)_{(x_{\tilde{k},l}:y_{\tilde{k},l}; x_{\tilde{k},l'}:y_{\tilde{k},l'})} \quad (5.14)$$

$$\Psi_{l,l'}^{(g_k)} = (\Psi^{(g)})_{(x_{\tilde{k},l}:y_{\tilde{k},l}; x_{k,l'}:y_{k,l'})} \quad (5.15)$$

In (5.14) and (5.15),

$$x_{k,l} \triangleq [(k-1)L + l]D_{\tilde{g}} + 1 \quad (5.16)$$

$$y_{k,l} \triangleq [(k-1)L + l]D_{\tilde{g}} + D_{\tilde{g}} \quad (5.17)$$

Finally,

$$\Phi_{sum} \triangleq \sum_{l=0}^{L-1} \Phi_{l,l} \quad (5.18)$$

and

$$\Psi_{sum}^{(g_k)} \triangleq \sum_{l=0}^{L-1} \Psi_{l,l}^{(g_k)}. \quad (5.19)$$

After these definitions, analytical expressions for $P_S^{(\tilde{g}_k),\text{CMF}}$ and $P_{IN}^{(\tilde{g}_k),\text{CMF}}$ are given in (5.20) and (5.21), respectively. The full derivation can be found in Appendix B.

$$P_S^{(\tilde{g}_k),\text{CMF}} = E_s^{(\tilde{g})} \left[|tr(\Phi_{sum})|^2 + \sum_{l_1=0}^{L-1} \sum_{l_2=0}^{L-1} tr(\Phi_{l_2,l_1} \Phi_{l_1,l_2}) \right] \quad (5.20)$$

$$\begin{aligned} P_{IN}^{(\tilde{g}_k),\text{CMF}} = & \sum_{g'=1}^G E_s^{(g')} \left[\sum_{k'=1}^{K_{g'}} \sum_{l=-(L-1)}^{L-1} \left| \sum_{l_1=0}^{L-1} tr(\Psi_{l_1,l+l_1}^{(g'_{k'})}) \right|^2 + \right. \\ & \left. K_{g'} tr \left(\Phi_{sum} \sum_{l=0}^L \mathbf{R}_{eff,l}^{(g')} \right) \right] \\ & + E_s^{(\tilde{g})} \left[|tr(\Phi_{sum})|^2 + \sum_{l_1=0}^{L-1} \sum_{l_2=0}^{L-1} tr(\Phi_{l_2,l_1} \Phi_{l_1,l_2}) \right] \quad (5.21) \\ & - 2E_s^{(\tilde{g})} Re \left\{ tr(\Psi_{sum}^{(\tilde{g}_k)})^* tr(\Phi_{sum}) \right. \\ & \left. + \sum_{l_1=0}^{L-1} \sum_{l_2=0}^{L-1} tr \left(\Phi_{l_2,l_1} \left[\Psi_{l_2,l_1}^{(\tilde{g}_k)} \right]^H \right) \right\} \\ & + N_0 tr \left(\Phi_{sum} [\mathbf{S}^{(\tilde{g})}]^H \mathbf{S}^{(\tilde{g})} \right) \end{aligned}$$

5.1.5 Analytically Calculated Approximation for Achievable Information Rate

When there is a single user in a group and SZF is not used (the last processing block is CMF), it is found that an approximation for AIR expression can be used as shown

below.

$$AIR^{(\hat{g})} = \frac{1}{K_{\hat{g}}} \sum_{k=1}^{K_{\hat{g}}} E \left[\log_2 \left(1 + \frac{P_S^{(\hat{g}_k)}}{P_{IN}^{(\hat{g}_k)}} \right) \right] \cong \frac{1}{K_{\hat{g}}} \sum_{k=1}^{K_{\hat{g}}} \log_2 \left(1 + \frac{E \left[P_S^{(\hat{g}_k)} \right]}{E \left[P_{IN}^{(\hat{g}_k)} \right]} \right). \quad (5.22)$$

The expectations of powers were expressed analytically in (5.20) and (5.21). They are substituted as shown below.

$$AIR^{(\hat{g})} \cong \frac{1}{K_{\hat{g}}} \sum_{k=1}^{K_{\hat{g}}} \log_2 \left(1 + \frac{P_S^{(\hat{g}_k), \text{CMF}}}{P_{IN}^{(\hat{g}_k), \text{CMF}}} \right). \quad (5.23)$$

Analytically calculated approximation for AIR and AIR obtained through Monte Carlo method are compared in Figure (5.1) for the group 1 in the scenario tabulated in Table 5.1.

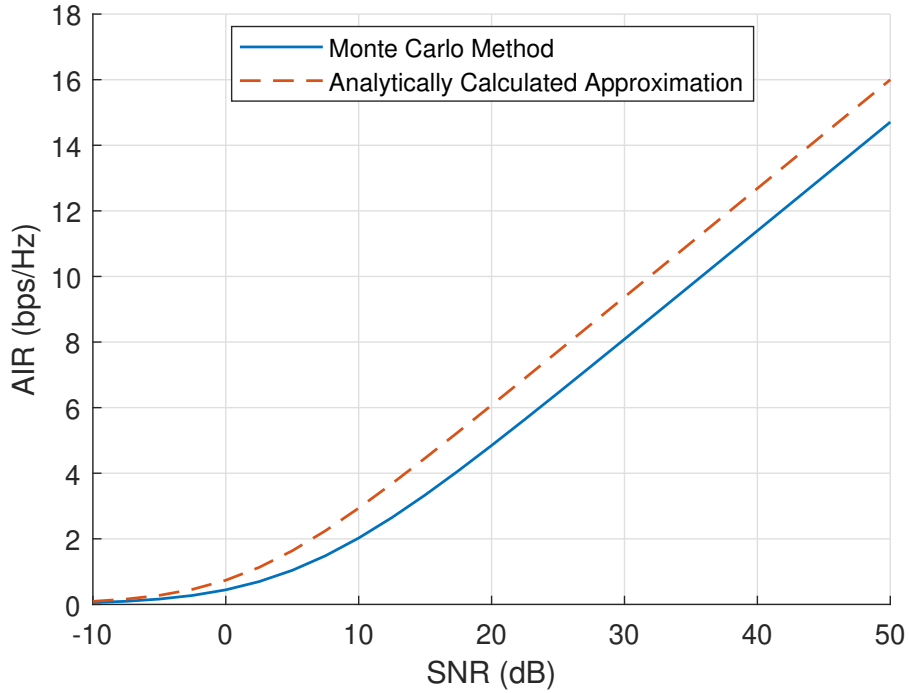


Figure 5.1: Comparison of analytically calculated approximation for AIR and AIR obtained through Monte Carlo method. (Group 1, GEB, CMF, perfect instantaneous channel estimation, perfect angular estimation)

This approximation is used in Figures from 5.6 to 5.11.

5.2 Sensitivity to Estimation Error for Long-Term Channel Parameters

Angular estimations are made by a block called *Joint Angle-Delay Sparsity Map And Power Profile*. This block produces estimates $\hat{\mu}_{\phi,l}^{(g)}$, $\hat{\sigma}_{\phi,l}^{(g)}$ and $\hat{\rho}_{\phi,l}^{(g)}(\phi)$, which are mean AoA, angular spread and power profile, respectively. This thesis does not offer a design method for this block and assumes that the estimates are given. Since the performance of the offered system is dependent on the accuracy of these estimates, the sensitivity to these estimates are assessed with given errors. These errors are

$$e_{\mu} = \hat{\mu}_{\phi,l}^{(g)} - \mu_{\phi,l}^{(g)} \quad (5.24)$$

and

$$e_{\sigma} = \hat{\sigma}_{\phi,l}^{(g)} - \sigma_{\phi,l}^{(g)} \quad (5.25)$$

The analog beamformer is constructed using $\hat{\mu}_{\phi,l}^{(g)}$ and $\hat{\sigma}_{\phi,l}^{(g)}$. Furthermore, in the construction of any processing stage, the CCMs which are calculated according to these estimates (such as $\hat{\mathbf{R}}_l^{(g)}$ or $\hat{\mathbf{R}}_y$) are used, if any needed. The response of the system to these errors will give an opinion about the needed accuracy level that might be expected from such an estimator.

5.3 Numerical Results

In this section, a number of simulation results will be given. Simulations are realized for a certain scenario. In this scenario, BS has $N = 100$ antenna elements. $G = 4$ groups exist where the first group has 3 MPCs and the others have 2 MPCs for each. Signal powers of groups are uniformly distributed among their MPCs. Groups 1, 2, 3 and 4 have 1, 2, 3 and 4 users and their signal powers are 1, 10, 100 and 1000, respectively. The total number of RF chains for a group is taken as the minimum of the number of MPCs and the number of users of that group. All the details are tabulated in Table 5.1. The sparsity map given in Figure 2.2 shows the placement in the angle-delay plane for this scenario. For each MPC, the power profile $\rho_{\phi,l}^{(g)}(\phi)$ is taken uniform in the indicated angular area and zero elsewhere. In some figures, a CMF bound is given for which fully digital beamformer is used by omitting the analog beamformer (e.g., $\mathbf{S}^{(g)} = \mathbf{I}_N$ and $D_g = N$), and SINR is calculated by taking

all the interference terms as zero, except the noise term. For instantaneous channel estimators, rows of Hadamard matrices are used as training sequences. Optimization of training sequences is out of scope of this thesis.

In Figure 5.2, GEB is used as the analog beamformer. Then, different schemes are used in the digital beamformer. These schemes are usage of regularized spatial zero forcing filter (SZF) after CMF, usage of TDMA method instead of SZF after CMF and usage of CMF alone. There are four graphs for four groups. The graph (a) is for the first group, which has a single user. In addition, it is a group that suffers from a great near-far effect. It has the minimum signal power in the scenario. The methods have equal performances as expected. The difference from the bound can be explained as the result of the inter-group interference. The rejection abilities of the GEB is successful enough for overall performance to follow the bound with a small difference, considering that the inter-group interference is huge for this group. In addition, as SNR increases, ISI would have caused a saturation in the performance, because it is an interference term in the denominator of the SINR that grows with the signal power that is the numerator of the SINR. Since there is no saturation, it is concluded that ISI is almost completely removed by the GEB analog beamformer. In the graphs (b), (c) and (d), it is seen that the performance generally drops for all methods, as the number of intra-group users increases. CMF without TDMA case saturates due to the multi-user interference. CMF with TDMA does not saturate, since it has one active user at a time and ISI is removed by the GEB, as in the first group. However, it suffers from a decrease in AIR due to the division of time between users. SZF usage after CMF outperforms other techniques at high SNR for intra-

Table 5.1: Angular sectors of multipath components

Group Index (g)	Center Angle (μ_ϕ)	Angular Spread (σ_ϕ)	Delay ($\mathcal{L}^{(g)}[m]$)	MPC Power Distribution	RF Chain ($d_m^{(g)}$)	Number of Users (K_g)	Signal Power ($E_s^{(g)}$)
1	(0°, 9.75°, 22°)	(3°, 2.5°, 3.5°)	(0, 5, 11)	(1/3, 1/3, 1/3)	(1, 1, 1)	1	1
2	(27.5°, 15.25°)	(3°, 2°)	(3, 9)	(1/2, 1/2)	(1, 1)	2	10
3	(-6.25°, -13.5°)	(3.5°, 3°)	(8, 17)	(1/2, 1/2)	(2, 1)	3	100
4	(-20.25°, -27°)	(3°, 3.5°)	(20, 29)	(1/2, 1/2)	(2, 2)	4	1000

group multiplexing, for groups 2 and 3. In this method, time or frequency is not divided, but the users are separated in the spatial dimension.

Figure 5.3 is similar to the Figure 5.2, but DFT beamformer is used in this case. It is seen that the performance is very limited compared to the GEB. The general performance increases from the first group to the fourth group, which shows the sensitivity of the DFT beamformer to the inter-group interference. In the graph (d), the CMF with TDMA case saturates although it belongs to the group that has the maximum signal power and minimum inter-group interference. Since there is only one active user, it shows the effect of ISI. Therefore, the ISI mitigation effect that is seen for the GEB is not present for the DFT beamformer.

Instantaneous channel estimation methods are compared in Figure 5.4 which is in the case of GEB usage. It is seen that the MMSE and BA-LS estimators are very successful. Conventional LS estimator performs similarly for groups 1 and 2 but its performance decreases for groups 3 and 4, when the same training length ($T = 4$) is applied for all groups.

In Figure 5.5, the effect of the training length is assessed when GEB is used. It is seen that MMSE and BA-LS can perform successfully even with very small training lengths, varying between 1 and 4 training symbols according to groups. In addition, critical training lengths are seen in the graphs. Before these critical values, estimators does not operate properly. After these values, performances of estimators converge slowly to the perfect knowledge case. These critical values are comparable with the number of intra-group users (1, 2, 3, 4 for groups 1, 2, 3, 4) for MMSE and BA-LS estimators, and they are comparable with the product of number of intra-group users and number of MPCs (3, 4, 6, 8 for groups 1, 2, 3, 4) for conventional LS estimator. It is also notable that for these critical values, performances of estimators are closest to the perfect channel estimation case for the group 4, and they decrease from that gradually as observed from group 3 to group 1. This is caused by near-far effect, or power of inter-group interference, which is most severe for the group 1.

In the next figures, the power levels will not be as shown in the Table 5.1, but will be specified for each figure. Figure 5.6 shows the dependency of the performance on the number of RF chains. RF chains are distributed to three MPCs of the first group

uniformly as far as possible. It is plotted for the group 1 where all the groups have same power levels. It is seen from this figure that after 12 RF chains, there is almost no performance increase as the number of RF chains increases.

In Figure 5.7, performances of GEB and DFT beamformer against near-far effect, or inter-group interference, are compared. All the inter groups are taken to have equal power levels, while the signal power of the intended group is changed along the x-axis, in order to achieve signal to interference ratio (SIR) indicated on the axis. It is seen in this figure that GEB is robust but DFT beamformer is very sensitive to the near-far effect.

The effect of the number of antennas is investigated in Figures 5.8 and 5.9. The traces of the CCMs are kept the same, so they show the diversity gain rather than array gain. When the number of RF chains remains the same, it is seen that GEB allows some decrease in the number of antennas, while performance decreases very sharply for number of antennas around 20, for both beamformers. When the number of antennas increases, the performance decreases. It is because the correspondent beamwidth per dimension gets narrower and cannot cover the spreads of the MPCs. When the number of RF chains are proportionally increased with the number of antennas in Figure 5.9, it is seen that the performance does not decrease, but it does not increase either. It is because the spatial diversity in the channel is limited.

Needed accuracy levels for CCMs are questioned in Figures 5.10 and 5.11. It is seen that performance immediately decreases with bias but there is a horizontal pattern for spread error in a wide range. Performances decrease below 2 bps/Hz with a 3° bias, which is around the average angular spread in the scenario. It is seen that bias in the angular estimation is more harmful than error in the angular spread estimate. It can be concluded from these figures that a design for joint angle-delay power profile estimator should primarily aim unbiased angular estimates while angular spread errors can be tolerated. It can also be interpreted as the accuracy of the angular spread in the design of the analog beamformer is not vital.

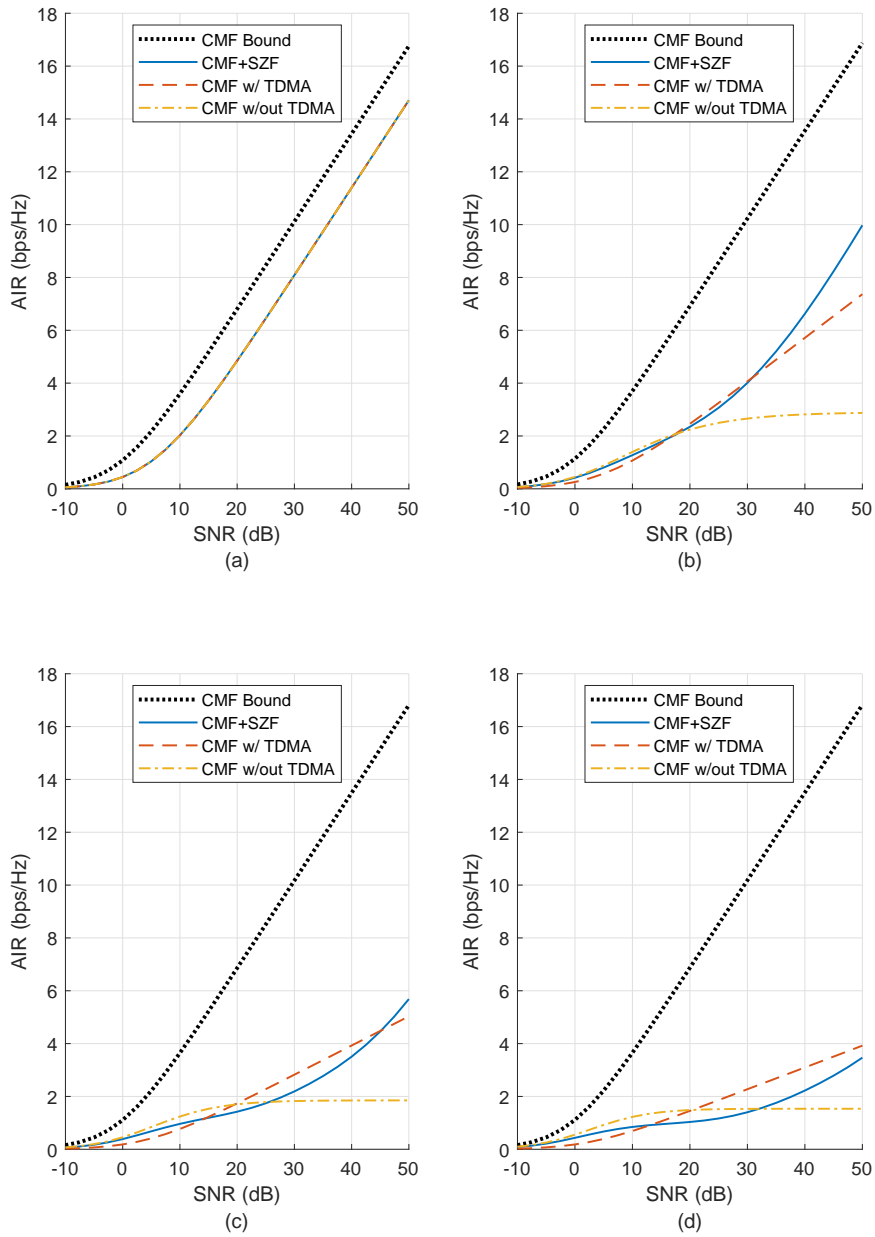


Figure 5.2: Performance of GEB and comparison of intra-group multiplexing techniques. (a) Group 1. (b) Group 2. (c) Group 3. (d) Group 4. (Perfect instantaneous channel estimation, perfect angular estimation)

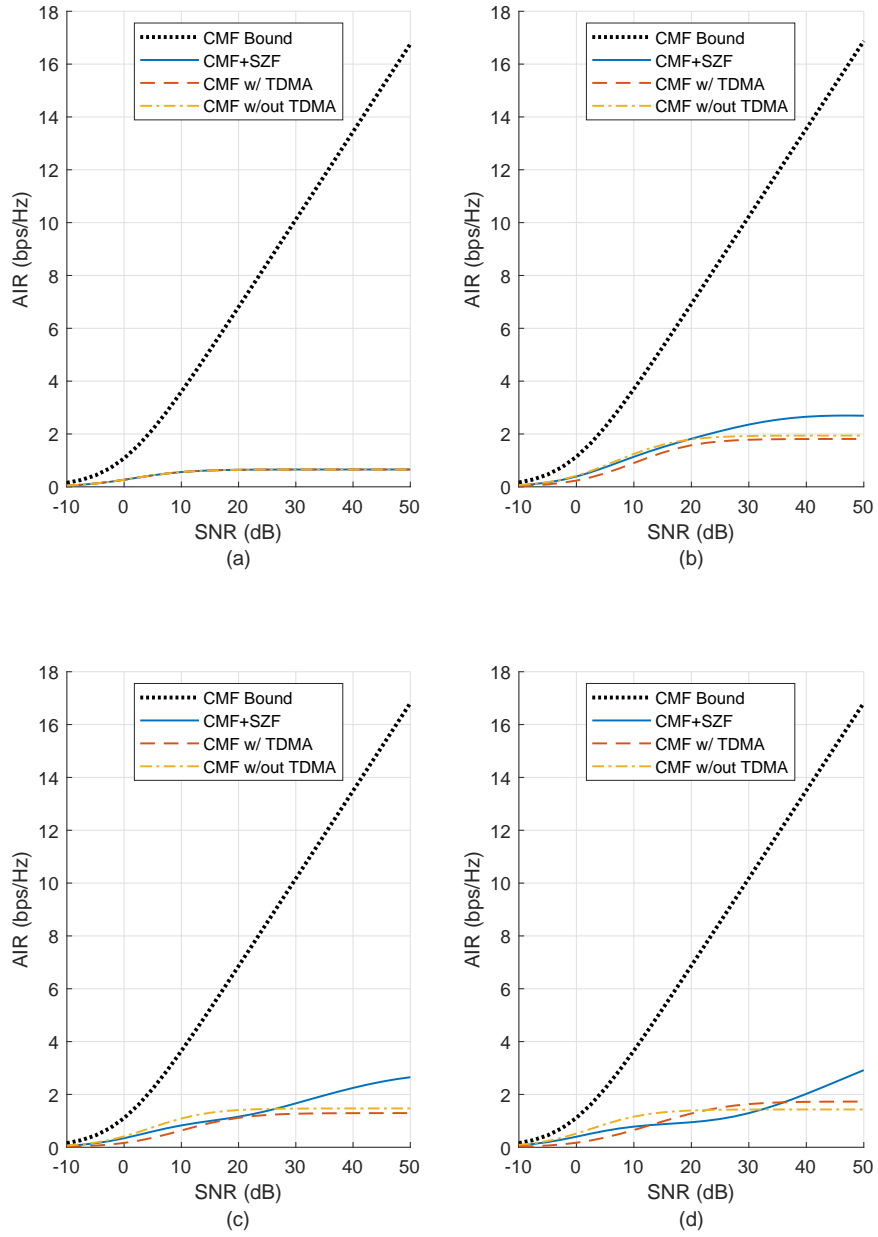


Figure 5.3: Performance of DFT beamformer and comparison of intra-group multiplexing techniques. (a) Group 1. (b) Group 2. (c) Group 3. (d) Group 4. (Perfect instantaneous channel estimation, perfect angular estimation)

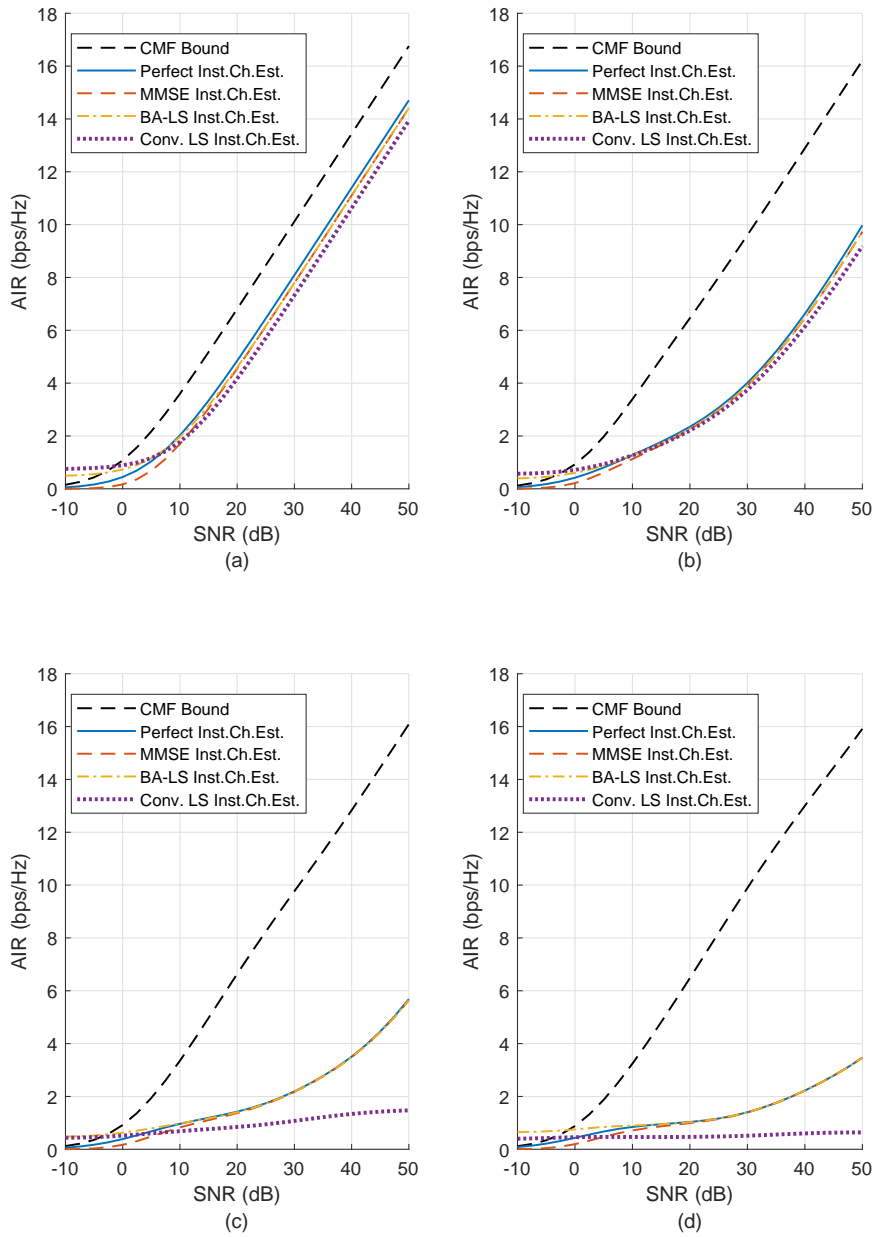


Figure 5.4: Comparison of instantaneous channel estimation techniques when GEB is used. (a) Group 1. (b) Group 2. (c) Group 3. (d) Group 4. (CMF with SZF, training length $T = 4$, perfect angular estimation)

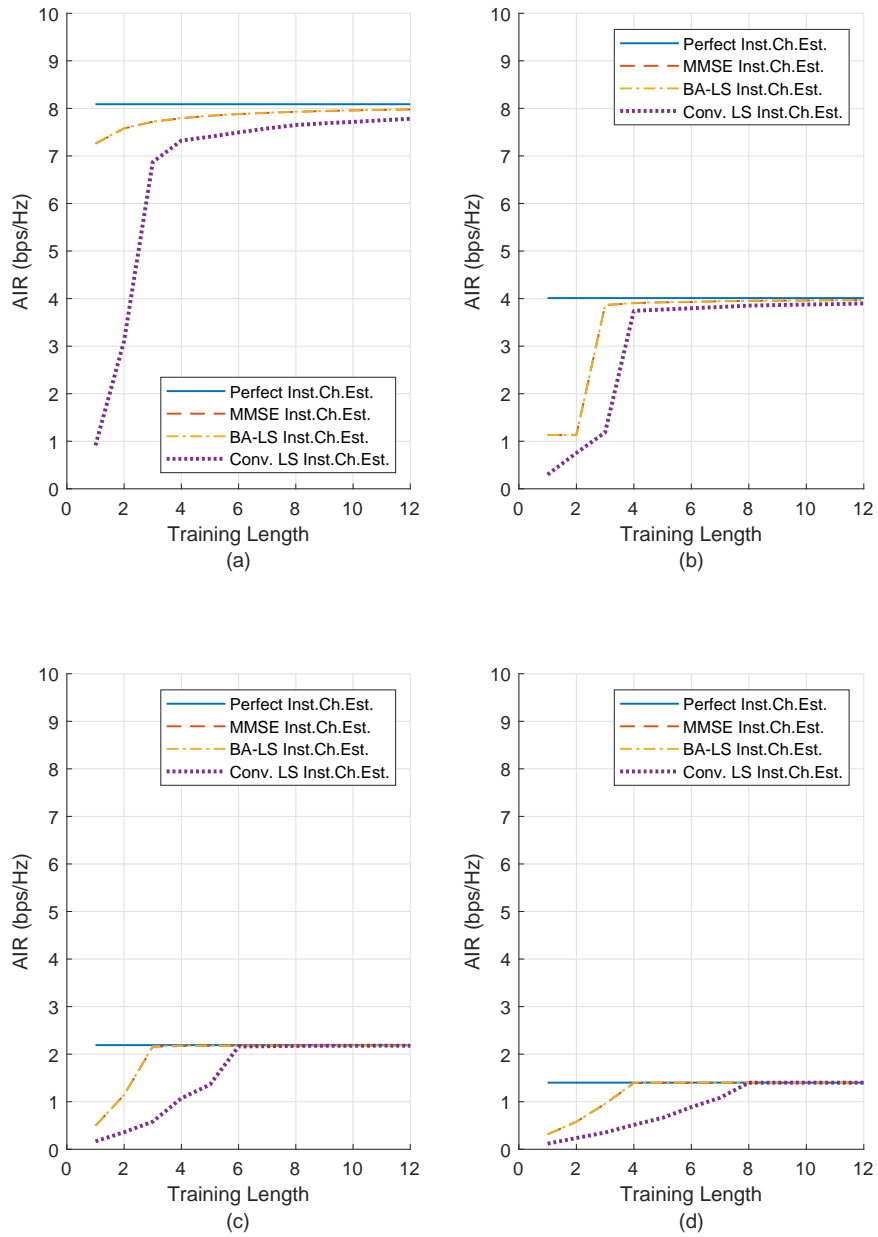


Figure 5.5: Performances of instantaneous channel estimation techniques versus training length when GEB is used. (a) Group 1. (b) Group 2. (c) Group 3. (d) Group 4. (CMF with SZF, 30 dB SNR, perfect angular estimation)

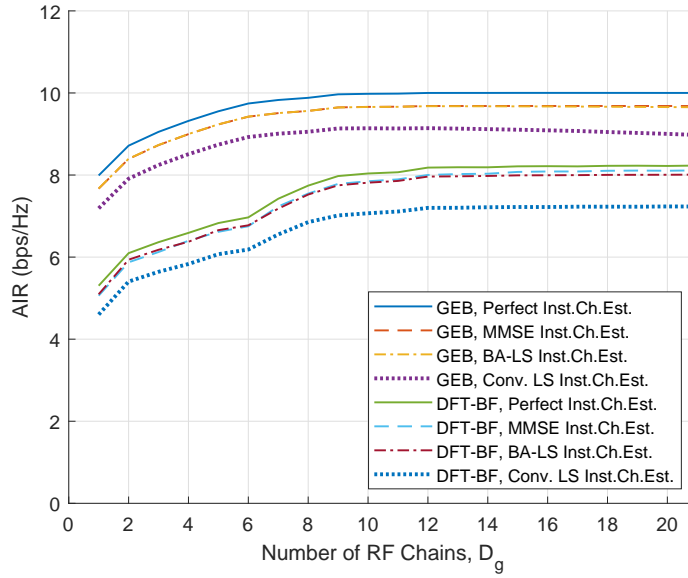


Figure 5.6: Performance of GEB and DFT-BF against number of RF chains D_g for the group 1. All the groups have equal signal powers. (30 dB SNR, CMF, training length $T = 4$, perfect angular estimation)

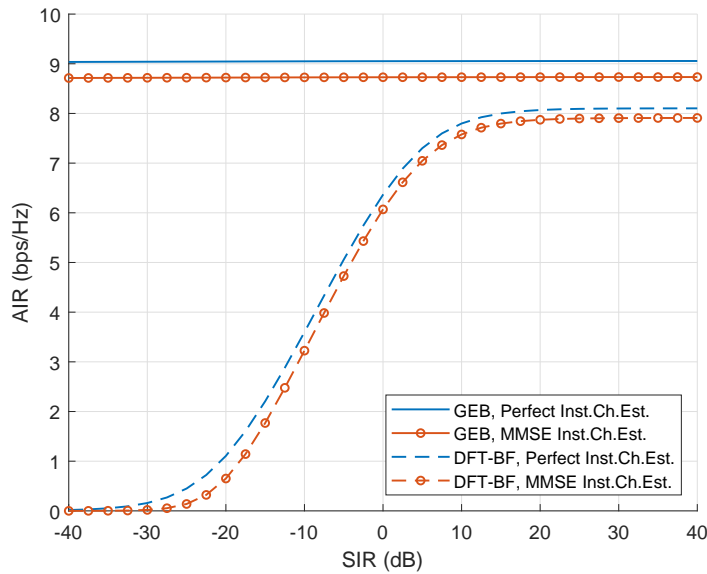


Figure 5.7: Performance of GEB and DFT-BF against near-far effect for the group 1. All inter-groups have equal signal powers, signal power of the intended group depends on SIR. (30 dB SNR, CMF, training length $T = 4$, perfect angular estimation)

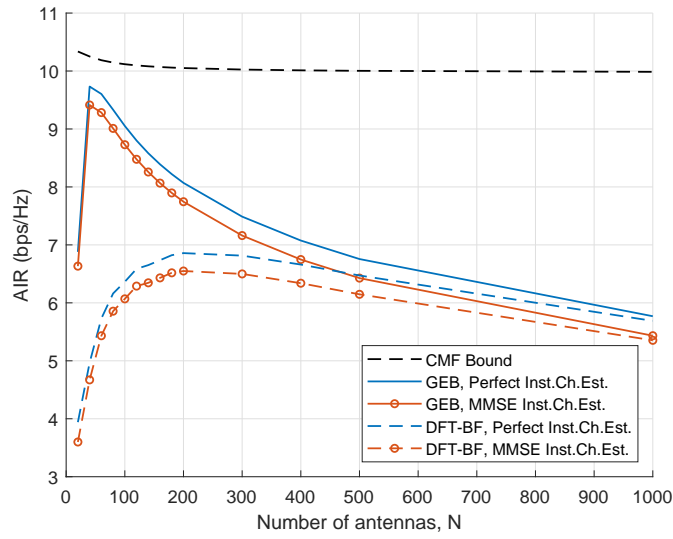


Figure 5.8: Performance of GEB and DFT-BF against number of antennas for the group 1. All the groups have equal signal powers. Number of RF chains is 3 and remains the same. (30 dB SNR, CMF, training length $T = 4$, perfect angular estimation)

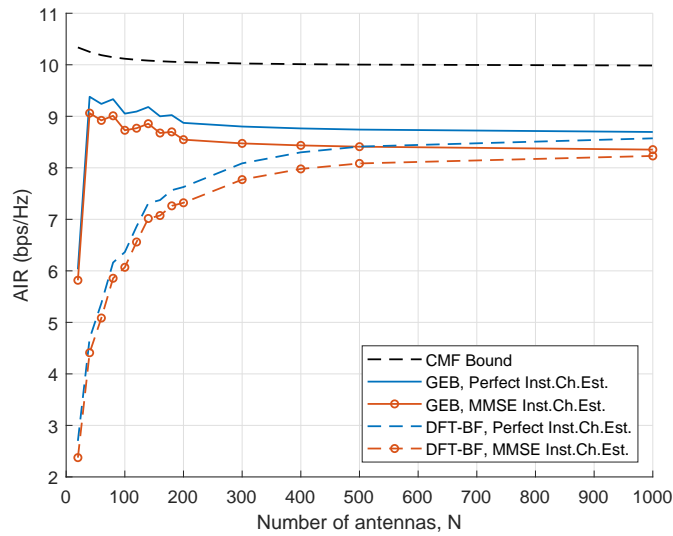


Figure 5.9: Performance of GEB and DFT-BF against number of antennas for the group 1. All the groups have equal signal powers. Number of RF chains is proportional to the number of antennas with ratio 3/100, ceiled if needed. (30 dB SNR, CMF, training length $T = 4$, perfect angular estimation)

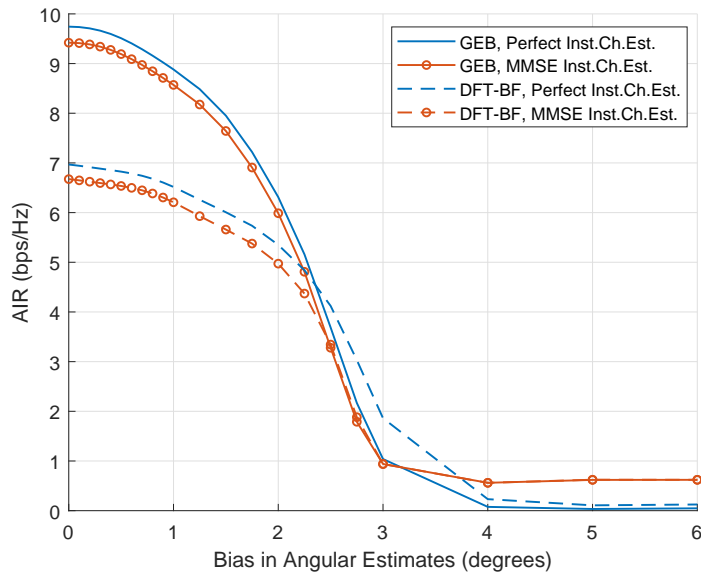


Figure 5.10: Performance against bias in angular estimation for the group 1. All the groups have equal signal powers. (30 dB SNR, 6 RF Chains, CMF, training length $T = 4$, no error in the estimate of angular spread)

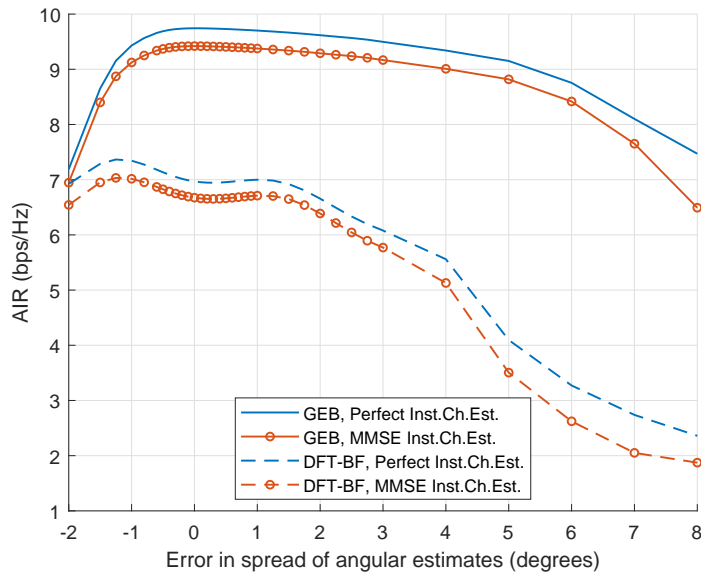


Figure 5.11: Performance against error in angular spread for the group 1. All the groups have equal signal powers. (30 dB SNR, 6 RF Chains, CMF, training length $T = 4$, unbiased angular estimates)

CHAPTER 6

ADAPTIVE CONSTRUCTION OF ANALOG BEAMFORMER

6.1 Slow-Time Adaptation

Long-term channel statistics, based on which analog beamformer is designed, is almost equivalent to the angular properties of the channel and angular positions of users. When users are mobile, analog beamformer needs to be updated. Digital beamformer also needs updates, even in a static channel. However, it is expected that the update need of the analog beamformer will not be as frequent as the digital beamformer. Therefore, slow-time and fast-time concepts, which are encountered in various signal processing areas, can be used to express the update interval of analog and digital beamformers, respectively. While the former is comparable with the length of data packages, the latter is comparable with symbol duration.

Digital beamformer and instantaneous channel estimator are placed after analog beamformer and operate in reduced-dimension, group-specific subspaces. Matrix inversions in the channel estimation procedure are done with small-size matrices. It is seen in the previous chapter that satisfying performance levels for instantaneous channel estimation can be achieved even with very small training lengths. In addition, digital beamforming is performed with digital circuitry, so updates can be applied easily. Therefore, mobility of users is not seen as a major problem for digital beamformer.

Generalized eigen-beamformer seems to be very successful design for the analog beamformer stage thanks to its interference rejection abilities; which enable ISI-free samples when properly used, robustness against near-far effect and a shorter training length for instantaneous channel estimation. Since generalized eigendecomposition of large matrices is needed in order to construct (or update) the GEB, it might be

computationally very complex, even if it is done in slow-time. In this chapter, channel mobility and adaptive construction of analog beamformer will be addressed.

6.2 Mobile Channel Model

Channel mobility is modeled as a change in center angle of each MPC $\mu_{\phi,l}^{(g)}$ with time, while angular spread $\sigma_{\phi,l}^{(g)}$ is kept constant. The center angle in the n^{th} time instance is

$$\mu_{\phi,l}^{(g)}[n] = \mu_{\phi,l}^{(g)}[0] + \Delta\mu_{\phi,l}^{(g)}[n], \quad (6.1)$$

where the mobility addend $\Delta\mu_{\phi,l}^{(g)}[n]$ is a stochastic process obtained by autoregressive first order (AR(1)) Markov process, shown as

$$\Delta\mu_{\phi,l}^{(g)}[n] = \alpha\Delta\mu_{\phi,l}^{(g)}[n-1] + \sqrt{1-\alpha^2}v[n] \text{ for } n = 1, 2, \dots \quad (6.2)$$

where $\Delta\mu_{\phi,l}^{(g)}[0] = 0$ and $0 < \alpha < 1$. In addition, $v[n] \sim \mathcal{N}(0, \sigma_v^2)$ and i.i.d. for different n .

Accordingly, the mobility term can also be written as

$$\Delta\mu_{\phi,l}^{(g)}[n] = \sqrt{1-\alpha^2}\alpha^n \sum_{k=1}^n \alpha^{-k}v[k] \text{ for } n = 1, 2, \dots \quad (6.3)$$

from which mean and variance of the elements can be written, according to the properties of $v[n]$, as

$$E \left[\Delta\mu_{\phi,l}^{(g)}[n] \right] = 0 \text{ for } n = 0, 1, 2, \dots, \quad (6.4)$$

$$\text{var} \left(\Delta\mu_{\phi,l}^{(g)}[n] \right) = (1 - \alpha^{2n}) \sigma_v^2 \text{ for } n = 1, 2, \dots \quad (6.5)$$

Therefore,

$$E \left[\mu_{\phi,l}^{(g)}[n] \right] = \mu_{\phi,l}^{(g)}[0] \text{ for } n = 0, 1, 2, \dots, \quad (6.6)$$

$$\text{var} \left(\mu_{\phi,l}^{(g)}[n] \right) = (1 - \alpha^{2n}) \sigma_v^2 \text{ for } n = 0, 1, 2, \dots \quad (6.7)$$

The autocorrelation function is

$$E \left[\Delta\mu_{\phi,l}^{(g)}[n_1] \left(\Delta\mu_{\phi,l}^{(g)}[n_2] \right)^* \right] = (1 - \alpha^{2n_1}) \alpha^{n_2 - n_1} \sigma_v^2 \text{ for } 0 < n_1 < n_2. \quad (6.8)$$

Accordingly, the AoA estimation $\hat{\mu}_{\phi,l}^{(g)}[n]$ is modeled as

$$\hat{\mu}_{\phi,l}^{(g)}[n] = \mu_{\phi,l}^{(g)}[n] + e[n] \quad (6.9)$$

where $e[n]$ is normally distributed, zero-mean and i.i.d. error term whose variance is σ_{est}^2 .

For each time instance n , variables will be denoted as $x[n]$, $\mathbf{x}[n]$ or $\mathbf{X}[n]$ such as $\hat{\mu}_{\phi,l}^{(g)}[n]$, $\hat{\mathbf{u}}_l^{(g)}[n]$ and $\mathbf{R}_y[n]$. Only exception will be $\rho_\theta(\theta, n)$ and $\rho_\phi(\phi, n)$.

6.3 Recursive Filtering of Matrices and Vectors

The analog beamformer is reconstructed according to $\hat{\mu}_{\phi,l}^{(g)}[n]$ for every n . Erroneous estimates can cause outages because the whole system is built on the interference rejection abilities of the analog beamformer. For example, digital beamformer and instantaneous channel estimator operate in the subspace constructed by the analog beamformer. Since the AoA related to an arbitrary user is expected to be highly correlated in time, it is reasonable for the analog beamformer to be constructed using previous estimates as well, along with the newest estimates. This approach might be applied on various matrices or vectors, resulted from a possible combination with the methods that will be discussed in the next sections. Therefore, it is beneficial to generalize the operation. Let $\mathcal{F}(\mathbf{R}[n], \beta)$ denote the recursive filtering operation on the arbitrary matrix series $\mathbf{R}[n]$ with the filter parameter $\beta \in [0, 1)$. Its output takes the letter f as superscript and shown as

$$\mathbf{R}^f[n] \triangleq \mathcal{F}(\mathbf{R}[n], \beta), \quad (6.10)$$

where

$$\mathbf{R}^f[n] = \beta \mathbf{R}^f[n-1] + (1 - \beta) \mathbf{R}[n]. \quad (6.11)$$

This operation will be indicated in later block diagrams as shown in Figure 6.1. The variable $\mathbf{R}^f[n-1]$ at the recursion input is implied by the output and it might be omitted in later usages for the sake of simplicity.

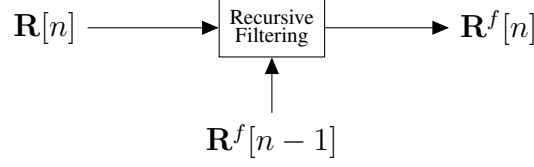


Figure 6.1: Recursive filtering block

6.4 Modifications on Channel Covariance Matrices

6.4.1 Azimuth Angle - Phase Transformation

The array response vector $\mathbf{u}(\phi)$ in (2.4) is dependent on azimuth angle ϕ through $\sin(\cdot)$ function. This fact is obstructive when trying to do derivations on CCMs, which are dependent on $\mathbf{u}(\phi)$. When the transformation

$$\theta \triangleq \pi \sin(\phi) \quad (6.12)$$

is performed, there exists a power profile $\rho_{\theta,l}^{(g)}(\theta)$ in phase domain which satisfies

$$\mathbf{R}_l^{(g)} = \int_{-\pi/2}^{\pi/2} \rho_{\phi,l}^{(g)}(\phi) \mathbf{u}(\phi) \mathbf{u}(\phi)^H d\phi = \int_{-\pi}^{\pi} \rho_{\theta,l}^{(g)}(\theta) \mathbf{q}(\theta) \mathbf{q}(\theta)^H d\theta, \quad (6.13)$$

where

$$\mathbf{q}(\theta) \triangleq \frac{1}{\sqrt{N}} [1 \ e^{j\theta} \ e^{j2\theta} \ \dots \ e^{j(N-1)\theta}]^T. \quad (6.14)$$

Noting that $\mathbf{q}(\pi \sin(\phi)) = \mathbf{u}(\phi)$ and $d\theta = \pi \cos(\phi) d\phi$, make a change of variables on the right hand side from θ to ϕ using (6.12).

$$\int_{-\pi/2}^{\pi/2} \rho_{\phi,l}^{(g)}(\phi) \mathbf{u}(\phi) \mathbf{u}(\phi)^H d\phi = \int_{-\pi/2}^{\pi/2} \rho_{\theta,l}^{(g)}(\pi \sin(\phi)) \mathbf{u}(\phi) \mathbf{u}(\phi)^H \pi \cos(\phi) d\phi \quad (6.15)$$

It is seen that

$$\rho_{\phi,l}^{(g)}(\phi) = \rho_{\theta,l}^{(g)}(\pi \sin(\phi)) \pi \cos(\phi). \quad (6.16)$$

or, through (6.12),

$$\rho_{\theta,l}^{(g)}(\theta) = \frac{\rho_{\phi,l}^{(g)}(\arcsin(\frac{\theta}{\pi}))}{\pi \cos(\arcsin(\frac{\theta}{\pi}))}. \quad (6.17)$$

Substituting $\cos(\arcsin(\frac{\theta}{\pi})) = \sqrt{1 - \frac{\theta^2}{\pi^2}}$,

$$\rho_{\theta,l}^{(g)}(\theta) = \frac{\rho_{\phi,l}^{(g)}(\arcsin(\frac{\theta}{\pi}))}{\sqrt{\pi^2 - \theta^2}}. \quad (6.18)$$

Consider a rectangular distribution of power along the angular domain where

$$\rho_{\phi,l}^{(g)}(\phi) = \begin{cases} A, & \mu_{\phi,l}^{(g)} - \frac{\sigma_{\phi,l}^{(g)}}{2} < \phi < \mu_{\phi,l}^{(g)} + \frac{\sigma_{\phi,l}^{(g)}}{2} \\ 0, & \textit{otherwise} \end{cases}. \quad (6.19)$$

Corresponding $\rho_{\theta,l}^{(g)}(\theta)$ can be found via (6.18), and obviously it is not a rectangular one when exactly transformed. However, it is expected to be close to a rectangle because nonlinearity coming with the sine function inside the transformation in (6.12) can be weak when the angular spread $\sigma_{\phi,l}^{(g)}$ is narrow enough. It resembles well-known small signal approximation where nonlinearity of the transformation is neglected when there is a small oscillation in the input about a mean value. $\rho_{\theta,l}^{(g)}(\theta)$ corresponding to $\rho_{\phi,l}^{(g)}(\phi)$ in (6.19) is approximated as

$$\rho_{\theta,l}^{(g)}(\theta) = \begin{cases} B, & \mu_{\theta,l}^{(g)} - \frac{\sigma_{\theta,l}^{(g)}}{2} < \theta < \mu_{\theta,l}^{(g)} + \frac{\sigma_{\theta,l}^{(g)}}{2} \\ 0, & \textit{otherwise} \end{cases}. \quad (6.20)$$

This approximation will aim to satisfy

- $\mu_{\theta,l}^{(g)} - \frac{\sigma_{\theta,l}^{(g)}}{2} = \pi \sin\left(\mu_{\phi,l}^{(g)} - \frac{\sigma_{\phi,l}^{(g)}}{2}\right)$
- $\mu_{\theta,l}^{(g)} + \frac{\sigma_{\theta,l}^{(g)}}{2} = \pi \sin\left(\mu_{\phi,l}^{(g)} + \frac{\sigma_{\phi,l}^{(g)}}{2}\right)$
- $\int_{-\pi}^{\pi} \rho_{\theta,l}^{(g)}(\theta) d\theta = \int_{-\frac{\pi}{2}}^{\frac{\pi}{2}} \rho_{\phi,l}^{(g)}(\phi) d\phi$

The first two criteria yield

$$\mu_{\theta,l}^{(g)} = \pi \sin\left(\mu_{\phi,l}^{(g)}\right) \cos\left(\frac{\sigma_{\phi,l}^{(g)}}{2}\right), \quad (6.21)$$

$$\sigma_{\theta,l}^{(g)} = 2\pi \sin\left(\frac{\sigma_{\phi,l}^{(g)}}{2}\right) \cos\left(\mu_{\phi,l}^{(g)}\right). \quad (6.22)$$

The criterion in the last bullet implies $A\sigma_{\phi,l}^{(g)} = B\sigma_{\theta,l}^{(g)}$. Therefore

$$B = A \frac{\sigma_{\phi,l}^{(g)}}{2\pi \sin\left(\frac{\sigma_{\phi,l}^{(g)}}{2}\right) \cos\left(\mu_{\phi,l}^{(g)}\right)}. \quad (6.23)$$

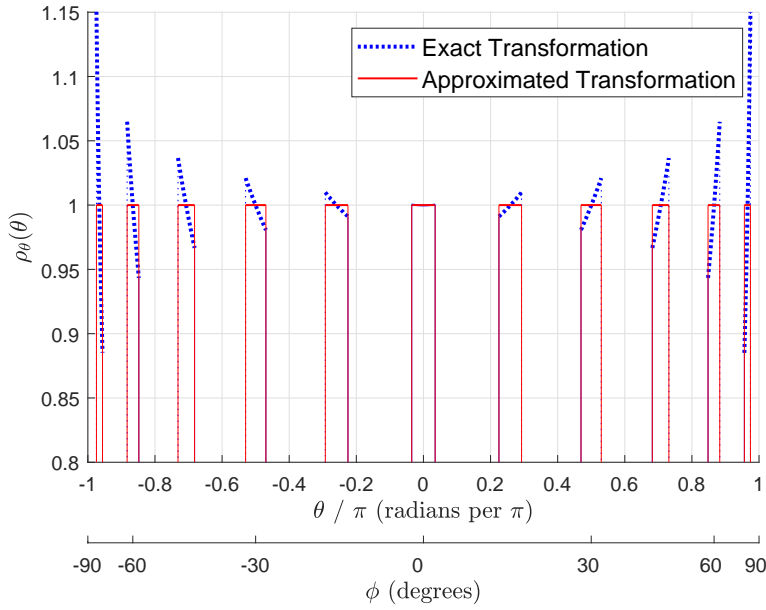


Figure 6.2: Comparison of exact and approximated angular transformations

A comparison between exact and approximated transforms are given in Figure 6.2 where transforms in the phase domain are plotted in the same axis for numerous different azimuthal rectangular power distributions $\rho_{\phi,l}^{(g)}(\phi)$ with widths $\sigma_{\phi,l}^{(g)}(\phi) = 4^\circ$ and different mean angles $\mu_{\phi,l}^{(g)}(\phi)$.

It is seen that the approximation is more successful with those having a center angle close to zero. The ratios of the integral of the absolute error to the integral of the exact transformation are 0.0652, 0.0303, 0.0175, 0.0101, 0.0047, 0.0002, 0.0047, 0.0101, 0.0175, 0.0302 and 0.0652 from left to the right. Since they are small, it is concluded that the approximation is successful and it will be used in further steps. It can be shown in later block diagrams as in Figure 6.3.

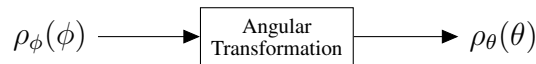


Figure 6.3: Angular transformation block

Note that the knowledge of $\rho_\phi(\phi)$ implies the knowledge of μ_ϕ and σ_ϕ , since $\mu_\phi - \frac{\sigma_\phi}{2}$ and $\mu_\phi + \frac{\sigma_\phi}{2}$ indicate the boundaries of the nonzero region of $\rho_\phi(\phi)$, given that $\rho_\phi(\phi)$ belongs to an MPC. Same is also valid for $\rho_\theta(\theta)$, μ_θ and σ_θ . Since this angular

transformation assumes a left-and-right-bounded input, this block is available only for the power profile of a single MPC.

6.4.2 Hadamard Factorization of Channel Covariance Matrices

Consider that the multipath of g^{th} group in the l^{th} delay is uniformly distributed in a restricted part of the angular domain with center $\mu_{\phi,l}^{(g)}(\phi)$, spread $\sigma_{\phi,l}^{(g)}(\phi)$ and power profile $\rho_{\phi,l}^{(g)}(\phi)$ which is equal to the one in (6.19). Assume that its CCM can be expressed as

$$\mathbf{R}_l^{(g)} = \int_{-\pi}^{\pi} \rho_{\phi,l}^{(g)}(\theta) \mathbf{q}(\theta) \mathbf{q}(\theta)^H d\theta, \quad (6.24)$$

where

$$\rho_{\phi,l}^{(g)}(\theta) = \begin{cases} \frac{1}{\sigma_{\theta,l}^{(g)}} & , \quad \mu_{\theta,l}^{(g)} - \frac{\sigma_{\theta,l}^{(g)}}{2} < \theta < \mu_{\theta,l}^{(g)} + \frac{\sigma_{\theta,l}^{(g)}}{2} \\ 0 & , \quad \text{otherwise} \end{cases}. \quad (6.25)$$

Therefore,

$$\mathbf{R}_l^{(g)} = \frac{1}{\sigma_{\theta,l}^{(g)}} \int_{\mu_{\theta,l}^{(g)} - \frac{\sigma_{\theta,l}^{(g)}}{2}}^{\mu_{\theta,l}^{(g)} + \frac{\sigma_{\theta,l}^{(g)}}{2}} \mathbf{q}(\theta) \mathbf{q}(\theta)^H d\theta \quad (6.26)$$

The entry in the m^{th} row and n^{th} column $(\mathbf{R}_l^{(g)})_{m,n}$ can be written as

$$(\mathbf{R}_l^{(g)})_{m,n} = \frac{1}{\sigma_{\theta,l}^{(g)}} \int_{\mu_{\theta,l}^{(g)} - \frac{\sigma_{\theta,l}^{(g)}}{2}}^{\mu_{\theta,l}^{(g)} + \frac{\sigma_{\theta,l}^{(g)}}{2}} \frac{1}{N} e^{j(m-n)\theta} d\theta. \quad (6.27)$$

Further steps are applied in the equations below.

$$(\mathbf{R}_l^{(g)})_{m,n} = \frac{1}{N\sigma_{\theta,l}^{(g)}} \left(\frac{e^{j(m-n)\theta}}{j(m-n)} \right) \Bigg|_{\mu_{\theta,l}^{(g)} - \frac{\sigma_{\theta,l}^{(g)}}{2}}^{\mu_{\theta,l}^{(g)} + \frac{\sigma_{\theta,l}^{(g)}}{2}} \quad (6.28)$$

$$(\mathbf{R}_l^{(g)})_{m,n} = \frac{1}{N\sigma_{\theta,l}^{(g)}} \frac{e^{j(m-n)\mu_{\theta,l}^{(g)}} 2j \sin \left((m-n) \frac{\sigma_{\theta,l}^{(g)}}{2} \right)}{j(m-n)} \quad (6.29)$$

$$(\mathbf{R}_l^{(g)})_{m,n} = \frac{e^{j(m-n)\mu_{\theta,l}^{(g)}} \sin \left((m-n) \frac{\sigma_{\theta,l}^{(g)}}{2} \right)}{N (m-n) \frac{\sigma_{\theta,l}^{(g)}}{2}} \quad (6.30)$$

$$\left(\mathbf{R}_l^{(g)}\right)_{m,n} = \left(\mathbf{q}(\mu_{\theta,l}^{(g)})\mathbf{q}(\mu_{\theta,l}^{(g)})^H\right)_{m,n} \text{sinc}\left((m-n)\frac{\sigma_{\theta,l}^{(g)}}{2\pi}\right) \quad (6.31)$$

Finally, it is found that

$$\mathbf{R}_l^{(g)} = \mathbf{R}_0(\mu_{\theta,l}^{(g)}) \odot \mathbf{D}(\sigma_{\theta,l}^{(g)}) \quad (6.32)$$

where $\mathbf{R}_0(\theta) \triangleq \mathbf{q}(\theta)\mathbf{q}(\theta)^H$, $(\mathbf{D}(\theta))_{m,n} \triangleq \text{sinc}\left((m-n)\frac{\theta}{2\pi}\right)$, and \odot is the Hadamard product operator. \mathbf{R} is the CCM of an MPC which is uniformly occupying an angular area with center $\mu_{\theta,l}^{(g)}$ and width $\sigma_{\theta,l}^{(g)}$. It is shown in this section that \mathbf{R} can be 'Hadamard-factorized' so that center angle is governed by a rank-1 matrix $\mathbf{R}_0(\mu_{\theta,l}^{(g)})$ and angular spread is governed by a Toeplitz matrix $\mathbf{D}(\sigma_{\theta,l}^{(g)})$.

6.4.3 Patching in Angular Domain

It is shown in the previous section that the CCM of an MPC can be Hadamard-factorized into two parts, one governing the mean angle and the other governing the angular spread. Unfortunately, it is only valid for rectangular power profiles which are uniform and nonzero only in one connected area of the angular axis. However, it would still be useful for a CCM with arbitrary power profile, for example \mathbf{R}_y ; if the power profile is separated into parts, each of which is appropriately approximated as uniform, Hadamard-factorized separately, and brought together by superposition to construct the CCM. When these angular parts have certain boundaries and equal length, it can be called patching in angular domain. This idea will be elaborated in this section.

Consider an arbitrary CCM \mathbf{R} with arbitrary angular power profile $\rho_\theta(\theta)$. If the angular domain is separated into parts by defining angular patches of width $\frac{2\pi}{N}$ about center angles $k\frac{2\pi}{N}$ for $k = 0, 1, \dots, N-1$, the spectrum can be approximated so that it is sum of whole patches with possibly different powers for each patch. In this way, for different patches, $\mathbf{D}(\sigma_\theta)$ is made constant with $\sigma_\theta = \frac{2\pi}{N}$ and the eigenvector of rank-one matrix $\mathbf{R}_0(\mu_\theta)$ is confined to be among the DFT vectors. Then, \mathbf{R} can be approximated as;

$$\mathbf{R} \cong \sum_k p_k \left(\mathbf{q}\left(\frac{2\pi}{N}k\right)\mathbf{q}\left(\frac{2\pi}{N}k\right)^H \odot \mathbf{D}\left(\frac{2\pi}{N}\right) \right), \quad (6.33)$$

where p_k are patch power levels to be determined. Since $\mathbf{D}(\frac{2\pi}{N})$ does not change for different k ,

$$\mathbf{R} \cong \left(\sum_k p_k \mathbf{q}(\frac{2\pi}{N}k) \mathbf{q}(\frac{2\pi}{N}k)^H \right) \odot \mathbf{D}(\frac{2\pi}{N}). \quad (6.34)$$

Then,

$$\mathbf{R} = (\mathbf{Q}\mathbf{P}\mathbf{Q}^H) \odot \mathbf{D}, \quad (6.35)$$

where $\mathbf{Q} \triangleq \begin{bmatrix} \mathbf{q}(0) & \mathbf{q}(\frac{2\pi}{N}) & \mathbf{q}(\frac{4\pi}{N}) & \cdots & \mathbf{q}((N-1)\frac{2\pi}{N}) \end{bmatrix}$ is the DFT matrix of size N , $\mathbf{P} \triangleq \text{diag} \left[\{p_k\}_{k=0}^{N-1} \right]$, and $\mathbf{D} \triangleq \mathbf{D}(\frac{2\pi}{N})$ for simplicity. Note that the matrices \mathbf{Q} and \mathbf{D} are constant matrices and only \mathbf{P} is specific to \mathbf{R} .

The aforementioned process is separated into two, and defined as system blocks for future references, as in Figure 6.4. The first block 'Patching' decides patch powers p_k from the angular power profile $\rho_\theta(\theta)$ and creates the diagonal matrix \mathbf{P} from them. The 'CCM Construction' block constructs a CCM using input patch powers, as shown in the equation (6.35).

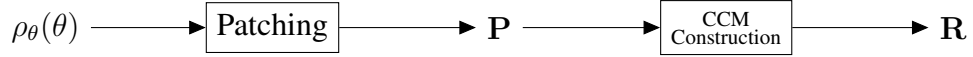


Figure 6.4: Patching and CCM Construction

The patching block can use different methods. While a correlator type model can be used as

$$p_k = \int_{k\frac{2\pi}{N} - \frac{\pi}{N}}^{k\frac{2\pi}{N} + \frac{\pi}{N}} \rho_\theta(\theta) d\theta, \quad (6.36)$$

a more straightforward method can be used too, where all the patches in which occupancy from $\rho_\theta(\theta)$ is found are awarded equal powers, and others assumed zero. It is a method selecting the narrowest set of consecutive patches covering the actual angular spread. It can be expressed as

$$p_k = \begin{cases} a, & \text{if } \mu_\theta + \frac{\sigma_\theta}{2} > k\frac{2\pi}{N} - \frac{\pi}{N} \text{ and } \mu_\theta - \frac{\sigma_\theta}{2} < k\frac{2\pi}{N} + \frac{\pi}{N} \\ 0, & \text{otherwise} \end{cases} \quad (6.37)$$

for $k = 0, \dots, N-1$, where a is selected to satisfy total power equality as

$$\sum_{k=0}^{N-1} p_k = \int_{-\pi}^{\pi} \rho_\theta(\theta) d\theta. \quad (6.38)$$

Note that an output power profile is implied after this process, even if it is not used explicitly. It can be expressed as

$$\rho_{\theta}^p(\theta) \triangleq \sum_{k=0}^{N-1} p_k \frac{\text{rect}\left(\frac{\theta - k\frac{2\pi}{N}}{\frac{2\pi}{N}}\right)}{\frac{2\pi}{N}} \quad (6.39)$$

where $\text{rect}(\theta)$ is well-known rectangular function, equal to one between $-\frac{1}{2}$ and $+\frac{1}{2}$ and zero otherwise.

It was shown in Chapter 5 that erroneously taking angular spread wider than its true value can be tolerated. Both methods have equal spreads but wider than the actual one, while the first one shrinks the edges of the related area in the output power profile. Although the first one is a more rigorous way, the second promises less complexity and change rate. Since the main motivation is to decrease these concepts, the second one is more preferable and it will be considered whenever the patching process is mentioned henceforward.

In the patching structure in (6.35), \mathbf{D} is actually equal to the CCM of an MPC having zero mean angle and $\frac{2\pi}{N}$ spread in phase domain. Each eigenvalue and eigenvector pair of $\mathbf{Q}\mathbf{P}\mathbf{Q}^H$ simply shifts and multiplies it, then the results are summed to achieve \mathbf{R} . This process resembles a convolution operation outputting the angular profile $\rho_{\theta}(\theta)$ of \mathbf{R} , where one of the operands is a rectangular function of width $\theta = \frac{2\pi}{N}$ and the other is sum of impulses at $\theta = \frac{2\pi}{N}k$ for $k = 0, 1, \dots, N - 1$ with different weights.

6.4.4 Quantization of Patch Power Levels

Consider the structure given in (6.35). The arbitrary CCM \mathbf{R} can be subjected to a change due to the mobility of the channel. Since the analog beamformer is constructed using CCMs in the GEB method which is focused on, this means a reconstruction process of the analog beamformer. As a complexity-lowering attempt, a scheme where a significant change in the CCMs (or the positions of the users) is waited for reconstruction can be considered. A practical way to utilize this scheme is to quantize the power levels p_k in the main diagonal of the matrix \mathbf{P} in (6.35).

A quantization process should take the expected magnitude of the subject into consideration. A usually smaller variable and a usually greater variable should be subjected to different quantization processes to achieve the expected representation size, change rate, etc. If \mathbf{R} in (6.35) is the observation covariance matrix \mathbf{R}_y , the power levels of the patches in \mathbf{P} can be very different indeed, because the observation consists of the MPCs of different users, most probably having very different expected power levels due to the near-far effect. In fact, the MPCs belonging to the same user can have different power levels. However, for the quantization of the power levels of a single MPC, a single quantizer can be used. Therefore, it is proposed to use different MPC-specific quantizers for different MPCs, if any needed. Then, the observation covariance matrix with quantized patch power levels can be obtained from a linear combination of those belonging to the MPCs, in a similar way to the one in (2.21). These MPC-specific quantizers should have an expectancy about the power levels, and appropriate level bounds accordingly. Let $Q_l^{(g)}(\mathbf{A}, k)$ be the quantizer for the MPC of the g^{th} group in the l^{th} delay, quantizing the entries in the arbitrary matrix \mathbf{A} of size $N \times N$ depending on the resolution parameter k and the expected power level for a patch deduced from parameters such as $\sigma_{\theta,l}^{(g)}$, $E_s^{(g)}$, K_g . It outputs \mathbf{A}^q as

$$\mathbf{A}^q \triangleq Q_l^{(g)}(\mathbf{A}, k). \quad (6.40)$$

Entries of \mathbf{A}^q are equal to one of the predetermined levels as

$$(\mathbf{A}^q)_{m,n} = r_{m,n} \frac{h_l^{(g)}}{k} \text{ for } m, n = 1, 2, \dots, N \quad (6.41)$$

where $\frac{h_l^{(g)}}{k}$ is the width of quantization levels, $r_{m,n}$ is the chosen level which is found as

$$r_{m,n} \triangleq \underset{\tilde{r}}{\operatorname{argmin}} \left| (\mathbf{A})_{m,n} - \tilde{r} \frac{h_l^{(g)}}{k} \right| \text{ for } \tilde{r} \in \mathbb{Z}, \quad (6.42)$$

and $h_l^{(g)}$ is the expected single patch power level, or height, which is calculated as

$$h_l^{(g)} \triangleq \frac{E_s^{(g)} K_g \operatorname{tr}(\mathbf{R}_l^{(g)})}{\left\lceil \frac{\sigma_\theta}{2\pi} \right\rceil}. \quad (6.43)$$

Note that the numerator is the power level that the related MPC of the related group represents in the total observation according to (2.21), and the nominator is the ceiled expected number of patches occupied by the MPC.

Let $\mathbf{P}_l^{(g)}$ be related to $\rho_{\theta,l}^{(g)}$ and $\mathbf{R}_l^{(g)}$ through patching and CCM construction operations explained in Section 6.4.3. When it is input to the quantizer $\mathcal{Q}_l^{(g)}$, the output is shown as

$$\mathbf{P}_l^{(g),q} \triangleq \mathcal{Q}_l^{(g)} \left(\mathbf{P}_l^{(g)}, k \right). \quad (6.44)$$

Quantized observation patch power matrix \mathbf{P}_y^q can be obtained as

$$\mathbf{P}_y^q \triangleq \sum_{g=1}^G K_g E_s^{(g)} \sum_{l=0}^{L-1} \mathbf{P}_l^{(g),q} + N_0 \mathbf{I}_N, \quad (6.45)$$

in accordance with (2.21). Then, the quantized observation CCM can be calculated as

$$\mathbf{R}_y^q = (\mathbf{Q} \mathbf{P}_y^q \mathbf{Q}^H) \odot \mathbf{D}, \quad (6.46)$$

in accordance with (6.35). This process is illustrated in Figure 6.5.

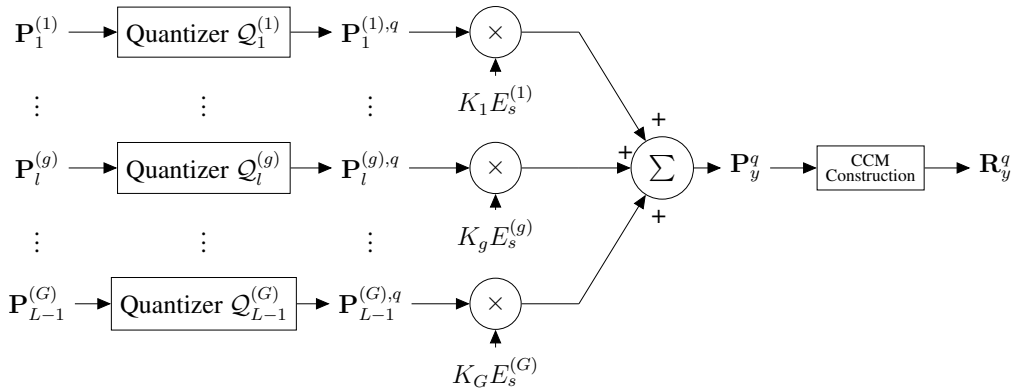


Figure 6.5: Separate quantization of MPC patch power levels

6.4.5 Update of Inverse of a Matrix with Patched Structure

Consider a CCM \mathbf{R} expressed in the structure given in (6.35). It was stated in Sections 6.4.2 and 6.4.3 that the matrix \mathbf{D} in (6.35) is such that

$$(\mathbf{D})_{m,n} = \text{sinc} \left(\frac{m-n}{N} \right). \quad (6.47)$$

The matrix \mathbf{D} is also equal to the CCM of an MPC having $\mu_\theta = 0$ center angle and $\sigma_\theta = \frac{2\pi}{N}$ angular spread. Since it is a small angular area with a large N , it is expected to be low-rank. That is, the majority of its eigenvalues is zero or very close to zero. In other words, some eigenvalue-eigenvector pairs are dominant compared to others.

Assume that the eigendecomposition of the matrix \mathbf{D} is

$$\mathbf{D} = \mathbf{F}\mathbf{\Lambda}\mathbf{F}^H, \quad (6.48)$$

where eigenvector \mathbf{f}_n is the n^{th} column of the matrix \mathbf{F} , and the eigenvalue λ_n is the n^{th} entry of the main diagonal of $\mathbf{\Lambda}$. So, it can be written as

$$\mathbf{D} = \sum_{n=1}^N \lambda_n \mathbf{f}_n \mathbf{f}_n^H, \quad (6.49)$$

where eigenvalues λ_n are assumed to be sorted in descending order as n increases. Separate $\mathbf{\Lambda}$ as $\mathbf{\Lambda} = \mathbf{\Lambda}^{\frac{1}{2}} \left[\mathbf{\Lambda}^{\frac{1}{2}} \right]^H$ and define $\mathbf{E} \triangleq \mathbf{F}\mathbf{\Lambda}^{\frac{1}{2}}$ so that

$$\mathbf{D} = \mathbf{E}\mathbf{E}^H \quad (6.50)$$

or

$$\mathbf{D} = \sum_{n=1}^N \mathbf{e}_n \mathbf{e}_n^H \quad (6.51)$$

where $\mathbf{E} = \begin{bmatrix} \mathbf{e}_1 & \mathbf{e}_2 & \cdots & \mathbf{e}_N \end{bmatrix}$. \mathbf{D} can be approximated with the matrix \mathbf{D}_r as

$$\mathbf{D}_r \triangleq \sum_{n=1}^r \mathbf{e}_n \mathbf{e}_n^H. \quad (6.52)$$

Then, \mathbf{D}_r can be used in the patching structure in (6.35) as

$$\mathbf{R} = (\mathbf{Q}\mathbf{P}\mathbf{Q}^H) \odot \mathbf{D}_r. \quad (6.53)$$

Also, $\mathbf{Q}\mathbf{P}\mathbf{Q}^H$ can be written in terms of vectors as

$$\mathbf{Q}\mathbf{P}\mathbf{Q}^H = \sum_{k=1}^N p_k \mathbf{q}_k \mathbf{q}_k^H, \quad (6.54)$$

where \mathbf{q}_k are columns of the matrix \mathbf{Q} so that

$$\mathbf{Q} = \begin{bmatrix} \mathbf{q}_1 & \mathbf{q}_2 & \cdots & \mathbf{q}_N \end{bmatrix}. \quad (6.55)$$

Then,

$$\mathbf{R} = \left(\sum_{k=1}^N p_k \mathbf{q}_k \mathbf{q}_k^H \right) \odot \left(\sum_{n=1}^r \mathbf{e}_n \mathbf{e}_n^H \right), \quad (6.56)$$

$$= \sum_{k=1}^N \sum_{n=1}^r p_k (\mathbf{q}_k \mathbf{q}_k^H) \odot (\mathbf{e}_n \mathbf{e}_n^H). \quad (6.57)$$

Since $(\mathbf{a}\mathbf{a}^H) \odot (\mathbf{b}\mathbf{b}^H) = (\mathbf{a} \odot \mathbf{b})(\mathbf{a} \odot \mathbf{b})^H$, the above equation can be rewritten as

$$\mathbf{R} = \sum_{k=1}^N \sum_{n=1}^r p_k (\mathbf{q}_k \odot \mathbf{e}_n) (\mathbf{q}_k \odot \mathbf{e}_n)^H. \quad (6.58)$$

Then, define

$$\mathbf{V} \triangleq \begin{bmatrix} \mathbf{V}_1 & \mathbf{V}_2 & \cdots & \mathbf{V}_N \end{bmatrix}, \quad (6.59)$$

where

$$\mathbf{V}_k \triangleq \begin{bmatrix} \mathbf{q}_k \odot \mathbf{e}_1 & \mathbf{q}_k \odot \mathbf{e}_2 & \cdots & \mathbf{q}_k \odot \mathbf{e}_r \end{bmatrix}. \quad (6.60)$$

Define also

$$\bar{\mathbf{P}} \triangleq \mathbf{P} \otimes \mathbf{I}_r, \quad (6.61)$$

where \otimes is the Kronecker product operator. Finally,

$$\mathbf{R} = \mathbf{V}\bar{\mathbf{P}}\mathbf{V}^H. \quad (6.62)$$

Note that the matrix \mathbf{V} is of size $N \times Nr$, and the matrix $\bar{\mathbf{P}}$ is of size $Nr \times Nr$.

After that, consider the series of matrices $\mathbf{R}[n]$ and its correspondent $\mathbf{P}[n]$ through (6.53). Let the update matrices be defined as

$$\Delta\mathbf{R}[n] \triangleq \mathbf{R}[n] - \mathbf{R}[n-1] \quad (6.63)$$

and

$$\Delta\mathbf{P}[n] \triangleq \mathbf{P}[n] - \mathbf{P}[n-1]. \quad (6.64)$$

The matrix pair $\Delta\mathbf{R}[n]$ and $\Delta\mathbf{P}[n]$ fits into the structure in (6.53) as

$$\Delta\mathbf{R}[n] = (\mathbf{Q}\Delta\mathbf{P}[n]\mathbf{Q}^H) \odot \mathbf{D}_r. \quad (6.65)$$

Then consider $\Delta\bar{\mathbf{P}}[n]$ which corresponds to $\Delta\mathbf{P}[n]$ through (6.61) as

$$\Delta\bar{\mathbf{P}}[n] \triangleq \Delta\mathbf{P}[n] \otimes \mathbf{I}_r. \quad (6.66)$$

Note that $\Delta\mathbf{R}[n]$ and $\Delta\bar{\mathbf{P}}[n]$ satisfies the relation in (6.62) as

$$\Delta\mathbf{R}[n] = \mathbf{V}\Delta\bar{\mathbf{P}}[n]\mathbf{V}^H. \quad (6.67)$$

$\Delta\mathbf{P}[n]$ and $\Delta\bar{\mathbf{P}}[n]$ involves the change in the patch powers. Then, only the powers of patches experiencing a movement are nonzero. This leads to secondary expressions of the structures in (6.53) and (6.62). The zero entries in the main diagonal of $\Delta\mathbf{P}[n]$

and the corresponding columns of \mathbf{Q} are not necessary. Consider that there are $N_{\Delta p}$ nonzero entries in the main diagonal of $\Delta\mathbf{P}[n]$. Express its location as $\Delta n[p] = n$ for $p = 1, \dots, N_{\Delta p}$ meaning p^{th} nonzero patch power is in the n^{th} position in the main diagonal of $\Delta\bar{\mathbf{P}}$. Then,

$$\Delta\mathbf{R}[n] = (\mathbf{Q}_{nz}\Delta\mathbf{P}_{nz}[n]\mathbf{Q}_{nz}^H) \odot \mathbf{D}_r, \quad (6.68)$$

where

$$\Delta\mathbf{P}_{nz}[n] \triangleq \text{diag} \left[\left\{ (\Delta\mathbf{P}[n])_{\Delta n[p], \Delta n[p]} \right\}_{p=1}^{N_{\Delta p}} \right], \quad (6.69)$$

and

$$\mathbf{Q}_{nz} \triangleq \begin{bmatrix} \mathbf{q}_{\Delta n[1]} & \mathbf{q}_{\Delta n[2]} & \cdots & \mathbf{q}_{\Delta n[N_{\Delta p}]} \end{bmatrix}. \quad (6.70)$$

This can also be expressed in the structure in (6.62) as

$$\Delta\mathbf{R}[n] = \mathbf{V}_{nz}\Delta\bar{\mathbf{P}}_{nz}[n]\mathbf{V}_{nz}^H, \quad (6.71)$$

where

$$\Delta\bar{\mathbf{P}}_{nz}[n] \triangleq \Delta\mathbf{P}_{nz}[n] \otimes \mathbf{I}_r. \quad (6.72)$$

and

$$\mathbf{V}_{nz} \triangleq \begin{bmatrix} \mathbf{V}_{\Delta n[1]} & \mathbf{V}_{\Delta n[2]} & \cdots & \mathbf{V}_{\Delta n[N_{\Delta p}]} \end{bmatrix}. \quad (6.73)$$

Note that the matrix \mathbf{V}_{nz} is of size $N \times N_{\Delta p}r$, and the matrix $\bar{\mathbf{P}}_{nz}[n]$ is of size $N_{\Delta p}r \times N_{\Delta p}r$. Then the inverse can be expressed as

$$\mathbf{R}^{-1}[n] = (\mathbf{R}[n-1] + \Delta\mathbf{R}[n])^{-1} \quad (6.74)$$

$$= (\mathbf{R}[n-1] + \mathbf{V}\Delta\bar{\mathbf{P}}[n]\mathbf{V}^H)^{-1} \quad (6.75)$$

$$= (\mathbf{R}[n-1] + \mathbf{V}_{nz}\Delta\bar{\mathbf{P}}_{nz}[n]\mathbf{V}_{nz}^H)^{-1}. \quad (6.76)$$

If $\mathbf{R}^{-1}[n-1]$ is known, $\mathbf{R}^{-1}[n]$ can be found through Woodbury matrix identity as

$$\begin{aligned} \mathbf{R}^{-1}[n] &= \mathbf{R}^{-1}[n-1] \\ &\quad - \mathbf{R}^{-1}[n-1]\mathbf{V}_{nz} \left(\Delta\bar{\mathbf{P}}_{nz}^{-1}[n] + \mathbf{V}_{nz}^H\mathbf{R}^{-1}[n-1]\mathbf{V}_{nz} \right)^{-1} \mathbf{V}_{nz}^H\mathbf{R}^{-1}[n-1]. \end{aligned} \quad (6.77)$$

The matrix inverse in the right hand side of (6.77) is on a matrix of size $N_{\Delta p}r \times N_{\Delta p}r$. The direct calculation of the matrix $\mathbf{R}^{-1}[n]$ would require a matrix inversion operation of size $N \times N$. In order for this method to be meaningful, $N_{\Delta p}r$ should be less than N . This issue will be addressed in the following sections.

When used after a patching process, this method can update the inverse of a matrix series $\mathbf{R}[n]$ with the input of $\Delta\mathbf{P}[n]$, promising low-complexity operation if the change rate of $\mathbf{R}[n]$ is slow. It can be represented in block diagrams in the next sections as shown in Figure 6.6.

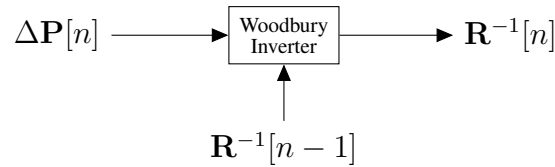


Figure 6.6: Woodbury inverter block

6.4.6 Summary of Blocks

So far, several operational blocks are introduced under Section 6.4. These are angular transformation, patching, CCM construction, patch power quantizer and Woodbury inverter. In addition, the recursive filtering block was introduced in Section 6.3.

Angular transformation overcomes the nonlinear nature of the array impulse response $\mathbf{u}(\phi)$ with a cost of an acceptable amount of error and allows analytical derivations on CCMs by providing a new angular support linearly related with the phase θ . However, this might not be needed at all in real applications, since an angular estimator most probably operates in the phase domain θ , and outputs $\hat{\mu}_\theta$, $\hat{\sigma}_\theta$ and $\hat{\rho}_\theta(\theta)$ instead of $\hat{\mu}_\phi$, $\hat{\sigma}_\phi$ and $\hat{\rho}_\phi(\phi)$.

Then, the power profile of the CCMs are patched. This operation represents the continuous angular power profile $\rho_\theta(\theta)$ with discrete series p_k , or equivalently the matrix \mathbf{P} . Therefore, manipulations on the power profile can be done more easily. In addition, patching brings a low-pass nature to the user movement, relying on the results given in Chapter 5 showing the tolerance to the spread errors.

A method for CCM construction has been introduced, which operates with constant matrices and only needs patch power levels. Also, this method is more practical compared to the one in (2.18) that requires numerical integrating methods. Therefore, it makes the MMSE channel estimation and generalized eigen-beamformer methods,

requiring CCM calculation, more affordable.

Recursive filtering is a caution for errors in the estimation of center angles of MPCs. It is expected to prevent instantaneous fading and outage. Patch power quantizer ensures the low adaptation rate. To do that, it is important that it is placed after recursive filtering stage. Then, a matrix inverse updater utilizing Woodbury matrix identity is introduced by the name Woodbury inverter. It only needs the change in patch power levels and the previous inverse. It inverts a matrix whose size is proportional with the number of changed patch powers, instead of the full size.

Input-output relations and output notations of the blocks are given in a generalized way on arbitrary matrices. However, they will be sorted one after another, and one will use the output of another as input. This brings a lot of new variables. These variables are shown in a compact way in Figure 6.7. Although blocks can be used in various orders theoretically, definitely all have a place, either implied by the input types or determined by the interest of the thesis. The flow of the quantities in Figure 6.7 will be the basis of a proposed method in next sections.

The horizontal passages between quantities (for example, from $\hat{\mathbf{P}}_l^{(g)}[n]$ to $\hat{\mathbf{P}}_y[n]$, $\hat{\mathbf{P}}_\eta^{(g)}[n]$, $\hat{\mathbf{P}}_{\eta,l}^{(g)}[n]$) require a similar usage of (2.21),(2.22) and (2.23). It is seen that all MPC variables have a passage to the observation or interference variables, and all the vertical operations are valid for both columns, except angular transformation and quantization. These are performed only on the MPC variables. Also note that the operations, passages and variables related to MPCs implies all MPCs, g from 1 to G and l from 0 to $L - 1$.

6.5 Modifications on Generalized Eigen-Beamformer

Generalized eigen-beamformer is constructed through generalized eigendecomposition of two matrices, namely the covariance matrices of intended signal and interference. Consider a one-rank Hermitian matrix $\mathbf{A} = \mathbf{u}\mathbf{u}^H$ and a full-rank positive-definite Hermitian matrix \mathbf{B} . A generalized eigenvalue λ and corresponding general-

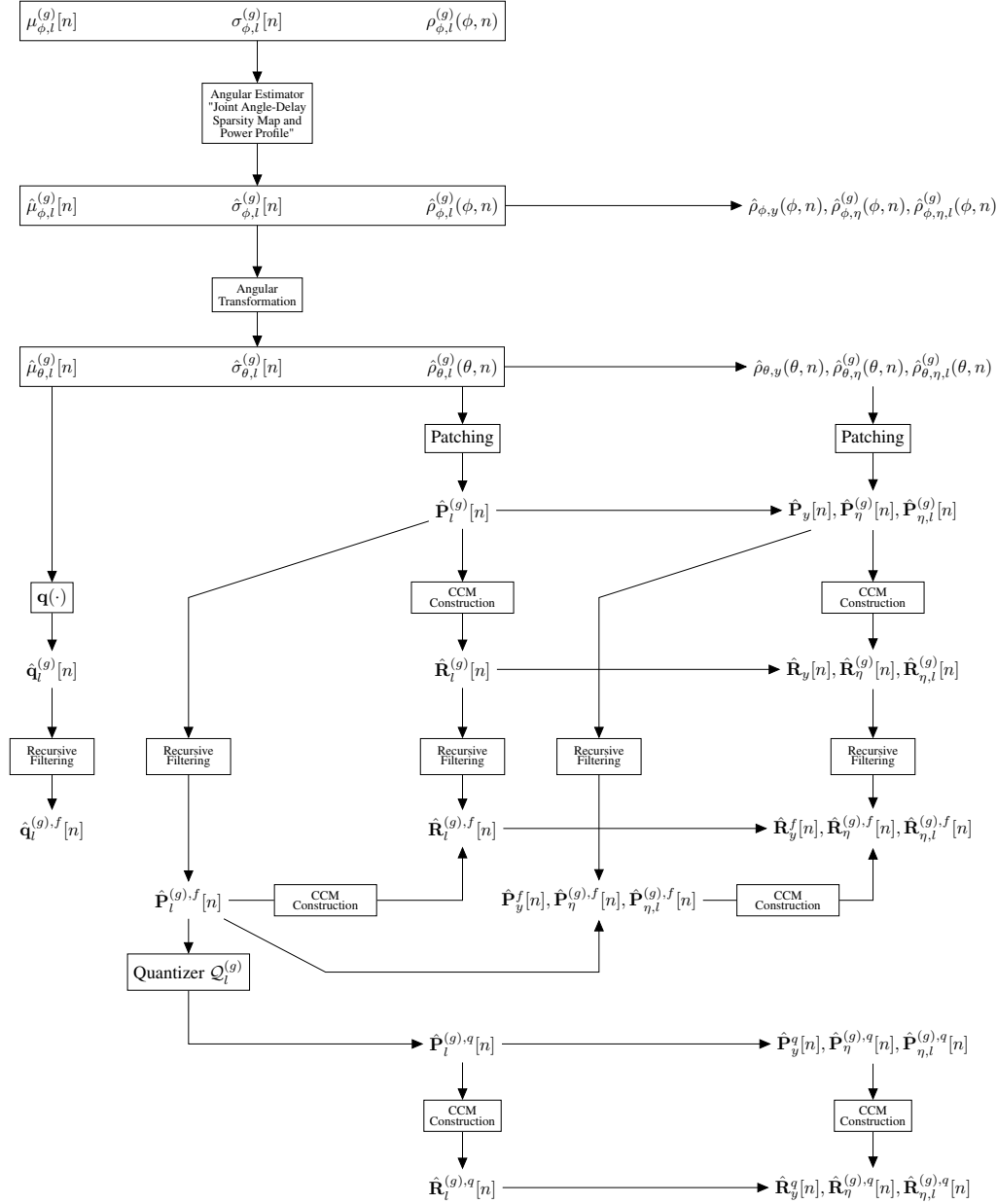


Figure 6.7: Map of Variables

ized eigenvector \mathbf{v} of the pair (\mathbf{A}, \mathbf{B}) satisfy the equation

$$\mathbf{A}\mathbf{v} = \lambda\mathbf{B}\mathbf{v}. \quad (6.78)$$

This equation is equivalent to

$$(\mathbf{A} - \lambda\mathbf{B})\mathbf{v} = \mathbf{0} \quad (6.79)$$

which implies, for a non-trivial solution of \mathbf{v} ,

$$\det(\mathbf{A} - \lambda\mathbf{B}) = 0. \quad (6.80)$$

Since \mathbf{B} is positive definite, there exists an inverse \mathbf{B}^{-1} , so it can be written that

$$\det(\mathbf{A}\mathbf{B}^{-1}\mathbf{B} - \lambda\mathbf{B}) = 0. \quad (6.81)$$

It follows as

$$\det(\mathbf{A}\mathbf{B}^{-1} - \lambda\mathbf{I})\det(\mathbf{B}) = 0 \quad (6.82)$$

and since $\det(\mathbf{B}) \neq 0$ because it is positive-definite,

$$\det(\mathbf{A}\mathbf{B}^{-1} - \lambda\mathbf{I}) = 0. \quad (6.83)$$

Substituting $\mathbf{A} = \mathbf{u}\mathbf{u}^H$ and dividing by $-\lambda$;

$$\det(\mathbf{I} - \frac{1}{\lambda}\mathbf{u}\mathbf{u}^H\mathbf{B}^{-1}) = 0. \quad (6.84)$$

Using Sylvester's determinant theorem, it can be converted to

$$\det(1 - \frac{1}{\lambda}\mathbf{u}^H\mathbf{B}^{-1}\mathbf{u}) = 0. \quad (6.85)$$

meaning

$$\lambda = \mathbf{u}^H\mathbf{B}^{-1}\mathbf{u}. \quad (6.86)$$

After achieving this; (6.78) is revisited. Substituting $\mathbf{A} = \mathbf{u}\mathbf{u}^H$ and making the guess that $\mathbf{v} = \mathbf{B}^{-1}\mathbf{u}$, the equation

$$\mathbf{u}\mathbf{u}^H\mathbf{B}^{-1}\mathbf{u} = \lambda\mathbf{u}. \quad (6.87)$$

is obtained. Note that $\mathbf{u}^H \mathbf{B}^{-1} \mathbf{u}$ on the left hand side is a scalar which is found, in (6.86), to be equal to the eigenvalue λ . Substituting λ in the related place, it is seen that the equation (6.78) is satisfied with

$$\mathbf{v} = \mathbf{B}^{-1} \mathbf{u}. \quad (6.88)$$

In conclusion, $\mathbf{B}^{-1} \mathbf{u}$ is the generalized eigenvector of the pair of matrices (\mathbf{A}, \mathbf{B}) , where $\mathbf{A} = \mathbf{u} \mathbf{u}^H$ is a rank-one Hermitian matrix and \mathbf{B} is a positive-definite Hermitian matrix.

This conclusion can be useful when it is combined with the fact that CCMs of MPCs $\mathbf{R}_l^{(g)}$ is obtained from angular profiles $\rho_l^{(g)}(\phi)$ which are nonzero over a very narrow angular interval. Looking to the parametric CCM construction equation (2.18), $\mathbf{R}_l^{(g)}$ can be expected to be very low-rank, and nearly one-rank. Therefore, as a suboptimal solution,

$$\mathbf{S}_m^{(g)} = \hat{\mathbf{R}}_y^{-1} \mathbf{q}(\hat{\mu}_{\theta,l}^{(g)}) \quad (6.89)$$

can be used when $d_m^{(g)} = 1$ where $l = \mathcal{L}^{(g)}[m]$. However, since $\mathbf{R}_l^{(g)}$ is not exactly rank-one matrix as \mathbf{A} , this solution can be improved further. In Section 6.4.2, it is shown that $\mathbf{R}_l^{(g)}$ can be written as

$$\mathbf{R}_l^{(g)} = \left(\mathbf{q}(\mu_{\theta,l}^{(g)}) \mathbf{q}^H(\mu_{\theta,l}^{(g)}) \right) \odot \mathbf{D}(\sigma_{\theta,l}^{(g)}). \quad (6.90)$$

Let the vector $\mathbf{d}_k(\sigma_{\theta,l}^{(g)})$ be the multiplication of the square root of the k^{th} eigenvalue and the k^{th} eigenvector of the matrix $\mathbf{D}(\sigma_{\theta,l}^{(g)})$, assuming eigenvalues are sorted in descending order as k increases. Then,

$$\mathbf{D}(\sigma_{\theta,l}^{(g)}) = \sum_{k=1}^N \mathbf{d}_k(\sigma_{\theta,l}^{(g)}) \mathbf{d}_k^H(\sigma_{\theta,l}^{(g)}). \quad (6.91)$$

Therefore,

$$\mathbf{R}_l^{(g)} = \left(\mathbf{q}(\mu_{\theta,l}^{(g)}) \mathbf{q}^H(\mu_{\theta,l}^{(g)}) \right) \odot \sum_{k=1}^N \mathbf{d}_k(\sigma_{\theta,l}^{(g)}) \mathbf{d}_k^H(\sigma_{\theta,l}^{(g)}) \quad (6.92)$$

$$= \sum_{k=1}^N \left(\mathbf{q}(\mu_{\theta,l}^{(g)}) \mathbf{q}^H(\mu_{\theta,l}^{(g)}) \right) \odot \left(\mathbf{d}_k(\sigma_{\theta,l}^{(g)}) \mathbf{d}_k^H(\sigma_{\theta,l}^{(g)}) \right) \quad (6.93)$$

$$= \sum_{k=1}^N \left(\mathbf{q}(\mu_{\theta,l}^{(g)}) \odot \mathbf{d}_k(\sigma_{\theta,l}^{(g)}) \right) \left(\mathbf{q}(\mu_{\theta,l}^{(g)}) \odot \mathbf{d}_k(\sigma_{\theta,l}^{(g)}) \right)^H \quad (6.94)$$

Note that, since magnitude of the entries in the $\mathbf{q}(\mu_{\theta,l}^{(g)})$ is constant, Hadamard product does not bring any damage to the orthogonality between the eigenvectors of the matrix $\mathbf{D}(\sigma_{\theta,l}^{(g)})$. In fact, $(\mathbf{q}(\mu_{\theta,l}^{(g)}) \odot \mathbf{d}_k(\sigma_{\theta,l}^{(g)}))$ from $k = 1, \dots, N$ are the eigenvectors of the CCM $\mathbf{R}_l^{(g)}$, except a scalar multiplier. Then, it is proposed to use these eigenvectors in the structure given in (6.89) instead of the lone steering vector. It is expressed as

$$\mathbf{S}_m^{(g)} = \hat{\mathbf{R}}_y^{-1} \left(\mathbf{q}(\hat{\mu}_{\theta,l}^{(g)}) \odot \mathbf{d}_1(\hat{\sigma}_{\theta,l}^{(g)}) \right) \quad (6.95)$$

for $d_m^{(g)} = 1$ where $l = \mathcal{L}^{(g)}[m]$. If more than one RF chain are attained to the m^{th} MPC of the g^{th} group which is in the l^{th} delay; that is $d_m^{(g)} > 1$, the structure below can be used.

$$\mathbf{S}_m^{(g)} = \hat{\mathbf{R}}_y^{-1} \left[\mathbf{q}(\hat{\mu}_{\theta,l}^{(g)}) \odot \mathbf{d}_1(\hat{\sigma}_{\theta,l}^{(g)}) \quad \mathbf{q}(\hat{\mu}_{\theta,l}^{(g)}) \odot \mathbf{d}_2(\hat{\sigma}_{\theta,l}^{(g)}) \quad \dots \quad \mathbf{q}(\hat{\mu}_{\theta,l}^{(g)}) \odot \mathbf{d}_{d_m^{(g)}}(\hat{\sigma}_{\theta,l}^{(g)}) \right] \quad (6.96)$$

6.6 Proposed Adaptive Construction Methods for Analog Beamformer

6.6.1 GEB with Recursively Filtered Channel Covariance Matrices

In the previous chapter, it is shown that the GEB is a powerful method, but vulnerable against the bias in the angular estimations. This method aims to exploit the advantages of the GEB in the presence of erroneous angular estimations. It is proposed to construct GEB with recursively filtered CCMs, instead of the last estimation. Doing that, it is aimed to benefit from the fact that the AoA of CCMs are correlated in time. First, the filtered covariance matrices of the intended signal and interference are obtained as

$$\hat{\mathbf{R}}_l^{(g),f}[n] \triangleq \beta \hat{\mathbf{R}}_l^{(g),f}[n-1] + (1 - \beta) \hat{\mathbf{R}}_l^{(g)}[n] \text{ for } n = 1, 2, 3, \dots \quad (6.97)$$

and

$$\hat{\mathbf{R}}_y^f[n] \triangleq \beta \hat{\mathbf{R}}_y^f[n-1] + (1 - \beta) \hat{\mathbf{R}}_y[n] \text{ for } n = 1, 2, 3, \dots \quad (6.98)$$

where $0 \leq \beta < 1$. Then, they are used in GEB construction, using generalized eigendecomposition of the filtered matrix pair $(\hat{\mathbf{R}}_l^{(g),f}[n], \hat{\mathbf{R}}_y^f[n])$ instead of the pair $(\hat{\mathbf{R}}_l^{(g)}[n], \hat{\mathbf{R}}_y[n])$. Note that the equation

$$\hat{\mathbf{R}}_y^f[n] = \sum_{g=1}^G K_g E_s^{(g)} \sum_{l=0}^{L-1} \hat{\mathbf{R}}_l^{(g),f}[n] + N_0 \mathbf{I}_N. \quad (6.99)$$

can also be used.

6.6.1.1 Asymptotic Analysis for the Recursive Filtering Output

Consider that there is only one user in the environment and it has only one MPC. Let its channel be static such that the center angle μ_θ and the angular spread σ_θ does not change with time. However, the estimate $\hat{\mu}_\theta[n]$ for the n^{th} time instance is erroneous such that

$$\hat{\mu}_\theta[n] = \mu_\theta + e_\theta[n] \quad (6.100)$$

where $e_\theta[n] \sim \mathcal{N}(0, \sigma_e^2)$ and i.i.d. for different n . In addition, the angular spread estimate is perfect such that $\hat{\sigma}_\theta[n] = \sigma_\theta$. The estimate CCM $\hat{\mathbf{R}}[n]$ is constructed according to values $\hat{\mu}_\theta[n]$ and σ_θ . The estimate CCM $\hat{\mathbf{R}}[n]$ can be expressed as

$$\hat{\mathbf{R}}[n] = \mathbf{R} \odot (\mathbf{q}(e_\theta[n])\mathbf{q}^H(e_\theta[n])), \quad (6.101)$$

meaning its entries are

$$\left(\hat{\mathbf{R}}[n]\right)_{ab} = (\mathbf{R})_{ab} e^{j(a-b)e_\theta[n]} \quad (6.102)$$

The mean, variance and cross correlation of the exponential term, with a normally distributed random variable in its exponent, can be expressed with the help of characteristic function for the normal random variables as shown below.

$$E \left[e^{j(a-b)e_\theta[n]} \right] = e^{-\frac{1}{2}(a-b)^2\sigma_e^2} \quad (6.103)$$

$$\text{var} \left(e^{j(a-b)e_\theta[n]} \right) = 1 - e^{-(a-b)^2\sigma_e^2} \quad (6.104)$$

$$E \left[\left(e^{j(a-b)e_\theta[n_1]} - E \left[e^{j(a-b)e_\theta[n_1]} \right] \right) \left(e^{j(a-b)e_\theta[n_2]} - E \left[e^{j(a-b)e_\theta[n_2]} \right] \right)^* \right] \quad (6.105)$$

$$= E \left[e^{j(a-b)(e_\theta[n_1]-e_\theta[n_2])} \right] - \left(e^{-\frac{1}{2}(a-b)^2\sigma_e^2} \right)^2 \quad (6.106)$$

$$= e^{-\frac{1}{2}(a-b)^2 2\sigma_e^2} - e^{-(a-b)^2\sigma_e^2} \quad (6.107)$$

$$= 0 \text{ for } n_1 \neq n_2 \quad (6.108)$$

Then, the mean and variance of the entries of the estimate CCM $\hat{\mathbf{R}}[n]$ are found to be as below.

$$E \left[\left(\hat{\mathbf{R}}[n] \right)_{ab} \right] = (\mathbf{R})_{ab} e^{-\frac{1}{2}(a-b)^2\sigma_e^2} \quad (6.109)$$

$$\text{var} \left(\left(\hat{\mathbf{R}}[n] \right)_{ab} \right) = ((\mathbf{R})_{ab})^2 \left(1 - e^{-(a-b)^2 \sigma_e^2} \right) \quad (6.110)$$

The output of the recursive filtering operation can be expressed as

$$\hat{\mathbf{R}}^f[n] = \beta \hat{\mathbf{R}}^f[n-1] + (1-\beta) \hat{\mathbf{R}}[n] \quad (6.111)$$

$$= \beta^n \hat{\mathbf{R}}[0] + (1-\beta) \beta^n \sum_{k=1}^n \beta^{-k} \hat{\mathbf{R}}[k] \quad (6.112)$$

The entries of the output are

$$\left(\hat{\mathbf{R}}^f[n] \right)_{ab} = \beta^n (\mathbf{R})_{ab} e^{j(a-b)e_\theta[0]} + (1-\beta) \beta^n \sum_{k=1}^n \beta^{-k} (\mathbf{R})_{ab} e^{j(a-b)e_\theta[k]} \quad (6.113)$$

Using the mean, variance and uncorrelatedness of the exponential random term which are found above, the mean and the variance of the entries of the filtered output CCM are calculated as below.

$$E \left[\left(\hat{\mathbf{R}}^f[n] \right)_{ab} \right] = \beta^n (\mathbf{R})_{ab} e^{-\frac{1}{2}(a-b)^2 \sigma_e^2} + (1-\beta) \beta^n \sum_{k=1}^n \beta^{-k} (\mathbf{R})_{ab} e^{-\frac{1}{2}(a-b)^2 \sigma_e^2} \quad (6.114)$$

$$= (\mathbf{R})_{ab} e^{-\frac{1}{2}(a-b)^2 \sigma_e^2} \quad (6.115)$$

$$\begin{aligned} \text{var} \left(\left(\hat{\mathbf{R}}^f[n] \right)_{ab} \right) &= \beta^{2n} (\mathbf{R})_{ab}^2 \left(1 - e^{-(a-b)^2 \sigma_e^2} \right) \\ &\quad + (1-\beta)^2 \beta^{2n} \sum_{k=1}^n \beta^{-2k} ((\mathbf{R})_{ab})^2 \left(1 - e^{-(a-b)^2 \sigma_e^2} \right) \end{aligned} \quad (6.116)$$

$$= (\mathbf{R})_{ab}^2 \left(1 - e^{-(a-b)^2 \sigma_e^2} \right) \left(\beta^{2n} + \frac{1-\beta}{1+\beta} (1-\beta^{2n}) \right) \quad (6.117)$$

$$\lim_{n \rightarrow \infty} \text{var} \left(\left(\hat{\mathbf{R}}^f[n] \right)_{ab} \right) = (\mathbf{R})_{ab}^2 \left(1 - e^{-(a-b)^2 \sigma_e^2} \right) \frac{1-\beta}{1+\beta} \quad (6.118)$$

$$\lim_{n \rightarrow \infty} \text{var} \left(\left(\hat{\mathbf{R}}^f[n] \right)_{ab} \right) = \frac{1-\beta}{1+\beta} \text{var} \left(\left(\hat{\mathbf{R}}[n] \right)_{ab} \right) \quad (6.119)$$

As it is seen, the variance decreases with filtering with a mean that is not the same as the actual CCM. The new mean of the filtered output CCM has wider spread in

angular domain than the actual CCM. The spreading effect of recursive filtering with erroneous estimates is shown in Figure 6.8 where

$$\mathbf{u}^H(\phi)E\left[\hat{\mathbf{R}}^f[n]\right]\mathbf{u}(\phi) \quad (6.120)$$

is plotted using (6.115) for various error levels.

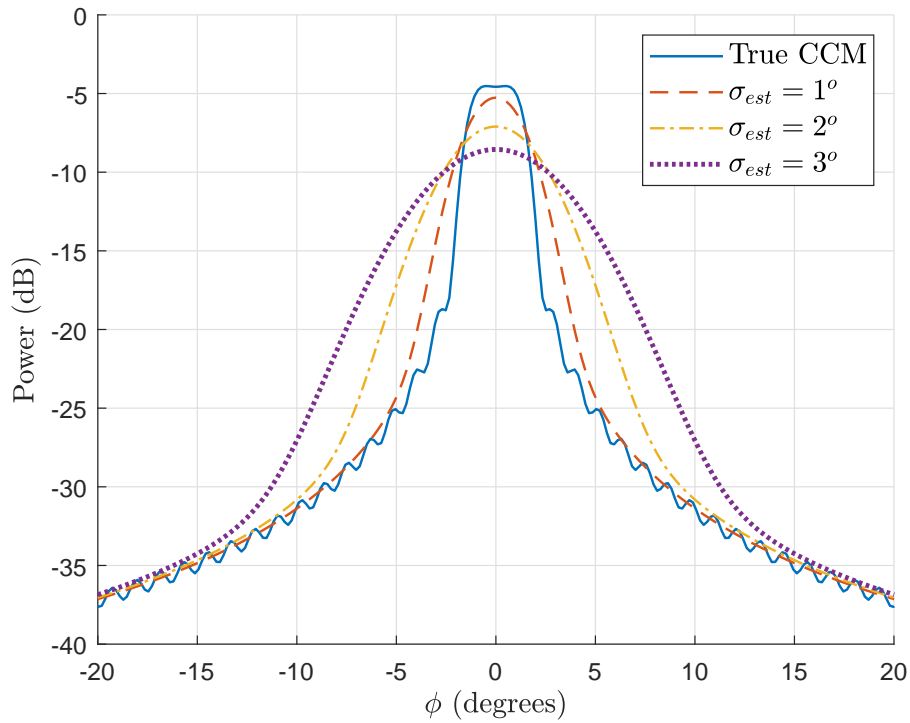


Figure 6.8: The spreading effect of recursive filtering with erroneous estimates

Although the mean calculated for the lastly estimated CCM is equal to the that calculated for the filtered one, it is the mean of the process. A single realization of this process is used every time which carries a biased mean AoA estimation. Therefore, while the usage of the last estimate CCM is related with biased estimation, the usage of recursively filtered estimate CCM is related with a spread error. In the previous chapter, it was shown that the system is vulnerable against the biased angular estimations but an error in the estimation of angular spread can be tolerated. Therefore, constructing GEB with recursively filtered CCMs promises a performance increase when the angular estimates are biased. However, the recursive filtering operation does not result in a convergence to the actual matrix. Therefore, there might be cases in which its usage is disadvantageous.

The error term $e_\phi[n]$ in terms of azimuth angle ϕ will be given in numerical results section as normally distributed with zero mean and standard deviation σ_{est} . In this section, analysis has been done as if the phase correspondent error term $e_\theta[n]$ is normally distributed for the sake of simplicity. In the numerical results, the maximum interested value of σ_{est} will be 3 degrees. It means that $e_\phi[n]$ will be between -9 degrees and +9 degrees with 99% probability. The linear approximation of $\sin(\phi)\pi$ is $\phi\pi$ by neglecting the higher order terms in its Taylor expression, where ϕ is in radians. For 9 degrees, or 0.1571 radians, $\theta = \sin(\phi)\pi$ is 0.4915 and the linear approximation $\phi\pi$ is 0.4935. They are very close and it shows that, for the aforementioned interval of $e_\phi[n]$, the $\theta = \sin(\phi)\pi$ relation is almost linear. Therefore, if $e_\phi[n]$ is given as normally distributed, $e_\theta[n]$ can be taken as normally distributed too.

6.6.2 Wiener Filter Type Analog Beamformer

It is proposed to construct the MPC-specific analog beamformer for the n^{th} time instance $\mathbf{S}_m^{(g)}[n]$ as

$$\mathbf{S}_m^{(g)}[n] = \left(\hat{\mathbf{R}}_y^q[n]\right)^{-1} \left[\left(\mathbf{q}_l^{(g),f}[n] \odot \mathbf{d}_1(\hat{\sigma}_{\theta,l}^{(g)})\right) \dots \left(\mathbf{q}_l^{(g),f}[n] \odot \mathbf{d}_{d_m^{(g)}}(\hat{\sigma}_{\theta,l}^{(g)})\right) \right], \quad (6.121)$$

where $\left(\hat{\mathbf{R}}_y^q[n]\right)^{-1}$ is obtained using the aforementioned processing blocks as shown in Figure 6.9. On the other hand,

$$\mathbf{q}_l^{(g),f}[n] \triangleq \beta \mathbf{q}_l^{(g),f}[n-1] + (1-\beta)\mathbf{q}_l^{(g)}[n], \quad (6.122)$$

where

$$\mathbf{q}_l^{(g)}[n] \triangleq \mathbf{q} \left(\hat{\mu}_{\theta,l}^{(g)}[n] \right). \quad (6.123)$$

In addition, $\mathbf{d}_k(\hat{\sigma}_{\theta,l}^{(g)})$ is the product of the square root of the k^{th} eigenvalue and its corresponding eigenvector of the matrix $\mathbf{D}(\hat{\sigma}_{\theta,l}^{(g)})$, as in (6.91). After constructing $\mathbf{S}_m^{(g)}[n]$ for $m = 1, \dots, M^{(g)}$, $\mathbf{S}^{(g)}[n]$ is obtained as shown in (3.1).

In Figure 6.9, it is seen that the angular profile obtained from the angular estimator is patched first. Then, recursive filtering and quantization operations are performed on the power levels of the patches, without constructing the CCM. Resulting patch power levels of MPCs are combined to obtain the total observation power levels, as in (6.45). Then, the inverse term is updated according to the patch powers which are different

than the previous ones. This method has three parameters: β from the recursive filtering of the patch power levels and the steering vector, k from the quantizer, and r from the reduced-rank expression \mathbf{D}_r of the matrix \mathbf{D} in Woodbury inverter.

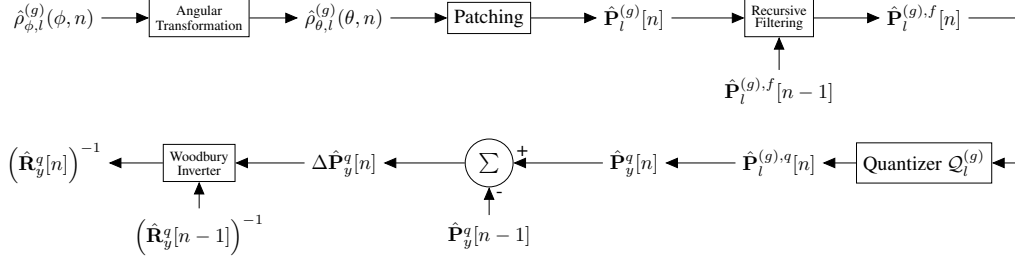


Figure 6.9: Adaptive analog beamformer construction

6.6.3 Whitening Filter Type Analog Beamformer

This filter is a variant of the Wiener filter type analog beamformer. Wiener filter type beamformer takes the whole observation as interference, using the inverse of $\hat{\mathbf{R}}_y^q[n]$. In Section 3.1.1, it is shown that whole observation correlation matrix and the MPC-specific interference covariance matrix can be taken as the interference matrix interchangeably, using them in the second place of the matrix pair to perform generalized eigendecomposition while constructing the GEB. However, GEB takes the CCM of the intended MPC as a whole for the intended part. Wiener filter type adaptive analog beamformer takes only some eigenvectors of the intended MPC for the intended signal. It might cause the suppression of the remaining eigenvectors of the intended MPC, which are present in the whole observation CCM. Therefore, this method excludes the components of the intended signal from the matrix whose inverse is taken. For this method, $\mathbf{S}_m^{(g)}[n]$ is constructed as

$$\mathbf{S}_m^{(g)}[n] = \left(\hat{\mathbf{R}}_{\eta,l}^{(g),q}[n] \right)^{-1} \left[\left(\mathbf{q}_l^{(g),f}[n] \odot \mathbf{d}_1(\hat{\sigma}_{\theta,l}^{(g)}) \right) \quad \dots \quad \left(\mathbf{q}_l^{(g),f}[n] \odot \mathbf{d}_{d_m^{(g)}}(\hat{\sigma}_{\theta,l}^{(g)}) \right) \right], \quad (6.124)$$

where $\left(\hat{\mathbf{R}}_{\eta,l}^{(g),q}[n] \right)^{-1}$ is obtained from $\left(\hat{\mathbf{R}}_y^q[n] \right)^{-1}$ through the block Woodbury inverter. In this case, the update input $\Delta \mathbf{P}[n]$ is equal to $-E_s^{(g)} K_g \hat{\mathbf{P}}_l^{(g),q}[n]$. That is, it can be thought that either the block Woodbury inverter is used twice, or the update power level matrices are merged together and the block is used once.

6.6.4 LMS Type Analog Beamformer

LMS (Least Mean Squares) filter is an adaptive filter which is mostly used for equalization purposes in communication systems. It mimics an unknown filter, which is the channel, in a training phase where the input signal is known, by trying to decrease the mean square error between the actual output and the synthetic one. In each iteration, the previous filter coefficients of the synthetic filter are updated in the direction in which the steepest descend in the mean square error occurs.

This adaptive analog beamformer construction method inspired from the LMS filter and aims to increase the SINR (Signal to interference-plus-noise ratio) at the output of the analog beamformer, in a similar way LMS decreases the mean square error. The gradient increasing the SINR is found, and the columns from the previous beamformer are updated by adding a vector in the direction that increases the SINR. It is assumed that GEB with recursive filtering in Section 6.6.1 is applied in the first time instance and this method is used to update it in next time instances. In addition, it operates on recursively filtered CCMs.

Consider the n^{th} time instance in which the analog beamformer $\mathbf{S}^{(g)}[n-1]$ will be updated to obtain $\mathbf{S}^{(g)}[n]$, which is constructed using the recursively filtered CCMs of MPCs $\hat{\mathbf{R}}_l^{(g),f}[n-1]$. Let this beamformer aim to select only one of the MPCs of a group and reject the other MPCs of this group besides those belonging to all inter-groups. Then, the covariance matrix of the interference and noise is $\hat{\mathbf{R}}_{\eta,l}^{(g),f}[n-1]$. If $\mathbf{x}[n-1]$ is a column in the $\mathbf{S}^{(g)}[n-1]$ which governs the RF chain which is reserved for the MPC in the delay l , the SINR at the output of this RF chain is

$$\gamma = \mathcal{R} \left(\hat{\mathbf{R}}_l^{(g),f}[n-1], \hat{\mathbf{R}}_{\eta,l}^{(g),f}[n-1], \mathbf{x}[n-1] \right) \quad (6.125)$$

where

$$\mathcal{R}(\mathbf{A}, \mathbf{B}, \mathbf{w}) \triangleq \frac{\mathbf{w}^H \mathbf{A} \mathbf{w}}{\mathbf{w}^H \mathbf{B} \mathbf{w}}. \quad (6.126)$$

In the next time instance, assume that the channel has changed, so the covariance matrices. However, assume that the analog beamformer for the RF chain has not been updated yet. The SINR in this case is

$$\gamma = \mathcal{R} \left(\hat{\mathbf{R}}_l^{(g),f}[n], \hat{\mathbf{R}}_{\eta,l}^{(g),f}[n], \mathbf{x}[n-1] \right). \quad (6.127)$$

The gradient is the derivative of the expression $\mathcal{R}(\mathbf{A}, \mathbf{B}, \mathbf{w})$ with respect to the vector \mathbf{w} , and it is found as

$$\frac{\partial \mathcal{R}(\mathbf{A}, \mathbf{B}, \mathbf{w})}{\partial \mathbf{w}} = \frac{2\mathbf{A}\mathbf{w}(\mathbf{w}^H \mathbf{B}\mathbf{w}) - 2\mathbf{B}\mathbf{w}(\mathbf{w}^H \mathbf{A}\mathbf{w})}{(\mathbf{w}^H \mathbf{B}\mathbf{w})^2} \quad (6.128)$$

in Appendix A.

Therefore, the update vector obtained from the gradient of the SINR term is

$$\mathbf{y}[n] = \frac{\partial \mathcal{R}(\hat{\mathbf{R}}_l^{(g),f}[n], \hat{\mathbf{R}}_{\eta,l}^{(g),f}[n], \mathbf{x}[n-1])}{\partial \mathbf{x}[n-1]}. \quad (6.129)$$

This gradient indicates the direction that brings the maximum increase in SINR when approached towards with an infinitesimal step from the position indicated by $\mathbf{x}[n-1]$ in N -dimensional space. Therefore, the beamformer matrix can be updated as

$$\mathbf{x}[n] = \mathbf{x}[n-1] + \mu \mathbf{y}[n] \quad (6.130)$$

where μ is a predetermined step size. However, this process can be performed more than one time as iterations inside the current time instance. Denoting the iteration index as a superscript, the starting point for the next time instance $\mathbf{x}^{(0)}[n] = \mathbf{x}[n-1]$.

Then,

$$\mathbf{x}^{(m)}[n] = \mathbf{x}^{(m-1)}[n] + \mu \mathbf{y}^{(m)}[n]. \quad (6.131)$$

for $m = 1, \dots, M$, where

$$\mathbf{y}^{(m)}[n] \triangleq \frac{\partial \mathcal{R}(\hat{\mathbf{R}}_l^{(g),f}[n], \hat{\mathbf{R}}_{\eta,l}^{(g),f}[n], \mathbf{x}^{(m-1)}[n])}{\partial \mathbf{x}^{(m-1)}[n]}. \quad (6.132)$$

After a predetermined number of iteration M , the result is assumed as the new beamformer vector as

$$\mathbf{x}[n] = \mathbf{x}^{(M)}[n]. \quad (6.133)$$

Note that the gradient is taken on a *a priori* SINR expression. Then the update vector is determined. Considering the output of the m^{th} iteration in the n^{th} time instance $\mathbf{x}^{(m)}[n]$, there is also an *a posteriori* SINR expression, which is given as

$$\gamma = \mathcal{R}(\hat{\mathbf{R}}_l^{(g),f}[n], \hat{\mathbf{R}}_{\eta,l}^{(g),f}[n], \mathbf{x}^{(m)}[n]) \quad (6.134)$$

$$= \mathcal{R}(\hat{\mathbf{R}}_l^{(g),f}[n], \hat{\mathbf{R}}_{\eta,l}^{(g),f}[n], \mathbf{x}^{(m-1)}[n] + \mu \mathbf{y}^{(m)}[n]), \quad (6.135)$$

$$= \frac{(\mathbf{x}^{(m-1)}[n] + \mu \mathbf{y}^{(m)}[n])^H \hat{\mathbf{R}}_l^{(g),f}[n] (\mathbf{x}^{(m-1)}[n] + \mu \mathbf{y}^{(m)}[n])}{(\mathbf{x}^{(m-1)}[n] + \mu \mathbf{y}^{(m)}[n])^H \hat{\mathbf{R}}_{\eta,l}^{(g),f}[n] (\mathbf{x}^{(m-1)}[n] + \mu \mathbf{y}^{(m)}[n])} \quad (6.136)$$

The only unknown is the step size μ . When the derivative of SINR with respect to μ is taken and equated to zero, a μ value that maximizes the SINR, only for the selected update vector, is found. This problem has a solution with very complex expression, but using the fact that the previous beamformer selects the signals represented by the CCM $\mathbf{R}_l^{(g)}[n]$ and rejects the signals represented by $\mathbf{R}_{\eta,l}^{(g)}[n]$ to the best of its ability, there are terms that are expected to be dominant than others. Then, the SINR-maximizing step size is approximately found as

$$\mu^{(m)}[n] = -\frac{\text{Re} \left\{ (\mathbf{x}^{(m-1)}[n])^H \mathbf{R}_{\eta,l}^{(g)}[n] \mathbf{y}^{(m)}[n] \right\}}{(\mathbf{y}^{(m)}[n])^H \mathbf{R}_{\eta,l}^{(g)}[n] \mathbf{y}^{(m)}[n]} \quad (6.137)$$

This adaptive step size is used in the update as

$$\mathbf{x}^{(m)}[n] = \mathbf{x}^{(m-1)}[n] + \mu^{(m)}[n] \mathbf{y}^{(m)}[n]. \quad (6.138)$$

This adaptive beamformer construction method has one design parameter, which is the number of iterations M . For each of column of the beamformer matrix $\mathbf{S}^{(g)}[n-1]$, this procedure is done starting from $\mathbf{x}^{(0)}[n] = \mathbf{x}[n-1]$ and finally $\mathbf{x}[n] = \mathbf{x}^{(M)}[n]$ is found. Then $\mathbf{S}^{(g)}[n]$ is reconstructed by placing the updated beamformer vectors into their respective columns.

6.7 Complexity Analysis

In previous sections, a lot of processing stages are explained and the proposed analog beamformer construction methods require the usage of all. Among these construction steps, the computational complexity of the matrix inverse in (6.77) in the Woodbury inverter block is considered to be dominant against others. Therefore, the size of this matrix inversion operation $N_{\Delta p} r$ is taken as the complexity measure of the proposed Wiener filter type analog beamformer construction.

For the whitening filter type analog beamformer construction, the conversion from $(\hat{\mathbf{R}}_y^g[n])^{-1}$ to $(\hat{\mathbf{R}}_{\eta,l}^{(g),q}[n])^{-1}$ should be considered too. Therefore, its complexity measure is taken as $(N_{\Delta p} + N_{p,l}^{(g)}) r$, where $N_{p,l}^{(g)}$ is the number of nonzero patches of the CCM of the group g in the delay l .

The complexity measure of the LMS type adaptive construction method is taken as M . It was taken as the inverse size for previous methods. The equivalence comes from the fact that the updates of the inverse matrices in previous methods can be performed by iterations so that only one-rank is updated at a time. Therefore, instead of taking an inverse at one time, previous methods can also be performed with a number of iterations which is equal to the size of matrix inversion, without needing any matrix inverse in those iterations. In addition, these iterations have a similar forms in terms of computation. Therefore, the number of iterations and matrix inversion size are assumed to be equivalent in terms of computational complexity, and the complexity measure of the LMS type method is taken as M .

The GEB method utilizes a generalized eigendecomposition operation on matrices of size $N \times N$. It is seen from the research on the algorithms used for this operation, such as Lanczos algorithm, that they employ a matrix inverse operation on the input matrices [33]. Therefore, the complexity measure of the GEB method is taken as N , the size of the covariance matrices.

6.8 Numerical Results

In this section, some numerical results will be given about the topics discussed in this chapter; namely, mobility in the channel and adaptive analog beamformer construction methods. The scenario in Chapter 5 will be used whose details can be seen in Table 5.1. The results are generally for the first group, assuming perfect instantaneous channel estimation, 30 dB input SNR and mobility parameter $\sigma_v = 3^\circ$ (which is the asymptotic AoA standard deviation through (6.7)), unless otherwise stated.

First of all, the movement created by the mobile channel model given in Section 6.2 can be observed in Figure 6.10 for $\alpha = 0.9, 0.99, 0.999, 0.9999$. It is seen that the CCMs move faster with smaller α , but around the starting point because the movement process is stationary in the mean as shown in (6.6). It is seen that the CCMs can move to become on top of each other. In these time intervals, grouping should be remade but this topic is out of scope of this thesis. As a result, the grouping stays the same and some fading will be seen for these intervals in the next figures.

Secondly, the estimated angle of arrivals $\hat{\mu}_{\phi,l}^{(g)}$ are shown in Figure 6.11 for $\alpha = 0.999$ with $\sigma_{est} = 0.1, 0.5, 1, 2$. The true movement is the same as the one in Figure 6.10, so that they can be compared. These α and σ_{est} values will be used in the next figures.

In Figure 6.12, the performance of the GEB method combined with the recursive filtering is given. The recursive filtering approach is actively used in the cases of $\beta = 0.5$ and $\beta = 0.9$. The $\beta = 0$ case corresponds to the GEB method without recursive filtering. It is seen that the bias in the angular estimation seriously affects the performance when recursive filtering is not used, while recursive filtering approach brings a remarkable robustness.

The next figures will show the time average performances. Figure 6.13 involves the response of the performance to the mobility parameter α , for selected β and σ_{est} parameters. The horizontal axis constructed as $-\log_{10}(1 - \alpha)$, considering the interested region of values this parameter takes. It corresponds to the interval between $\alpha = 1 - 10^{-0.5} = 0.684$ (fast channel) and $\alpha = 1 - 10^{-5} = 0.99999$ (slow channel). It is seen that the performance generally drops as the mobility gets faster. It is also seen that the usage of recursive filtering should be avoided when there is a fast channel and the angular estimation is successful. When the channel is slow and the estimation is not perfect, recursive filtering approach is undoubtedly the better option because the last estimation is not trustworthy and previous information can be used since the channel is slow and AoA are highly correlated in time.

The change of performance against the recursive filtering parameter β is given in Figure 6.14. When subplots are compared focusing on the more accurate angular estimate curves with $\sigma_{est} = 0.1$, it is seen that the usage of recursive filtering in fast channels decreases the performance, while the parameter β does not differ the performance in a wide range for slow channels.

When the angular estimation accuracy decreases (as σ_{est} increases), an optimum value for the β parameter starts to be apparent in related curves. For $\sigma_{est} = 2$, the optimum value is the most apparent and it is about $\beta = 0.5$.

The change of performance against the standard deviation of the angular estimation error σ_{est} is given in Figure 6.15. The vulnerability against estimation errors that

is subjected when recursive filtering is not used can be seen in the figure. On the other hand, the recursive filtering method is seen to bring a robustness against angular estimation errors. In addition, it is also seen in the first subplot that recursive filtering is not helpful for very fast channels, if the estimation is not erroneous.

Experiments for probability of outage were conducted for Figures 6.16 and 6.17, in which input SNR is held at 30 dB and output SINR below 20 dB is assumed as outage. It is seen from these figures that outage due to high channel estimation error can be decreased via proposed recursive filtering scheme. However, the presence of an optimum value should be noted. In addition, in very small channel estimation error cases, it is seen that the proposed method should be avoided. Finally, it is seen once more that a large β value should be used for large σ_{est} , and vice versa.

For the complexity analysis, complexity measure is calculated as $N_{\Delta p}r$ and $(N_{\Delta p} + N_{p,l}^{(g)})r$ for the Wiener filter type and whitening filter type methods, respectively. r is a design variable. A Monte Carlo analysis performed for $N_{\Delta p}$, which is dependent on the mobility of the channel. The results are given in Tables 6.1, 6.2 and 6.3. It is seen that the change in the quantized patch power levels are greater with faster channels, larger estimation errors and more detailed quantization, as expected. On the other hand, the usage of the recursive filtering with large β parameter is seen to decrease the change remarkably. However, this decrease is beneficial only if it does not bring a significant decrease in the performance.

For the whitening filter type method, $N_{p,l}^{(g)}$ is taken as 3, which is consistent with the angular spreads given for the scenario in Table 5.1. For complexity and performance comparison of the proposed adaptive methods, Figures 6.18, 6.19 and 6.20 are prepared. Since neither of complexity and performance is a design variable for Wiener type and whitening type adaptive analog beamformer construction methods, they are scatter plots, where each dot or marker indicates a beamformer type designed with a selected set of parameters.

In the plots, marker triplets of same shape and color have the same effective rank r for the matrix \mathbf{D} , for Wiener and whitening filter types. The three markers in those triplets differ in the quantization depth k given in (6.40), (6.41) and (6.42). The leftmost is always for $k = 1$, the rightmost is for $k = 4$ and the one in between is

for $k = 2$. For the LMS type method, the complexity measure is equal to the number of iterations and it is a design variable. Markers for the LMS type method are given for 2, 5, 10, 20, 50 and 100 iterations. For GEB methods, the complexity is taken as $N = 100$, as explained before.

The set of basis values 0.99, 0.9 and 0.5 are selected for the parameters α , β and σ_{est} , respectively. Then, in each figure, three scatter plots are given where only the one of the parameters varies from the basis values, while others are same. In each figure, the effect of the varying parameter will be seen.

In Figure 6.18, there are three plots for 0.9, 0.99 and 0.999 values of α parameter, which governs the channel mobility rate. Generally, the left and upper part of the plots shows the effective methods, which decrease the complexity without a significant decrease in the performance. The plot (b) belongs to the selected set of parameters. It is seen that $r = 1$ does not give good results in terms of performance. When r change is followed for 2,3 and 4 for the same filter type; in other words, when the yellow, red and blue markers are followed for the same marker type, it is seen that red and blue markers are increasing in terms of complexity but stay almost the same in terms of performance. Therefore, $r = 2$ seems as the optimum selection in terms of efficiency. When Wiener and whitening filters are observed for the same r and quantization depth; in other words, dots and crosses are compared for the same color and same position in the triplets, it is seen that the whitening Filter increases performance by increasing the complexity. LMS type adaptive construction immediately achieves high output SINR with extremely low complexity but does not improve further. Positions of the GEB methods and the cluster of proposed adaptive methods show that the proposed methods promises remarkable decrease in the complexity while not losing much from the performance.

Looking to graphs (a), (b) and (c) in the same figure, it is seen that when the channel mobility increases, adaptive methods experience a decrease in the performance and an increase in the complexity, and vice versa. However, the graph (a) belongs to the case where $\alpha = 0.9$, which is the fastest channel that is considered in this chapter. Also, there are some markers whose vertical decrease is limited, for example the whitening filter with $r = 2$ and $k = 2$. It is 4 dB below the best GEB solution that works with

estimated CCMs even in the fastest case, which is GEB without recursive filtering indicated with black cross, while still providing a significant complexity decrease. In other cases, its output SINR loss is around 1 dB.

In Figure 6.19, the effect of the recursive filtering parameter β is shown. It is seen that small β values significantly increases the complexity measure, which is related with the change rate of the patch power levels. It was shown in previous figures that β parameter has an apparent optimum value only for some cases, which is about 0.5. For most of the cases, there is a wide range of β values that can be selected without experiencing a significant difference in the performance. Then, for the complexity of the adaptive methods, it is concluded that the β value should be chosen around 0.9 if there is no reason to do otherwise.

The effect of erroneous AoA estimations is seen in Figure 6.20. It is seen that it results in both a decrease in the performance and increase in the complexity. But the whitening filter with $r = 2$ and $k = 2$ seems to preserve the performance given by the best GEB method that works with the estimated CCMs, while providing a low complexity measure around 16, for the case in which $\sigma_{est} = 2$.

It is seen from Figures 6.18, 6.19 and 6.20 that the GEB method for the analog beam-former design, whose advantages are mentioned in the previous chapter, can be replaced by a lower complexity adaptive method without losing from its performance level. Note that these adaptive methods are inspired from the GEB method. They are proposed as a result of the modifications performed on the GEB method and channel covariance matrices.

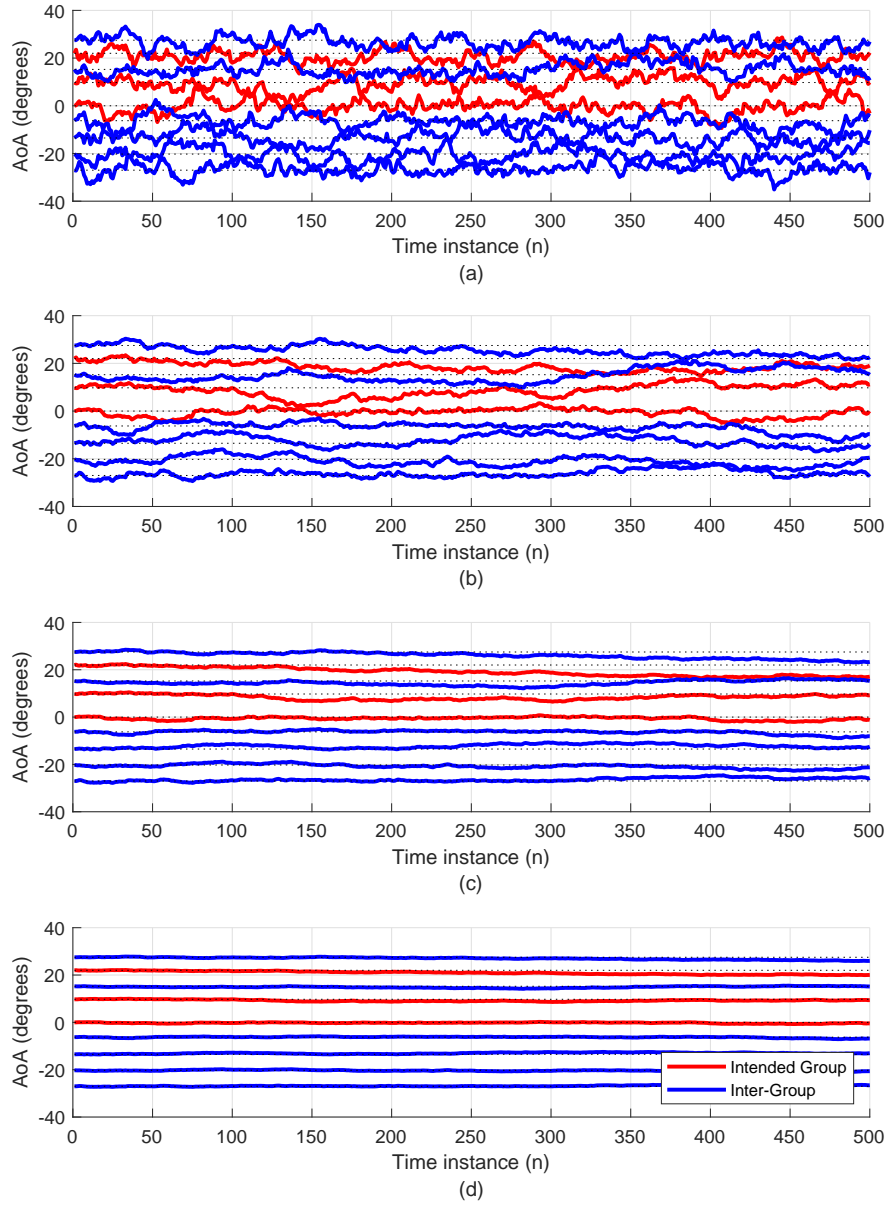


Figure 6.10: Angular Movement of the MPCs. (a) $\alpha = 0.9$. (b) $\alpha = 0.99$. (c) $\alpha = 0.999$. (d) $\alpha = 0.9999$.

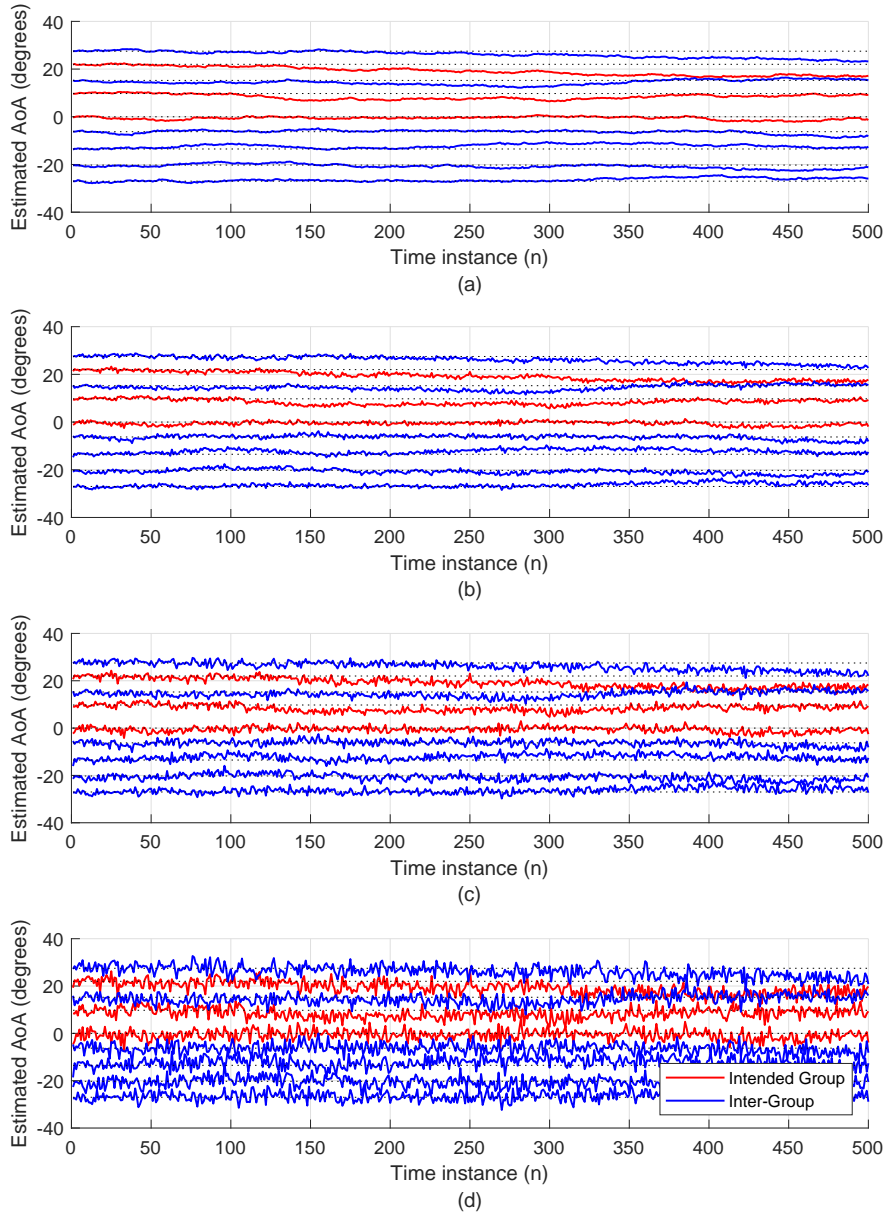


Figure 6.11: Estimated Angular positions of the MPCs for $\alpha = 0.999$. (a) $\sigma_{est} = 0.1$. (b) $\sigma_{est} = 0.5$. (c) $\sigma_{est} = 1$. (d) $\sigma_{est} = 2$.

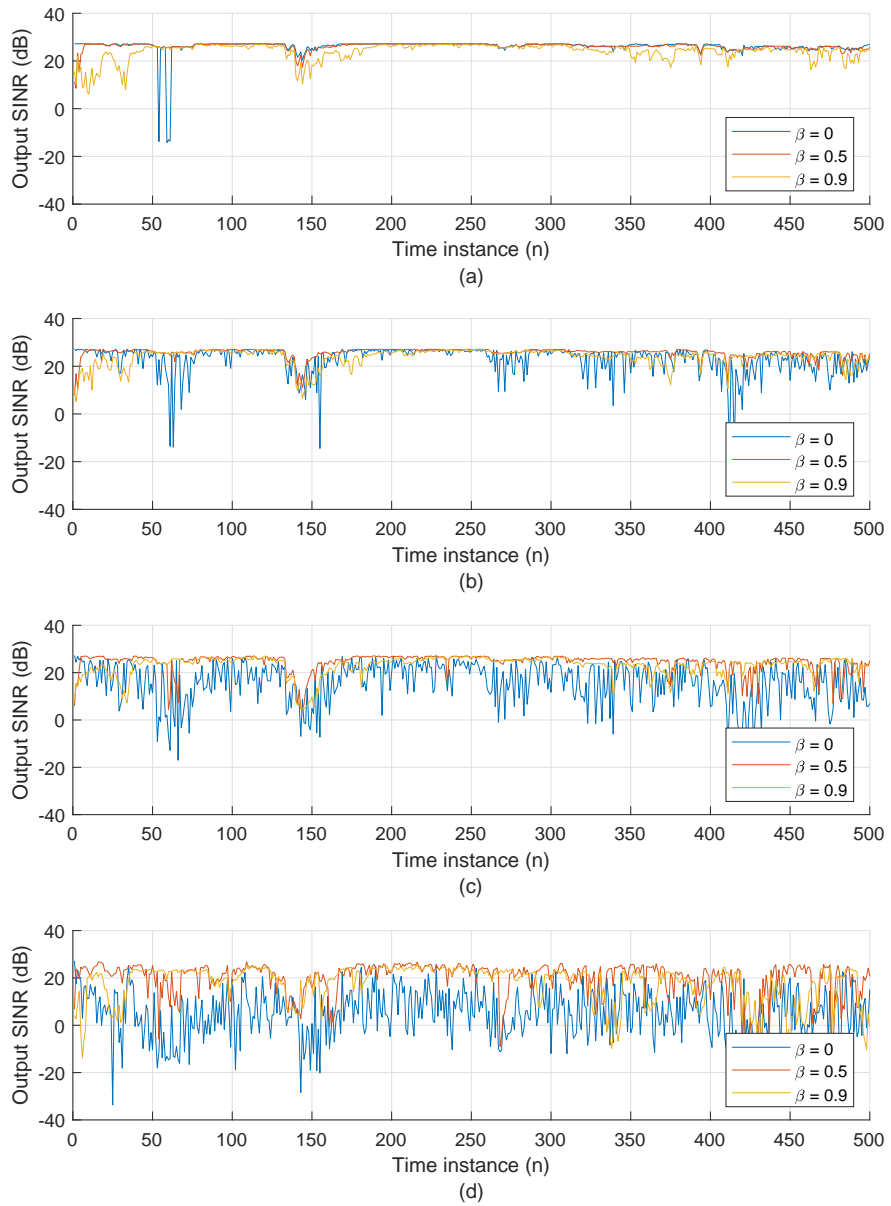


Figure 6.12: The performance of the recursive filtering combined with GEB for the mobile channel with $\alpha = 0.999$. (a) $\sigma_{est} = 0.1$. (b) $\sigma_{est} = 0.5$. (c) $\sigma_{est} = 1$. (d) $\sigma_{est} = 2$.

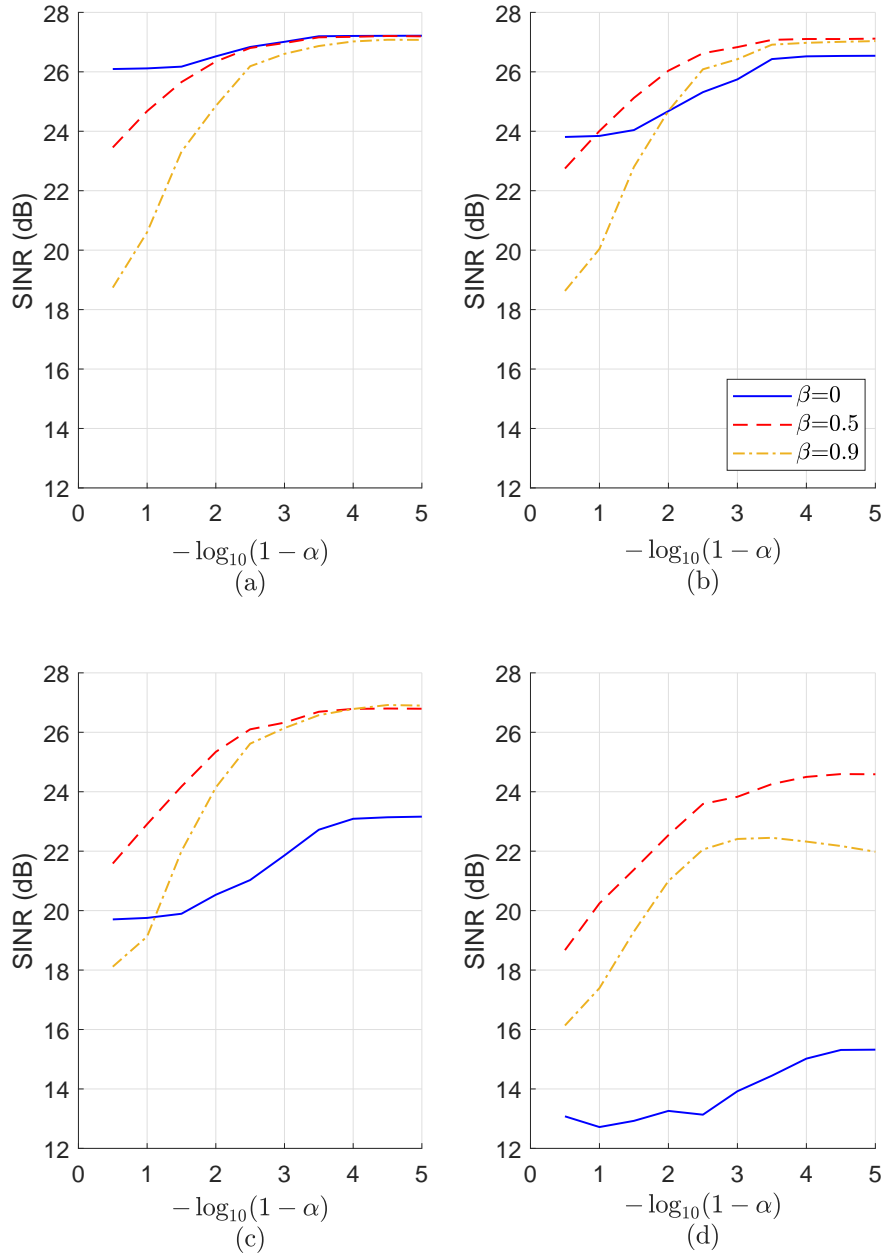


Figure 6.13: Performance against channel mobility index α . (a) $\sigma_{est} = 0.1$. (b) $\sigma_{est} = 0.5$. (c) $\sigma_{est} = 1$. (d) $\sigma_{est} = 2$.

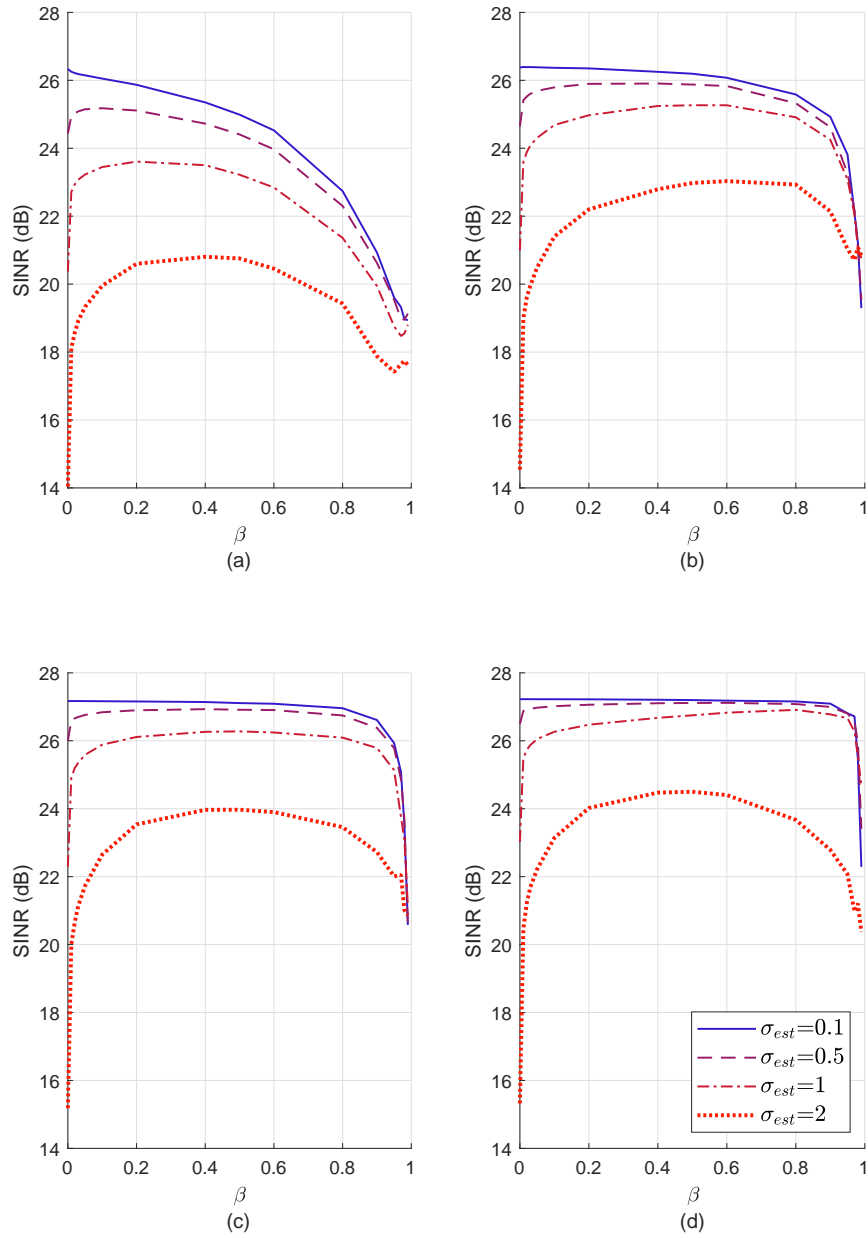


Figure 6.14: Performance against recursive filtering parameter β . (a) $\alpha = 0.9$. (b) $\alpha = 0.99$. (c) $\alpha = 0.999$. (d) $\alpha = 0.9999$.

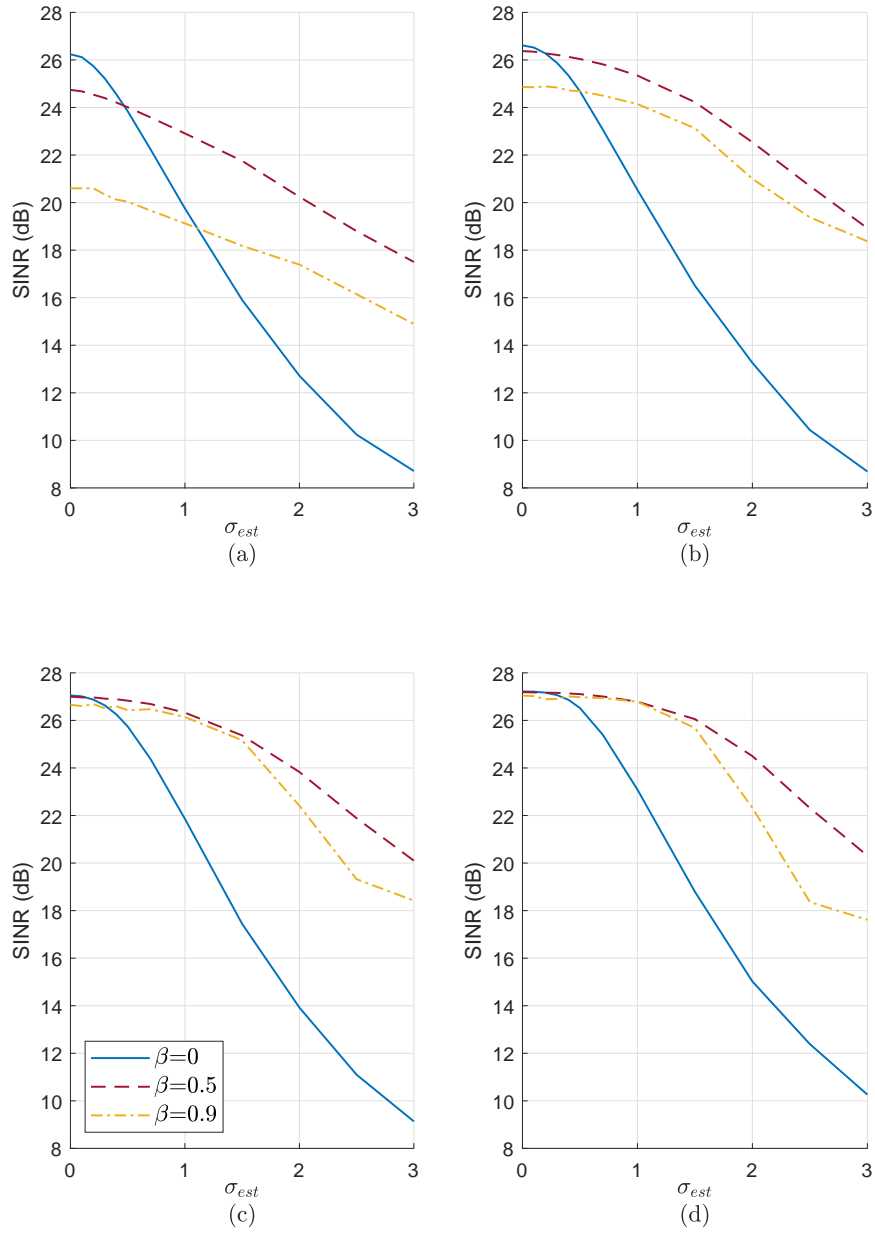


Figure 6.15: Performance against standard deviation of the channel estimation error σ_{est} . (a) $\alpha = 0.9$. (b) $\alpha = 0.99$. (c) $\alpha = 0.999$. (d) $\alpha = 0.9999$.

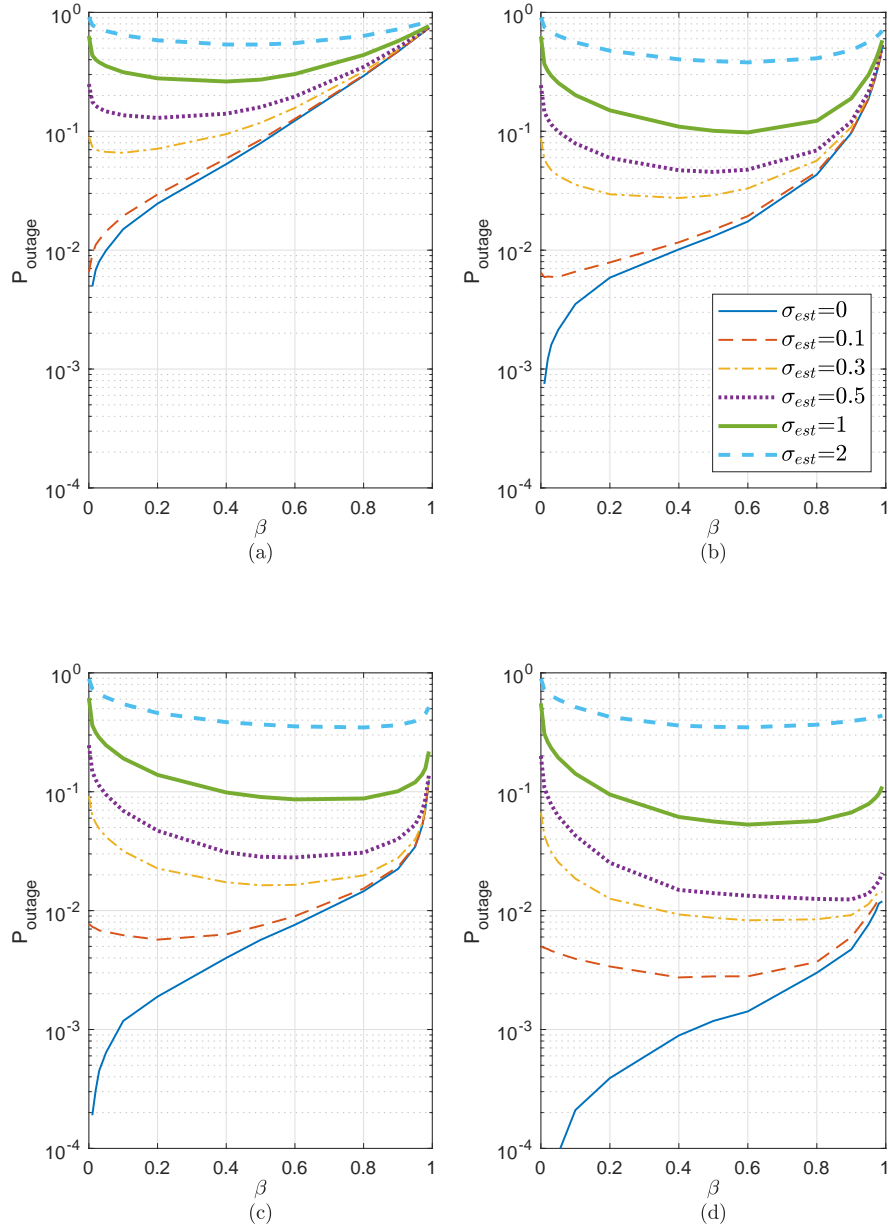


Figure 6.16: Change of probability of outage with recursive filtering parameter β . (a) $\alpha = 0.9$. (b) $\alpha = 0.99$. (c) $\alpha = 0.999$. (d) $\alpha = 0.9999$.

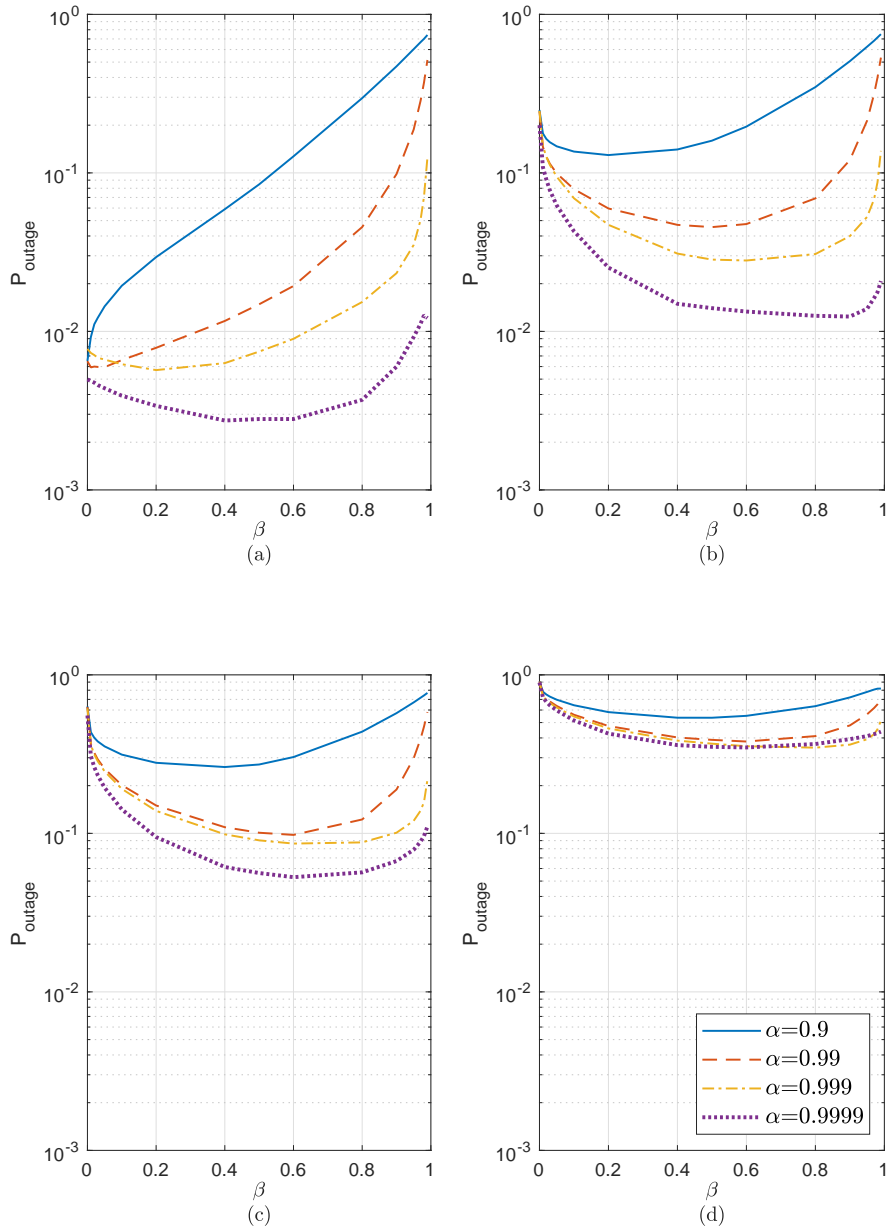


Figure 6.17: Change of probability of outage with recursive filtering parameter β . (a) $\sigma_{est} = 0.1$. (b) $\sigma_{est} = 0.5$. (c) $\sigma_{est} = 1$. (d) $\sigma_{est} = 2$.

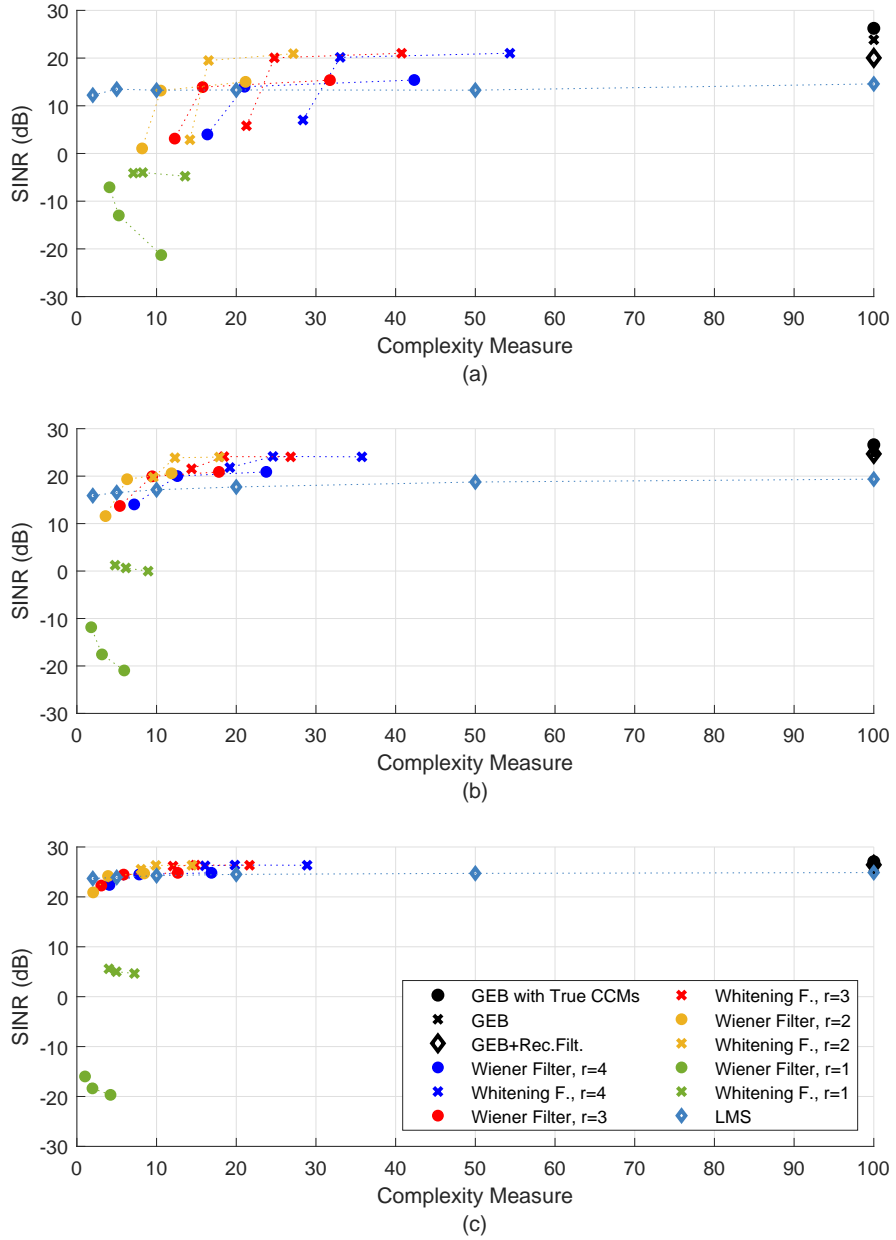


Figure 6.18: Comparison of complexity and performance of different methods for $\beta = 0.9$ and $\sigma_{est} = 0.5$. (a) $\alpha = 0.9$. (b) $\alpha = 0.99$. (c) $\alpha = 0.999$.

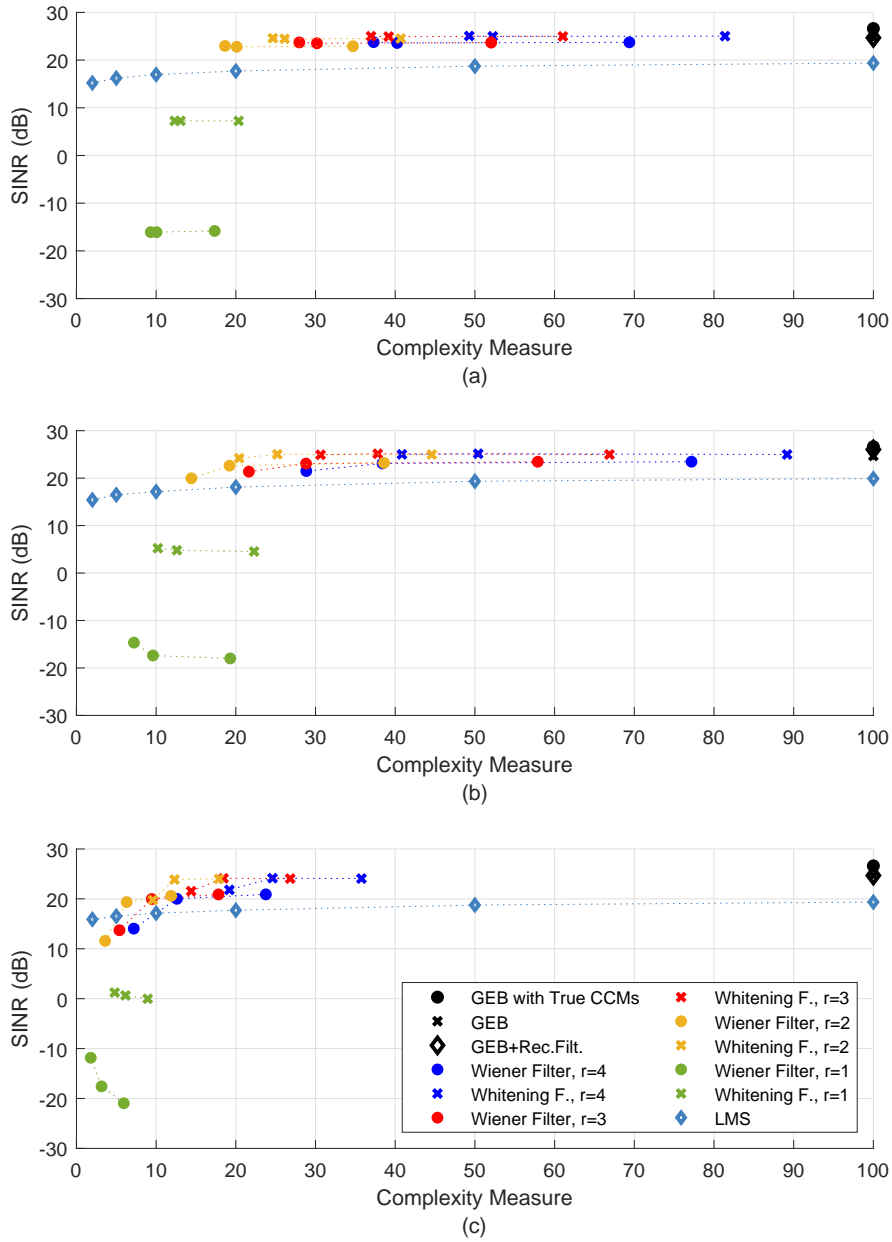


Figure 6.19: Comparison of complexity and performance of different methods for $\alpha = 0.99$ and $\sigma_{est} = 0.5$. (a) $\beta = 0$. (b) $\beta = 0.5$. (c) $\beta = 0.9$.

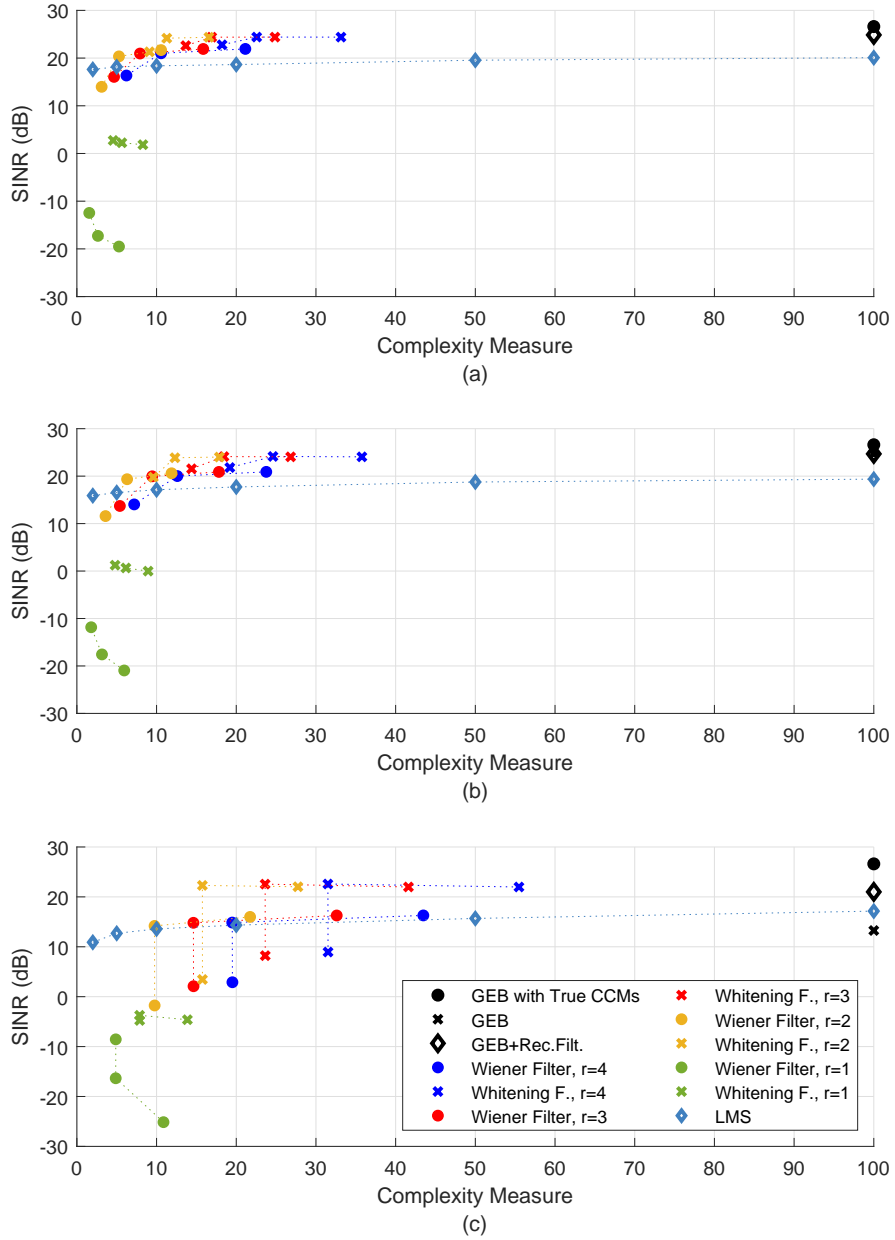


Figure 6.20: Comparison of complexity and performance of different methods for $\alpha = 0.99$ and $\beta = 0.9$. (a) $\sigma_{est} = 0.1$. (b) $\sigma_{est} = 0.5$. (c) $\sigma_{est} = 2$.

Table 6.1: Average number of changes in the quantized patch power levels for quantization parameter 1

α	0.9			0.99			0.999			0.9999		
β	0	0.5	0.9	0	0.5	0.9	0	0.5	0.9	0	0.5	0.9
$\sigma_{est} = 0$	14.84	12.46	3.93	4.98	3.96	1.5	1.59	1.21	0.48	0.52	0.4	0.16
$\sigma_{est} = 0.1$	14.78	12.57	3.97	5.19	4.15	1.55	2.29	1.63	0.5	1.77	1.15	0.26
$\sigma_{est} = 0.3$	15.36	12.95	4.03	6.9	5.3	1.63	5.16	3.63	0.71	4.89	3.43	0.56
$\sigma_{est} = 0.5$	16.51	13.86	4.09	9.32	7.21	1.8	8.17	5.94	1.02	8.22	5.88	0.9
$\sigma_{est} = 1$	20.35	16.89	4.44	16.16	12.77	2.58	15.67	12	1.93	15.68	12.35	1.88
$\sigma_{est} = 2$	27.62	22.17	4.51	26.44	21.03	4.88	26.2	21.09	4.62	26.73	21.31	4.52

Table 6.2: Average number of changes in the quantized patch power levels for quantization parameter 2

α	0.9			0.99			0.999			0.9999		
β	0	0.5	0.9	0	0.5	0.9	0	0.5	0.9	0	0.5	0.9
$\sigma_{est} = 0$	15.42	17.14	5.18	5.77	6.35	2.64	1.95	1.86	0.86	0.61	0.58	0.26
$\sigma_{est} = 0.1$	15.36	17.18	5.13	5.96	6.58	2.64	2.8	2.43	0.97	2.17	1.47	0.39
$\sigma_{est} = 0.3$	15.89	17.6	5.17	7.71	7.78	2.87	5.93	5	1.4	5.65	4.57	1.05
$\sigma_{est} = 0.5$	17.02	18.28	5.26	10.06	9.6	3.15	8.95	7.62	1.96	9.05	7.46	1.78
$\sigma_{est} = 1$	20.78	20.62	5.39	16.69	14.98	4.05	16.22	13.72	3.32	16.21	14.16	3.2
$\sigma_{est} = 2$	27.87	25.74	6.75	26.73	23.71	4.87	26.48	23.63	4.72	27	23.78	4.62

Table 6.3: Average number of changes in the quantized patch power levels for quantization parameter 4

α	0.9			0.99			0.999			0.9999		
β	0	0.5	0.9	0	0.5	0.9	0	0.5	0.9	0	0.5	0.9
$\sigma_{est} = 0$	21.79	26.96	10.35	13.42	15.07	5.21	5.62	6.29	2.46	2.06	2.22	0.86
$\sigma_{est} = 0.1$	21.75	27.07	10.29	13.58	15.45	5.29	7.68	8.44	2.59	6.25	6.42	1.49
$\sigma_{est} = 0.3$	22.13	27.43	10.37	15.46	17.15	5.53	13.83	14.45	3.54	13.75	14.12	3.02
$\sigma_{est} = 0.5$	22.92	28.34	10.58	17.35	19.29	5.94	16.32	17.87	4.22	17.65	17.79	3.86
$\sigma_{est} = 1$	25.91	31.38	11.19	22.91	25.49	7.41	22.52	23.6	6.19	22.51	25.19	6.15
$\sigma_{est} = 2$	31.4	37.69	12.65	30.49	35.3	10.87	30.21	35.6	10.56	31.22	36.04	10.55

CHAPTER 7

CONCLUSIONS

In this thesis, design methods for analog and digital stages of hybrid beamformer and instantaneous channel estimator in reduced-dimension subspace are given from Chapters 2 to 4, together with a static channel model. In Chapter 5, performances of these design methods are assessed in the static scenario, with metrics of AIR and output SINR covering the whole system performance. For the analog beamformer, it is seen that the proposed generalized eigen-beamformer (GEB) outperforms the conventional DFT beamformer, with its abilities of ISI mitigation and inter-group interference rejection, which enables the multiplexing of inter-group users. For the digital beamformer, a spatio-temporal matched filtering scheme is offered, named as CMF. It is seen that it successfully combines the delayed multipaths of the intended group and cooperates with the analog beamformer in ISI mitigation. For multiple intra-group users, proposed SZF filter is shown to perform better than TDMA utilization in high SNR and low number of intra-group users. For instantaneous channel estimation, it is seen that well-known MMSE estimator and the proposed low-complexity BA-LS method perform almost equally. Their performances converge to that of the perfect channel knowledge case with very short lengths of training. In addition, they are shown to outperform the conventional LS estimator when short training length is used. For estimation of the angular (long-term) properties of the channel, a design method is not proposed. However, the needed accuracy level for angular estimates is tested with given errors. It is seen that the system is vulnerable against a bias in the estimation, while it is tolerant to errors in estimates of the angular spread. All these assessments generally assumed 2,3 or 4 RF chains per group (It was taken as the minimum of the number of MPCs and users in a group). It shows the level of decrease of RF chains compared to the fully digital beamformer.

In Chapter 6, movements are added to each MPC and channel is mobilized through a correlated movement model in time. In addition, erroneous estimates of mean AoA are assumed. A recursive filtering approach is proposed against the erroneous estimates, benefiting from the correlation of the true angular positions of MPCs in time. It is seen that, recursive filtering approach decreases variations of the performance and prevents outages. Then, analytical modifications on the construction of GEB and structure of CCMs are made, aiming to reduce complexity of constructing GEB, which requires generalized eigendecomposition each time. Firstly, for MPCs for narrow angular spread, it is found that generalized eigendecomposition operation can be modified so that it fits in the structure of Wiener and whitening filters. Then, a method utilizing Woodbury matrix identity is proposed to adaptively update the matrix inversions in the structure of these filters. Their complexity is found to be dependent on the parameters of the mobile channel, such as their performances. Then, another method inspired from LMS filter is proposed, with a gradient based operation and a step size adaptation. The efficiencies of these methods are compared with standard GEB construction on the performance versus complexity graphs. It is seen that there are bunch of realizations of these methods (differing in selection of parameters) that are similar in performance but lower in complexity. GEB was shown to be very successful in static case, but its complexity of construction was disregarded in Chapter 5. Its modified versions for mobile channel can be used in mobility without the concern of computational complexity.

This thesis assumes that angular estimations, power levels and amount of delays are all given. Also, it studies on the scenarios where users are perfectly grouped. In addition, there might be constraints on phase shifters and attenuators in the analog beamformer. Angular power profile estimation, grouping algorithms and design of analog beamformer under constraints might be the subjects of the future work.

REFERENCES

- [1] J. G. Andrews, S. Buzzi, W. Choi, S. V. Hanly, A. Lozano, A. C. K. Soong, and J. C. Zhang, “What will 5G be?,” *IEEE Journal on Selected Areas in Communications*, vol. 32, pp. 1065–1082, June 2014.
- [2] A. Adhikary, E. A. Safadi, M. K. Samimi, R. Wang, G. Caire, T. S. Rappaport, and A. F. Molisch, “Joint spatial division and multiplexing for mm-wave channels,” *IEEE Journal on Selected Areas in Communications*, vol. 32, pp. 1239–1255, June 2014.
- [3] T. S. Rappaport, S. Sun, R. Mayzus, H. Zhao, Y. Azar, K. Wang, G. N. Wong, J. K. Schulz, M. Samimi, and F. Gutierrez, “Millimeter wave mobile communications for 5G cellular: It will work!,” *IEEE Access*, vol. 1, pp. 335—349, May 2013.
- [4] A. F. Molisch, V. V. Ratnam, S. Han, Z. Li, S. L. H. Nguyen, L. Li, and K. Haneda, “Hybrid beamforming for massive MIMO: A survey,” *IEEE Communications Magazine*, vol. 55, no. 9, pp. 134–141, 2017.
- [5] Z. Li, S. Han, S. Sangodoyin, R. Wang, and A. F. Molisch, “Joint optimization of hybrid beamforming for multi-user massive MIMO downlink,” *IEEE Transactions on Wireless Communications*, vol. 17, pp. 3600–3614, June 2018.
- [6] A. Adhikary, J. Nam, J. Y. Ahn, and G. Caire, “Joint spatial division and multiplexing: The large-scale array regime,” *IEEE Transactions on Information Theory*, vol. 59, pp. 6441–6463, October 2013.
- [7] J. Nam, A. Adhikary, J. Y. Ahn, and G. Caire, “Joint spatial division and multiplexing: Opportunistic beamforming, user grouping and simplified downlink scheduling,” *IEEE Journal of Selected Topics in Signal Processing*, vol. 8, pp. 876—890, October 2014.
- [8] D. Kim, G. Lee, and Y. Sung, “Two-stage beamformer design for massive

- MIMO downlink by trace quotient formulation,” *IEEE Transactions on Communications*, vol. 63, pp. 2200–2211, June 2015.
- [9] G. M. Guvensen and E. Ayanoglu, “A generalized framework on beamformer design and CSI acquisition for single-carrier massive MIMO systems in millimeter wave channels,” in *IEEE Globecom Workshops (GC Wkshps)*, pp. 1–7, 2016.
- [10] J. Chen and D. Gesbert, “Joint user grouping and beamforming for low complexity massive MIMO systems,” in *IEEE International Workshop on Signal Processing Advances in Wireless Communications (SPAWC)*, 2016.
- [11] E. G. Larsson, O. Edfors, F. Tufvesson, and T. L. Marzetta, “Massive MIMO for next generation wireless systems,” *IEEE Communications Magazine*, vol. 52, pp. 186–195, February 2014.
- [12] L. You, X. Gao, A. L. Swindlehurst, and W. Zhong, “Channel acquisition for massive MIMO-OFDM with adjustable phase shift pilots,” *IEEE Transactions on Signal Processing*, vol. 64, pp. 1461–1476, March 2016.
- [13] W. U. Bajwa, A. Sayeed, and R. Nowak, “Sparse multipath channels: Modeling and estimation,” *IEEE 13th Digital Signal Processing Workshop*, pp. 320–325, January 2009.
- [14] Z. Chen and C. Yang, “Pilot decontamination in wideband massive MIMO systems by exploiting channel sparsity,” *IEEE Transactions on Wireless Communications*, vol. 15, pp. 5087–5100, July 2016.
- [15] A. Ghosh, T. A. Thomas, M. C. Cudak, R. Ratasuk, P. Moorut, F. W. Vook, T. S. Rappaport, G. R. MacCartney, S. Sun, and S. Nie, “Millimeter-wave enhanced local area systems: A high-data-rate approach for future wireless networks,” *IEEE Journal on Selected Areas in Communications*, vol. 32, pp. 1152–1163, June 2014.
- [16] A. L. Swindlehurst, E. Ayanoglu, P. Heydari, and F. Capolino, “Millimeter-wave massive MIMO: The next wireless revolution?,” *IEEE Communications Magazine*, vol. 52, pp. 56–62, September 2014.

- [17] A. Pitarokoilis, S. K. Mohammed, and E. G. Larsson, "On the optimality of single-carrier transmission in large-scale antenna systems," *IEEE Wireless Communications Letters*, vol. 1, pp. 276–279, August 2012.
- [18] J. Jose, A. Ashikhmin, T. L. Marzetta, and S. Vishwanath, "Pilot contamination and precoding in multi-cell TDD systems," *IEEE Transactions on Wireless Communications*, vol. 10, pp. 2640—2651, August 2011.
- [19] A. Alkhateeb, O. E. Ayach, G. Leus, and R. W. Heath, "Channel estimation and hybrid precoding for millimeter wave cellular systems," *IEEE Journal of Selected Topics in Signal Processing*, vol. 8, pp. 831—846, October 2014.
- [20] L. You, X. Gao, X. G. Xia, N. Ma, and Y. Peng, "Pilot reuse for massive MIMO transmission over spatially correlated rayleigh fading channels," *IEEE Transactions on Wireless Communications*, vol. 14, pp. 3352—3366, June 2015.
- [21] X. Rao and V. K. N. Lau, "Distributed compressive CSIT estimation and feedback for FDD multi-user massive MIMO systems," *IEEE Transactions on Signal Processing*, vol. 62, p. 3261–3271, June 2014.
- [22] J. C. Shen, J. Zhang, E. Alsusa, and K. B. Letaief, "Compressed CSI acquisition in FDD massive MIMO: How much training is needed?," *IEEE Transactions on Wireless Communications*, vol. 15, pp. 4145–4156, June 2016.
- [23] J. Chen and V. K. N. Lau, "Two-tier precoding for FDD multi-cell massive MIMO time-varying interference networks," *IEEE Journal on Selected Areas in Communications*, vol. 32, pp. 1230—1238, June 2014.
- [24] O. E. Ayach, S. Rajagopal, S. Abu-Surra, Z. Pi, and R. W. Heath, "Spatially sparse precoding in millimeter wave MIMO systems," *IEEE Transactions on Wireless Communications*, vol. 13, pp. 1499—1513, March 2014.
- [25] A. Liu and V. Lau, "Phase only RF precoding for massive MIMO systems with limited RF chains," *IEEE Transactions on Signal Processing*, vol. 62, pp. 4505—4515, September 2014.
- [26] S. Noh, M. D. Zoltowski, and D. J. Love, "Training sequence design for feedback assisted hybrid beamforming in massive MIMO systems," *IEEE Transactions on Communications*, vol. 64, pp. 187—200, January 2016.

- [27] C. Zhang, D. Guo, and P. Fan, “Tracking angles of departure and arrival in a mobile millimeter wave channel,” in *IEEE International Conference on Communications (ICC)*, 2016.
- [28] V. Va, H. Vikalo, and R. W. Heath, “Beam tracking for mobile millimeter wave communication systems,” in *IEEE Global Conference on Signal and Information Processing (GlobalSIP)*, 2016.
- [29] S. Jayaprakasam, X. Ma, J. W. Choi, and S. Kim, “Robust beam-tracking for mmWave mobile communications,” *IEEE Communications Letters*, vol. 21, pp. 2654–2657, December 2017.
- [30] H. Yu, Y. Sung, H. Kim, and Y. H. Lee, “Beam tracking for interference alignment in slowly fading MIMO interference channels: A perturbations approach under a linear framework,” *IEEE Transactions on Signal Processing*, vol. 60, pp. 1910–1926, April 2012.
- [31] A. Kurt and G. M. Guvensen, “An efficient hybrid beamforming and channel acquisition for wideband mm-wave massive MIMO channels,” in *IEEE International Conference on Communications (ICC)*, 2019.
- [32] S. M. Kay, *Fundamentals of Statistical Signal Processing, Vol. I - Estimation Theory*. Prentice Hall, 1993.
- [33] Z. Bai, J. Demmel, J. Dongarra, A. Ruhe, and H. van der Vorst, eds., *Templates for the Solution of Algebraic Eigenvalue Problems: A Practical Guide*. Philadelphia: SIAM, 2000.

Appendix A

GENERALIZED HERMITIAN EIGENDECOMPOSITION

Let \mathbf{A} and \mathbf{B} be two Hermitian matrices of size N . In addition, assume that \mathbf{B} is also a positive-definite matrix. The generalized eigenvector \mathbf{v}_k and the generalized eigenvalue λ_k of the matrix pair (\mathbf{A}, \mathbf{B}) satisfy

$$\mathbf{A}\mathbf{v}_k = \lambda_k\mathbf{B}\mathbf{v}_k, \quad (\text{A.1})$$

$$\mathbf{v}_k^H \mathbf{A} \mathbf{v}_{k'} = \lambda_k \delta_{kk'}, \quad (\text{A.2})$$

and

$$\mathbf{v}_k^H \mathbf{B} \mathbf{v}_{k'} = \delta_{kk'}. \quad (\text{A.3})$$

Another representation would involve all the eigenvalue and eigenvector pairs in the main diagonal of an eigenvalue matrix $\mathbf{\Lambda}$ and in the columns of an eigenvector matrix \mathbf{V} , respectively. That is,

$$\mathbf{\Lambda} \triangleq \begin{bmatrix} \lambda_1 & 0 & \cdots & 0 \\ 0 & \lambda_2 & \cdots & 0 \\ \vdots & \vdots & \ddots & \vdots \\ 0 & 0 & \cdots & \lambda_N \end{bmatrix}, \quad (\text{A.4})$$

and

$$\mathbf{V} \triangleq \begin{bmatrix} \mathbf{v}_1 & \mathbf{v}_2 & \cdots & \mathbf{v}_N \end{bmatrix}. \quad (\text{A.5})$$

In this way, the above relations given in (A.1), (A.2) and (A.3) can be equivalently expressed as

$$\mathbf{A}\mathbf{V} = \mathbf{B}\mathbf{V}\mathbf{\Lambda}, \quad (\text{A.6})$$

$$\mathbf{V}^H \mathbf{A} \mathbf{V} = \mathbf{\Lambda}, \quad (\text{A.7})$$

and

$$\mathbf{V}^H \mathbf{B} \mathbf{V} = \mathbf{I}_N. \quad (\text{A.8})$$

Generalized Hermitian eigendecomposition is performed generally by transforming the problem to the standard Hermitian eigendecomposition problem by using decompositions on the matrix \mathbf{B} (such as Cholesky decomposition), making some arrangements on the expression so that it fits into the standard Eigenvalue problem, finding the congruent eigenvalue-eigenvector pairs and finally transforming them back into the sought pairs [33]. Therefore, most of the known methods and algorithms for standard Hermitian eigenvalue problem have variants for the generalized case. Some of these methods are the power method, Lanczos method and Jacobi-Davidson methods. As a practical engineering tool, the MATLAB functions *eig* and *eigs* can calculate the generalized eigenvalues and eigenvectors.

A.1 A Congruence Related with Generalized Eigen-pairs

Add $\alpha\lambda_k \mathbf{A} \mathbf{v}_k$ to the both sides of (A.1).

$$(1 + \alpha\lambda_k) \mathbf{A} \mathbf{v}_k = \lambda_k (\mathbf{B} + \alpha \mathbf{A}) \mathbf{v}_k \quad (\text{A.9})$$

Then, divide both sides by $(1 + \alpha\lambda_k)$ to get

$$\mathbf{A} \mathbf{v}_k = \frac{\lambda_k}{(1 + \alpha\lambda_k)} (\mathbf{B} + \alpha \mathbf{A}) \mathbf{v}_k \quad (\text{A.10})$$

It resembles to the eigendecomposition structure in (A.1), with generalized eigenvalue $\frac{\lambda_k}{(1 + \alpha\lambda_k)}$, generalized eigenvector \mathbf{v}_k and the matrix pair $(\mathbf{A}, \mathbf{B} + \alpha \mathbf{A})$. However, check the conditions in (A.2) and (A.3).

$$\mathbf{v}_k^H \mathbf{A} \mathbf{v}_{k'} = \lambda_k \delta_{kk'}, \quad (\text{A.11})$$

$$\mathbf{v}_k^H (\mathbf{B} + \alpha \mathbf{A}) \mathbf{v}_{k'} = (1 + \alpha\lambda_k) \delta_{kk'}. \quad (\text{A.12})$$

It is seen that they are not satisfied. Then, define

$$\mathbf{y}_k \triangleq \frac{1}{\sqrt{1 + \alpha\lambda_k}} \mathbf{v}_k. \quad (\text{A.13})$$

Dividing both sides of (A.10) by $\sqrt{1 + \alpha\lambda_k}$,

$$\mathbf{A}\mathbf{y}_k = \frac{\lambda_k}{(1 + \alpha\lambda_k)} (\mathbf{B} + \alpha\mathbf{A}) \mathbf{y}_k \quad (\text{A.14})$$

is obtained. Checking the conditions in (A.2) and (A.3),

$$\mathbf{y}_k^H \mathbf{A} \mathbf{y}_{k'} = \frac{\lambda_k}{(1 + \alpha\lambda_k)} \delta_{kk'}, \quad (\text{A.15})$$

$$\mathbf{y}_k^H (\mathbf{B} + \alpha\mathbf{A}) \mathbf{y}_{k'} = \delta_{kk'}; \quad (\text{A.16})$$

it is seen that all the conditions are satisfied. It is shown that, if λ_k and \mathbf{v}_k are the generalized eigenvalue and eigenvectors of the matrix pair (\mathbf{A}, \mathbf{B}) ; then $\frac{\lambda_k}{(1 + \alpha\lambda_k)}$ and $\frac{1}{\sqrt{1 + \alpha\lambda_k}} \mathbf{v}_k$ are the generalized eigenvalue and eigenvectors of the matrix pair $(\mathbf{A}, \mathbf{B} + \alpha\mathbf{A})$. In addition, the derivative of the new eigenvalue with respect to the old eigenvalue

$$\frac{\partial}{\partial \lambda_k} \left(\frac{\lambda_k}{(1 + \alpha\lambda_k)} \right) = \frac{1}{(1 + \alpha\lambda_k)^2} \quad (\text{A.17})$$

is nonnegative. It means that if the old eigenvalue and eigenvector pairs have descending or ascending order, it holds also for the new pairs.

A.2 The Relation with Rayleigh Quotient

Rayleigh quotient is

$$\mathcal{R}(\mathbf{w}) = \frac{\mathbf{w}^H \mathbf{A} \mathbf{w}}{\mathbf{w}^H \mathbf{B} \mathbf{w}} \quad (\text{A.18})$$

where \mathbf{w} is a column vector of length N . Note that $\mathcal{R}(\mathbf{w})$, $\mathbf{w}^H \mathbf{A} \mathbf{w}$ and $\mathbf{w}^H \mathbf{B} \mathbf{w}$ are scalar values. The derivative of the Rayleigh quotient with respect to the vector \mathbf{w} becomes zero when \mathbf{w} is equal to one of the generalized eigenvectors of the matrix pair (\mathbf{A}, \mathbf{B}) . The derivative of the scalar $\mathcal{R}(\mathbf{w})$ with respect to \mathbf{w} , which is a vector, means

$$\frac{\partial \mathcal{R}(\mathbf{w})}{\partial \mathbf{w}} = \left[\frac{\partial \mathcal{R}(\mathbf{w})}{\partial w_1} \quad \frac{\partial \mathcal{R}(\mathbf{w})}{\partial w_2} \quad \dots \quad \frac{\partial \mathcal{R}(\mathbf{w})}{\partial w_N} \right]^T \quad (\text{A.19})$$

where w_k is the k^{th} entry of the vector \mathbf{w} . Then, it is straightforward to write

$$\frac{\partial \mathcal{R}(\mathbf{w})}{\partial \mathbf{w}} = \frac{\left(\frac{\partial}{\partial \mathbf{w}} \mathbf{w}^H \mathbf{A} \mathbf{w} \right) (\mathbf{w}^H \mathbf{B} \mathbf{w}) - \left(\frac{\partial}{\partial \mathbf{w}} \mathbf{w}^H \mathbf{B} \mathbf{w} \right) (\mathbf{w}^H \mathbf{A} \mathbf{w})}{(\mathbf{w}^H \mathbf{B} \mathbf{w})^2}. \quad (\text{A.20})$$

It is known from the matrix calculus that

$$\frac{\partial}{\partial \mathbf{w}} \mathbf{w}^H \mathbf{X} \mathbf{w} = 2\mathbf{X}\mathbf{w} \quad (\text{A.21})$$

for an arbitrary Hermitian matrix of size N . Applying this,

$$\frac{\partial \mathcal{R}(\mathbf{w})}{\partial \mathbf{w}} = \frac{2\mathbf{A}\mathbf{w} (\mathbf{w}^H \mathbf{B}\mathbf{w}) - 2\mathbf{B}\mathbf{w} (\mathbf{w}^H \mathbf{A}\mathbf{w})}{(\mathbf{w}^H \mathbf{B}\mathbf{w})^2} \quad (\text{A.22})$$

is obtained. For $\frac{\partial \mathcal{R}(\mathbf{w})}{\partial \mathbf{w}} = 0$, the vector \mathbf{w} should satisfy

$$\mathbf{A}\mathbf{w} (\mathbf{w}^H \mathbf{B}\mathbf{w}) = \mathbf{B}\mathbf{w} (\mathbf{w}^H \mathbf{A}\mathbf{w}). \quad (\text{A.23})$$

On the other hand, the generalized eigenvector \mathbf{v}_k and the generalized eigenvalue λ_k of the matrix pair (\mathbf{A}, \mathbf{B}) satisfy

$$\mathbf{A}\mathbf{v}_k = \lambda_k \mathbf{B}\mathbf{v}_k, \quad (\text{A.24})$$

$$\mathbf{v}_k^H \mathbf{A}\mathbf{v}_{k'} = \lambda_k \delta_{kk'}, \quad (\text{A.25})$$

and

$$\mathbf{v}_k^H \mathbf{B}\mathbf{v}_{k'} = \delta_{kk'}. \quad (\text{A.26})$$

With this information, when the generalized eigenvector \mathbf{v}_k is substituted on the left hand side of (A.23),

$$\mathbf{A}\mathbf{v}_k (\mathbf{v}_k^H \mathbf{B}\mathbf{v}_k) = \mathbf{A}\mathbf{v}_k \quad (\text{A.27})$$

is obtained. When it is substituted on the right hand side of (A.23),

$$\mathbf{B}\mathbf{v}_k (\mathbf{v}_k^H \mathbf{A}\mathbf{v}_k) = \lambda_k \mathbf{B}\mathbf{v}_k \quad (\text{A.28})$$

is obtained. It is seen that the two are equal according to the definition of generalized eigendecomposition, and the generalized eigenvector \mathbf{v}_k satisfies (A.23). Therefore, it is concluded that the generalized eigenvector \mathbf{v}_k of the matrix pair (\mathbf{A}, \mathbf{B}) makes the derivative of the Rayleigh quotient given in (A.18) zero. Also note that, when a generalized eigenvector is substituted in the Rayleigh quotient, the result is the corresponding eigenvalue as shown below.

$$\mathcal{R}(\mathbf{v}_k) = \frac{\mathbf{v}_k^H \mathbf{A}\mathbf{v}_k}{\mathbf{v}_k^H \mathbf{B}\mathbf{v}_k} = \frac{\lambda_k}{1}, \quad (\text{A.29})$$

$$\mathcal{R}(\mathbf{v}_k) = \lambda_k. \quad (\text{A.30})$$

Appendix B

DERIVATION OF ANALYTICAL EXPRESSIONS FOR SIGNAL POWERS AT THE OUTPUT OF THE CHANNEL MATCHED FILTER

B.1 Components in the Channel Matched Filter Output

From (3.12),

$$\mathbf{r}_n^{(g)} = \sum_{l=-(L-1)}^{L-1} \mathbf{R}_l^{\hat{h}h} \mathbf{x}_{n-l}^{(g)} + \sum_{l=0}^{L-1} \left[\hat{\mathbf{H}}_{eff,l}^{(g)} \right]^H \boldsymbol{\eta}_{eff,n+l}^{(g)} \quad (\text{B.1})$$

where the first addend comes from the intended group and the second is the sum of inter-group interference and noise. The second can be separated into two as

$$\sum_{l=0}^{L-1} \left[\hat{\mathbf{H}}_{eff,l}^{(g)} \right]^H \boldsymbol{\eta}_{eff,n+l}^{(g)} = \sum_{l=0}^{L-1} \left[\hat{\mathbf{H}}_{eff,l}^{(g)} \right]^H [\mathbf{S}^{(g)}]^H \boldsymbol{\eta}_{n+l}^{(g)} \quad (\text{B.2})$$

$$\begin{aligned} &= \sum_{l=0}^{L-1} \mathbf{e}_k^H \left[\hat{\mathbf{H}}_{eff,l}^{(g)} \right]^H [\mathbf{S}^{(g)}]^H \boldsymbol{\xi}_{n+l}^{(g)} \\ &+ \sum_{l=0}^{L-1} \mathbf{e}_k^H \left[\hat{\mathbf{H}}_{eff,l}^{(g)} \right]^H [\mathbf{S}^{(g)}]^H \mathbf{n}_{n+l} \end{aligned} \quad (\text{B.3})$$

The k^{th} entry of the vector $\mathbf{r}_n^{(g)}$ belongs to the k^{th} user. Select it with the selection vector \mathbf{e}_k as

$$r_n^{(gk)} = \mathbf{e}_k^H \mathbf{r}_n^{(g)} \quad (\text{B.4})$$

$$\begin{aligned} r_n^{(gk)} &= \underbrace{\sum_{l=-(L-1)}^{L-1} \mathbf{e}_k^H \mathbf{R}_l^{\hat{h}h} \mathbf{x}_{n-l}^{(g)}}_{\text{Intended Group (IG)}} \\ &+ \underbrace{\sum_{l=0}^{L-1} \mathbf{e}_k^H \left[\hat{\mathbf{H}}_{eff,l}^{(g)} \right]^H [\mathbf{S}^{(g)}]^H \boldsymbol{\xi}_{n+l}^{(g)}}_{\text{Inter-Group Interference (IGI)}} + \underbrace{\sum_{l=0}^{L-1} \mathbf{e}_k^H \left[\hat{\mathbf{H}}_{eff,l}^{(g)} \right]^H [\mathbf{S}^{(g)}]^H \mathbf{n}_{n+l}}_{\text{Noise}} \end{aligned} \quad (\text{B.5})$$

At the first glance, the output belonging to the k^{th} user includes components from the intended group, inter-group and noise. The intended group term can also be separated into its components.

$$\underbrace{\sum_{l=-(L-1)}^{L-1} \mathbf{e}_k^H \mathbf{R}_l^{\hat{h}h} \mathbf{x}_{n-l}^{(g)}}_{\text{Intended Group (IG)}} = \underbrace{\sum_{l=-(L-1)}^{L-1} \mathbf{e}_k^H \mathbf{R}_l^{\hat{h}h} \mathbf{e}_k x_{n-l}^{(g_k)}}_{\text{Intended User (IU)}} + \underbrace{\sum_{l=-(L-1)}^{L-1} \sum_{\substack{k'=1 \\ k' \neq k}}^K \mathbf{e}_k^H \mathbf{R}_l^{\hat{h}h} \mathbf{e}_{k'} x_{n-l}^{(g_{k'})}}_{\text{Multi-User Interference (MUI)}} \quad (\text{B.6})$$

$$\underbrace{\sum_{l=-(L-1)}^{L-1} \mathbf{e}_k^H \mathbf{R}_l^{\hat{h}h} \mathbf{e}_k x_{n-l}^{(g_k)}}_{\text{Intended User (IU)}} = \underbrace{\mathbf{e}_k^H \mathbf{R}_0^{\hat{h}h} \mathbf{e}_k x_n^{(g_k)}}_{\text{Intended Signal+ (S+)}} + \underbrace{\sum_{\substack{l=-(L-1) \\ l \neq 0}}^{L-1} \mathbf{e}_k^H \mathbf{R}_l^{\hat{h}h} \mathbf{e}_k x_{n-l}^{(g_k)}}_{\text{Inter-Symbol Interference (ISI)}} \quad (\text{B.7})$$

$$\underbrace{\mathbf{e}_k^H \mathbf{R}_0^{\hat{h}h} \mathbf{e}_k x_n^{(g_k)}}_{\text{Intended Signal+ (S+)}} = \underbrace{\mathbf{e}_k^H \mathbf{R}_0^{\hat{h}h} \mathbf{e}_k x_n^{(g_k)}}_{\text{Intended Signal (S)}} + \underbrace{\mathbf{e}_k^H \mathbf{R}_0^{\hat{h}e} \mathbf{e}_k x_n^{(g_k)}}_{\text{Self-Interference due to Ch. Est. Error (SICEE)}}, \quad (\text{B.8})$$

where

$$\mathbf{R}_l^{\hat{h}e} = \mathbf{R}_l^{\hat{h}h} - \mathbf{R}_l^{\hat{h}\hat{h}}. \quad (\text{B.9})$$

The terms can be shown as

$$r_n^{(g_k)} = \underbrace{S + SICEE}_{S^+} + \underbrace{ISI + MUI + IGI}_{\text{Intended User (IU)}} + \text{Noise} \quad (\text{B.10})$$

Intended Group (IG)

B.2 Expression of the Power of Components in Terms of Effective Channel Matrices

The components are shown below once more in a compact way.

$$\begin{aligned}
r_n^{(g_k)} &= \underbrace{\mathbf{e}_k^H \mathbf{R}_0^{\hat{h}\hat{h}} \mathbf{e}_k x_n^{(g_k)}}_{\text{Intended Signal (S)}} + \underbrace{\mathbf{e}_k^H \mathbf{R}_0^{\hat{h}e} \mathbf{e}_k x_n^{(g_k)}}_{\text{Self-Interference due to Ch. Est. Error (SICEE)}} + \underbrace{\sum_{\substack{l=-(L-1) \\ l \neq 0}}^{L-1} \mathbf{e}_k^H \mathbf{R}_l^{\hat{h}h} \mathbf{e}_k x_{n-l}^{(g_k)}}_{\text{Inter-Symbol Interference (ISI)}} \\
&+ \underbrace{\sum_{l=-(L-1)}^{L-1} \sum_{\substack{k'=1 \\ k' \neq k}}^K \mathbf{e}_k^H \mathbf{R}_l^{\hat{h}h} \mathbf{e}_{k'} x_{n-l}^{(g_{k'})}}_{\text{Multi-User Interference (MUI)}} + \underbrace{\sum_{l=0}^{L-1} \mathbf{e}_k^H \left[\hat{\mathbf{H}}_{eff,l}^{(g)} \right]^H \left[\mathbf{S}^{(g)} \right]^H \boldsymbol{\xi}_{n+l}^{(g)}}_{\text{Inter-Group Interference (IGI)}} \\
&+ \underbrace{\sum_{l=0}^{L-1} \mathbf{e}_k^H \left[\hat{\mathbf{H}}_{eff,l}^{(g)} \right]^H \left[\mathbf{S}^{(g)} \right]^H \mathbf{n}_{n+l}}_{\text{Noise}} \tag{B.11}
\end{aligned}$$

Powers of these terms are equal to expected values of the absolute squares of these terms. Note that these components are all scalars and their conjugate is equal to their Hermitian. Also, the fact that random data symbols are independent from the random channels will be used in the procedure below. In addition, $\mathbf{E}_{kk} \triangleq \mathbf{e}_k \mathbf{e}_k^H$ is the square matrix of size K , whose entry in its k^{th} row and k^{th} column is 1, and the others are all zero.

$$P_S = E \left\{ \left| \mathbf{e}_k^H \mathbf{R}_0^{\hat{h}\hat{h}} \mathbf{e}_k x_n^{(g_k)} \right|^2 \right\} \tag{B.12}$$

$$= E \left\{ \mathbf{e}_k^H \mathbf{R}_0^{\hat{h}\hat{h}} \mathbf{e}_k x_n^{(g_k)} \left[\mathbf{e}_k^H \mathbf{R}_0^{\hat{h}\hat{h}} \mathbf{e}_k x_n^{(g_k)} \right]^H \right\} \tag{B.13}$$

$$= \mathbf{e}_k^H E \left\{ \mathbf{R}_0^{\hat{h}\hat{h}} \mathbf{e}_k \left(x_n^{(g_k)} (x_n^{(g_k)})^* \right) \mathbf{e}_k^H \left[\mathbf{R}_0^{\hat{h}\hat{h}} \right]^H \right\} \mathbf{e}_k \tag{B.14}$$

$$= \mathbf{e}_k^H E \left\{ \mathbf{R}_0^{\hat{h}\hat{h}} \mathbf{E}_{kk} \left[\mathbf{R}_0^{\hat{h}\hat{h}} \right]^H \right\} \mathbf{e}_k E_s^{(g)} \tag{B.15}$$

$$\begin{aligned}
&= \mathbf{e}_k^H E \left\{ \sum_{l_1=0}^{L-1} \left[\hat{\mathbf{H}}_{eff,l_1}^{(g)} \right]^H \hat{\mathbf{H}}_{eff,l_1}^{(g)} \mathbf{E}_{kk} \right. \\
&\quad \left. \left[\sum_{l_2=0}^{L-1} \left[\hat{\mathbf{H}}_{eff,l_2}^{(g)} \right]^H \hat{\mathbf{H}}_{eff,l_2}^{(g)} \right]^H \right\} \mathbf{e}_k E_s^{(g)} \tag{B.16}
\end{aligned}$$

$$= E_s^{(g)} \sum_{l_1=0}^{L-1} \sum_{l_2=0}^{L-1} \mathbf{e}_k^H E \left\{ \left[\hat{\mathbf{H}}_{eff,l_1}^{(g)} \right]^H \hat{\mathbf{H}}_{eff,l_1}^{(g)} \mathbf{E}_{kk} \left[\hat{\mathbf{H}}_{eff,l_2}^{(g)} \right]^H \hat{\mathbf{H}}_{eff,l_2}^{(g)} \right\} \mathbf{e}_k \quad (\text{B.17})$$

$$P_{S^+} = E \left\{ \left| \mathbf{e}_k^H \mathbf{R}_0^{\hat{h}h} \mathbf{e}_k x_n^{(g_k)} \right|^2 \right\} \quad (\text{B.18})$$

$$= E \left\{ \mathbf{e}_k^H \mathbf{R}_0^{\hat{h}h} \mathbf{e}_k x_n^{(g_k)} \left[\mathbf{e}_k^H \mathbf{R}_0^{\hat{h}h} \mathbf{e}_k x_n^{(g_k)} \right]^H \right\} \quad (\text{B.19})$$

$$= \mathbf{e}_k^H E \left\{ \mathbf{R}_0^{\hat{h}h} \mathbf{e}_k \left(x_n^{(g_k)} \left(x_n^{(g_k)} \right)^* \right) \mathbf{e}_k^H \left[\mathbf{R}_0^{\hat{h}h} \right]^H \right\} \mathbf{e}_k \quad (\text{B.20})$$

$$= \mathbf{e}_k^H E \left\{ \mathbf{R}_0^{\hat{h}h} \mathbf{E}_{kk} \left[\mathbf{R}_0^{\hat{h}h} \right]^H \right\} \mathbf{e}_k E_s^{(g)} \quad (\text{B.21})$$

$$= \mathbf{e}_k^H E \left\{ \sum_{l_1=0}^{L-1} \left[\hat{\mathbf{H}}_{eff,l_1}^{(g)} \right]^H \mathbf{H}_{eff,l_1}^{(g)} \mathbf{E}_{kk} \left[\sum_{l_2=0}^{L-1} \left[\hat{\mathbf{H}}_{eff,l_2}^{(g)} \right]^H \mathbf{H}_{eff,l_2}^{(g)} \right]^H \right\} \mathbf{e}_k E_s^{(g)} \quad (\text{B.22})$$

$$= E_s^{(g)} \sum_{l_1=0}^{L-1} \sum_{l_2=0}^{L-1} \mathbf{e}_k^H E \left\{ \left[\hat{\mathbf{H}}_{eff,l_1}^{(g)} \right]^H \mathbf{H}_{eff,l_1}^{(g)} \mathbf{E}_{kk} \left[\mathbf{H}_{eff,l_2}^{(g)} \right]^H \hat{\mathbf{H}}_{eff,l_2}^{(g)} \right\} \mathbf{e}_k \quad (\text{B.23})$$

$$P_{SICEE} = E \left\{ \left| \mathbf{e}_k^H \mathbf{R}_0^{\hat{h}e} \mathbf{e}_k x_n^{(g_k)} \right|^2 \right\} \quad (\text{B.24})$$

$$= E \left\{ \mathbf{e}_k^H \mathbf{R}_0^{\hat{h}e} \mathbf{e}_k x_n^{(g_k)} \left[\mathbf{e}_k^H \mathbf{R}_0^{\hat{h}e} \mathbf{e}_k x_n^{(g_k)} \right]^H \right\} \quad (\text{B.25})$$

$$= \mathbf{e}_k^H E \left\{ \mathbf{R}_0^{\hat{h}e} \mathbf{E}_{kk} \left[\mathbf{R}_0^{\hat{h}e} \right]^H \right\} \mathbf{e}_k E_s^{(g)} \quad (\text{B.26})$$

$$= \mathbf{e}_k^H E \left\{ \left[\mathbf{R}_0^{\hat{h}h} - \mathbf{R}_0^{\hat{h}h} \right] \mathbf{E}_{kk} \left[\mathbf{R}_0^{\hat{h}h} - \mathbf{R}_0^{\hat{h}h} \right]^H \right\} \mathbf{e}_k E_s^{(g)} \quad (\text{B.27})$$

$$= P_{S^+} + P_S - \mathbf{e}_k^H E \left\{ \mathbf{R}_0^{\hat{h}h} \mathbf{E}_{kk} \left[\mathbf{R}_0^{\hat{h}h} \right]^H \right\} \mathbf{e}_k E_s^{(g)} \\ - \mathbf{e}_k^H E \left\{ \mathbf{R}_0^{\hat{h}h} \mathbf{E}_{kk} \left[\mathbf{R}_0^{\hat{h}h} \right]^H \right\} \mathbf{e}_k E_s^{(g)} \quad (\text{B.28})$$

$$= P_{S^+} + P_S - 2Re \left\{ \mathbf{e}_k^H E \left\{ \mathbf{R}_0^{\hat{h}h} \mathbf{E}_{kk} \left[\mathbf{R}_0^{\hat{h}h} \right]^H \right\} \mathbf{e}_k \right\} E_s^{(g)} \quad (\text{B.29})$$

$$= P_{S^+} + P_S - P_{CC} \quad (\text{B.30})$$

$$P_{CC} \triangleq 2Re \left\{ \mathbf{e}_k^H E \left\{ \mathbf{R}_0^{\hat{h}h} \mathbf{E}_{kk} \left[\mathbf{R}_0^{\hat{h}h} \right]^H \right\} \mathbf{e}_k \right\} E_s^{(g)} \quad (\text{B.31})$$

$$= 2Re \left\{ \mathbf{e}_k^H E \left\{ \sum_{l_1=0}^{L-1} \left[\hat{\mathbf{H}}_{eff,l_1}^{(g)} \right]^H \mathbf{H}_{eff,l_1}^{(g)} \mathbf{E}_{kk} \right. \right. \\ \left. \left. \left[\sum_{l_2=0}^{L-1} \left[\hat{\mathbf{H}}_{eff,l_2}^{(g)} \right]^H \hat{\mathbf{H}}_{eff,l_2}^{(g)} \right]^H \right\} \mathbf{e}_k \right\} E_s^{(g)} \quad (\text{B.32})$$

$$= 2Re \left\{ \sum_{l_1=0}^{L-1} \sum_{l_2=0}^{L-1} \mathbf{e}_k^H E \left\{ \left[\hat{\mathbf{H}}_{eff,l_1}^{(g)} \right]^H \mathbf{H}_{eff,l_1}^{(g)} \mathbf{E}_{kk} \left[\hat{\mathbf{H}}_{eff,l_2}^{(g)} \right]^H \hat{\mathbf{H}}_{eff,l_2}^{(g)} \right\} \mathbf{e}_k \right\} E_s^{(g)} \quad (\text{B.33})$$

$$P_{IU} = E \left\{ \left| \sum_{l=-(L-1)}^{L-1} \mathbf{e}_k^H \mathbf{R}_l^{\hat{h}h} \mathbf{e}_k x_{n-l}^{(g_k)} \right|^2 \right\} \quad (\text{B.34})$$

$$= E \left\{ \sum_{l=-(L-1)}^{L-1} \mathbf{e}_k^H \mathbf{R}_l^{\hat{h}h} \mathbf{e}_k x_{n-l}^{(g_k)} \left[\sum_{l=-(L-1)}^{L-1} \mathbf{e}_k^H \mathbf{R}_l^{\hat{h}h} \mathbf{e}_k x_{n-l}^{(g_k)} \right]^H \right\} \quad (\text{B.35})$$

$$= E \left\{ \sum_{l_a=-(L-1)}^{L-1} \sum_{l_b=-(L-1)}^{L-1} \mathbf{e}_k^H \mathbf{R}_{l_a}^{\hat{h}h} \mathbf{e}_k \left(x_{n-l_a}^{(g_k)} \left(x_{n-l_b}^{(g_k)} \right)^* \right) \mathbf{e}_k^H \left[\mathbf{R}_{l_b}^{\hat{h}h} \right]^H \mathbf{e}_k \right\} \quad (\text{B.36})$$

$$= E \left\{ \sum_{l_a=-(L-1)}^{L-1} \sum_{l_b=-(L-1)}^{L-1} \mathbf{e}_k^H \mathbf{R}_{l_a}^{\hat{h}h} \mathbf{e}_k \left(\delta_{l_a l_b} E_s^{(g)} \right) \mathbf{e}_k^H \left[\mathbf{R}_{l_b}^{\hat{h}h} \right]^H \mathbf{e}_k \right\} \quad (\text{B.37})$$

$$= \mathbf{e}_k^H E \left\{ \sum_{l=-(L-1)}^{L-1} \mathbf{R}_l^{\hat{h}h} \mathbf{E}_{kk} \left[\mathbf{R}_l^{\hat{h}h} \right]^H \right\} \mathbf{e}_k E_s^{(g)} \quad (\text{B.38})$$

$$= \mathbf{e}_k^H E \left\{ \sum_{l=-(L-1)}^{L-1} \sum_{l_1=0}^{L-1} \left[\hat{\mathbf{H}}_{eff,l_1}^{(g)} \right]^H \mathbf{H}_{eff,l+l_1}^{(g)} \mathbf{E}_{kk} \right. \\ \left. \left[\sum_{l_2=0}^{L-1} \left[\hat{\mathbf{H}}_{eff,l_2}^{(g)} \right]^H \mathbf{H}_{eff,l+l_2}^{(g)} \right]^H \right\} \mathbf{e}_k E_s^{(g)} \quad (\text{B.39})$$

$$= \sum_{l=-(L-1)}^{L-1} \sum_{l_1=0}^{L-1} \sum_{l_2=0}^{L-1} \mathbf{e}_k^H E \left\{ \left[\hat{\mathbf{H}}_{eff,l_1}^{(g)} \right]^H \mathbf{H}_{eff,l+l_1}^{(g)} \mathbf{E}_{kk} \right. \\ \left. \left[\mathbf{H}_{eff,l+l_2}^{(g)} \right]^H \hat{\mathbf{H}}_{eff,l_2}^{(g)} \right\} \mathbf{e}_k E_s^{(g)} \quad (\text{B.40})$$

$$P_{IG} = E \left\{ \left| \sum_{l=-(L-1)}^{L-1} \mathbf{e}_k^H \mathbf{R}_l^{\hat{h}h} \mathbf{x}_{n-l}^{(g)} \right|^2 \right\} \quad (\text{B.41})$$

$$= E \left\{ \sum_{l=-(L-1)}^{L-1} \mathbf{e}_k^H \mathbf{R}_l^{\hat{h}h} \mathbf{x}_{n-l}^{(g)} \left[\sum_{l=-(L-1)}^{L-1} \mathbf{e}_k^H \mathbf{R}_l^{\hat{h}h} \mathbf{x}_{n-l}^{(g)} \right]^H \right\} \quad (\text{B.42})$$

$$= E \left\{ \sum_{l_a=-(L-1)}^{L-1} \sum_{l_b=-(L-1)}^{L-1} \mathbf{e}_k^H \mathbf{R}_{l_a}^{\hat{h}h} \left(\mathbf{x}_{n-l_a}^{(g)} \left[\mathbf{x}_{n-l_b}^{(g)} \right]^H \right) \left[\mathbf{R}_{l_b}^{\hat{h}h} \right]^H \mathbf{e}_k \right\} \quad (\text{B.43})$$

$$= E \left\{ \sum_{l_a=-(L-1)}^{L-1} \sum_{l_b=-(L-1)}^{L-1} \mathbf{e}_k^H \mathbf{R}_{l_a}^{\hat{h}h} (\delta_{l_a l_b} E_s^{(g)} \mathbf{I}_N) \left[\mathbf{R}_{l_b}^{\hat{h}h} \right]^H \mathbf{e}_k \right\} \quad (\text{B.44})$$

$$= \mathbf{e}_k^H E \left\{ \sum_{l=-(L-1)}^{L-1} \mathbf{R}_l^{\hat{h}h} \left[\mathbf{R}_l^{\hat{h}h} \right]^H \right\} \mathbf{e}_k E_s^{(g)} \quad (\text{B.45})$$

$$= \mathbf{e}_k^H E \left\{ \sum_{l=-(L-1)}^{L-1} \sum_{l_1=0}^{L-1} \left[\hat{\mathbf{H}}_{eff,l_1}^{(g)} \right]^H \mathbf{H}_{eff,l+l_1}^{(g)} \right. \\ \left. \left[\sum_{l_2=0}^{L-1} \left[\hat{\mathbf{H}}_{eff,l_2}^{(g)} \right]^H \mathbf{H}_{eff,l+l_2}^{(g)} \right]^H \right\} \mathbf{e}_k E_s^{(g)} \quad (\text{B.46})$$

$$= \sum_{l=-(L-1)}^{L-1} \sum_{l_1=0}^{L-1} \sum_{l_2=0}^{L-1} \mathbf{e}_k^H E \left\{ \left[\hat{\mathbf{H}}_{eff,l_1}^{(g)} \right]^H \mathbf{H}_{eff,l+l_1}^{(g)} \right. \\ \left. \left[\mathbf{H}_{eff,l+l_2}^{(g)} \right]^H \hat{\mathbf{H}}_{eff,l_2}^{(g)} \right\} \mathbf{e}_k E_s^{(g)} \quad (\text{B.47})$$

$$P_{IGI} = E \left\{ \left| \sum_{l=0}^{L-1} \mathbf{e}_k^H \left[\hat{\mathbf{H}}_{eff,l}^{(g)} \right]^H \left[\mathbf{S}^{(g)} \right]^H \boldsymbol{\xi}_{n+l}^{(g)} \right|^2 \right\} \quad (\text{B.48})$$

$$= E \left\{ \sum_{l=0}^{L-1} \mathbf{e}_k^H \left[\hat{\mathbf{H}}_{eff,l}^{(g)} \right]^H \left[\mathbf{S}^{(g)} \right]^H \boldsymbol{\xi}_{n+l}^{(g)} \right. \\ \left. \left[\sum_{l=0}^{L-1} \mathbf{e}_k^H \left[\hat{\mathbf{H}}_{eff,l}^{(g)} \right]^H \left[\mathbf{S}^{(g)} \right]^H \boldsymbol{\xi}_{n+l}^{(g)} \right]^H \right\} \quad (\text{B.49})$$

$$= E \left\{ \sum_{l_1=0}^{L-1} \sum_{l_2=0}^{L-1} \mathbf{e}_k^H \left[\hat{\mathbf{H}}_{eff,l_1}^{(g)} \right]^H \left[\mathbf{S}^{(g)} \right]^H \boldsymbol{\xi}_{n+l_1}^{(g)} \left[\boldsymbol{\xi}_{n+l_2}^{(g)} \right]^H \mathbf{S}^{(g)} \hat{\mathbf{H}}_{eff,l_2}^{(g)} \mathbf{e}_k \right\} \quad (\text{B.50})$$

$$= \sum_{l_1=0}^{L-1} \sum_{l_2=0}^{L-1} \mathbf{e}_k^H E \left\{ \left[\hat{\mathbf{H}}_{eff,l_1}^{(g)} \right]^H \left[\mathbf{S}^{(g)} \right]^H \left[\sum_{g' \neq g} \sum_{l_3=0}^{L-1} \mathbf{H}_{l_3}^{(g')} \mathbf{x}_{n+l_1-l_3}^{(g')} \right] \right\}$$

$$\left\{ \left[\sum_{g'' \neq g} \sum_{l_4=0}^{L-1} \mathbf{H}_{l_4}^{(g'')} \mathbf{x}_{n+l_2-l_4}^{(g'')} \right]^H \mathbf{S}^{(g)} \hat{\mathbf{H}}_{eff,l_2}^{(g)} \right\} \mathbf{e}_k \quad (\text{B.51})$$

$$= \sum_{l_1=0}^{L-1} \cdots \sum_{l_4=0}^{L-1} \sum_{g' \neq g} \sum_{g'' \neq g} \mathbf{e}_k^H E \left\{ \left[\hat{\mathbf{H}}_{eff,l_1}^{(g)} \right]^H \mathbf{H}_{eff,l_3}^{(g')} \left(\delta_{g'g''} \delta_{l_1-l_2-l_3+l_4} E_s^{(g')} \mathbf{I}_N \right) \right. \\ \left. \left[\mathbf{H}_{eff,l_4}^{(g'')} \right]^H \hat{\mathbf{H}}_{eff,l_2}^{(g)} \right\} \mathbf{e}_k \quad (\text{B.52})$$

$$= \sum_{g' \neq g} E_s^{(g')} \sum_{l_1=0}^{L-1} \sum_{l_2=0}^{L-1} \sum_{l_3=0}^{L-1} \mathbf{e}_k^H E \left\{ \left[\hat{\mathbf{H}}_{eff,l_1}^{(g)} \right]^H \mathbf{H}_{eff,l_3}^{(g')} \right. \\ \left. \left[\mathbf{H}_{eff,l_3-l_1+l_2}^{(g')} \right]^H \hat{\mathbf{H}}_{eff,l_2}^{(g)} \right\} \mathbf{e}_k \quad (\text{B.53})$$

$$= \sum_{g' \neq g} E_s^{(g')} \sum_{l=-(L-1)}^{L-1} \sum_{l_1=0}^{L-1} \sum_{l_2=0}^{L-1} \mathbf{e}_k^H E \left\{ \left[\hat{\mathbf{H}}_{eff,l_1}^{(g)} \right]^H \mathbf{H}_{eff,l+l_1}^{(g')} \right. \\ \left. \left[\mathbf{H}_{eff,l+l_2}^{(g')} \right]^H \hat{\mathbf{H}}_{eff,l_2}^{(g)} \right\} \mathbf{e}_k \quad (\text{B.54})$$

$$P_{Noise} = E \left\{ \left| \sum_{l=0}^{L-1} \mathbf{e}_k^H \left[\hat{\mathbf{H}}_{eff,l}^{(g)} \right]^H \left[\mathbf{S}^{(g)} \right]^H \mathbf{n}_{n+l} \right|^2 \right\} \quad (\text{B.55})$$

$$= E \left\{ \sum_{l=0}^{L-1} \mathbf{e}_k^H \left[\hat{\mathbf{H}}_{eff,l}^{(g)} \right]^H \left[\mathbf{S}^{(g)} \right]^H \mathbf{n}_{n+l} \right. \\ \left. \left[\sum_{l=0}^{L-1} \mathbf{e}_k^H \left[\hat{\mathbf{H}}_{eff,l}^{(g)} \right]^H \left[\mathbf{S}^{(g)} \right]^H \mathbf{n}_{n+l} \right]^H \right\} \quad (\text{B.56})$$

$$= E \left\{ \sum_{l_1=0}^{L-1} \sum_{l_2=0}^{L-1} \mathbf{e}_k^H \left[\hat{\mathbf{H}}_{eff,l_1}^{(g)} \right]^H \left[\mathbf{S}^{(g)} \right]^H \mathbf{n}_{n+l_1} \left[\mathbf{n}_{n+l_2} \right]^H \mathbf{S}^{(g)} \hat{\mathbf{H}}_{eff,l_2}^{(g)} \mathbf{e}_k \right\} \quad (\text{B.57})$$

$$= \sum_{l_1=0}^{L-1} \sum_{l_2=0}^{L-1} \mathbf{e}_k^H E \left\{ \left[\hat{\mathbf{H}}_{eff,l_1}^{(g)} \right]^H \left[\mathbf{S}^{(g)} \right]^H \left(\delta_{l_1 l_2} N_0 \mathbf{I}_N \right) \mathbf{S}^{(g)} \hat{\mathbf{H}}_{eff,l_2}^{(g)} \right\} \mathbf{e}_k \quad (\text{B.58})$$

$$= N_0 \sum_{l_1=0}^{L-1} \mathbf{e}_k^H E \left\{ \left[\hat{\mathbf{H}}_{eff,l_1}^{(g)} \right]^H \left[\mathbf{S}^{(g)} \right]^H \mathbf{S}^{(g)} \hat{\mathbf{H}}_{eff,l_1}^{(g)} \right\} \mathbf{e}_k \quad (\text{B.59})$$

$$P_{IN} = P_{SICEE} + P_{ISI} + P_{MUI} + P_{IGI} + P_{Noise} \quad (\text{B.60})$$

$$= P_{S+} + P_S - P_{CC} + P_{ISI} + P_{MUI} + P_{IGI} + P_{Noise} \quad (\text{B.61})$$

$$= P_{IG} + P_{IGI} + P_{Noise} + P_S - P_{CC} \quad (\text{B.62})$$

S^+ , ISI and MUI are independent.

$$P_{ISI} = P_{IU} - P_{S^+} \quad (\text{B.63})$$

$$P_{MUI} = P_{IG} - P_{IU} \quad (\text{B.64})$$

S and SICEE are correlated.

$$S + SICEE = S^+ \quad (\text{B.65})$$

$$P_S + P_{SICEE} \neq P_{S^+} \quad (\text{B.66})$$

B.2.1 Summary

$$P_S = E_s^{(g)} \sum_{l_1=0}^{L-1} \sum_{l_2=0}^{L-1} \mathbf{e}_k^H E \left\{ \left[\hat{\mathbf{H}}_{eff,l_1}^{(g)} \right]^H \hat{\mathbf{H}}_{eff,l_1}^{(g)} \mathbf{E}_{kk} \left[\hat{\mathbf{H}}_{eff,l_2}^{(g)} \right]^H \hat{\mathbf{H}}_{eff,l_2}^{(g)} \right\} \mathbf{e}_k \quad (\text{B.67})$$

$$P_{S^+} = E_s^{(g)} \sum_{l_1=0}^{L-1} \sum_{l_2=0}^{L-1} \mathbf{e}_k^H E \left\{ \left[\hat{\mathbf{H}}_{eff,l_1}^{(g)} \right]^H \mathbf{H}_{eff,l_1}^{(g)} \mathbf{E}_{kk} \left[\mathbf{H}_{eff,l_2}^{(g)} \right]^H \hat{\mathbf{H}}_{eff,l_2}^{(g)} \right\} \mathbf{e}_k \quad (\text{B.68})$$

$$P_{CC} = 2\text{Re} \left\{ \sum_{l_1=0}^{L-1} \sum_{l_2=0}^{L-1} \mathbf{e}_k^H E \left\{ \left[\hat{\mathbf{H}}_{eff,l_1}^{(g)} \right]^H \mathbf{H}_{eff,l_1}^{(g)} \mathbf{E}_{kk} \left[\hat{\mathbf{H}}_{eff,l_2}^{(g)} \right]^H \hat{\mathbf{H}}_{eff,l_2}^{(g)} \right\} \mathbf{e}_k \right\} E_s^{(g)} \quad (\text{B.69})$$

$$P_{IU} = \sum_{l=-(L-1)}^{L-1} \sum_{l_1=0}^{L-1} \sum_{l_2=0}^{L-1} \mathbf{e}_k^H E \left\{ \left[\hat{\mathbf{H}}_{eff,l_1}^{(g)} \right]^H \mathbf{H}_{eff,l+l_1}^{(g)} \mathbf{E}_{kk} \left[\mathbf{H}_{eff,l+l_2}^{(g)} \right]^H \hat{\mathbf{H}}_{eff,l_2}^{(g)} \right\} \mathbf{e}_k E_s^{(g)} \quad (\text{B.70})$$

$$P_{IG} = \sum_{l=-(L-1)}^{L-1} \sum_{l_1=0}^{L-1} \sum_{l_2=0}^{L-1} \mathbf{e}_k^H E \left\{ \left[\hat{\mathbf{H}}_{eff,l_1}^{(g)} \right]^H \mathbf{H}_{eff,l+l_1}^{(g)} \left[\mathbf{H}_{eff,l+l_2}^{(g)} \right]^H \hat{\mathbf{H}}_{eff,l_2}^{(g)} \right\} \mathbf{e}_k E_s^{(g)} \quad (\text{B.71})$$

$$P_{IGI} = \sum_{g' \neq g} E_s^{(g')} \sum_{l=-(L-1)}^{L-1} \sum_{l_1=0}^{L-1} \sum_{l_2=0}^{L-1} \mathbf{e}_k^H E \left\{ \left[\hat{\mathbf{H}}_{eff,l_1}^{(g)} \right]^H \mathbf{H}_{eff,l+l_1}^{(g')} \left[\mathbf{H}_{eff,l+l_2}^{(g')} \right]^H \hat{\mathbf{H}}_{eff,l_2}^{(g)} \right\} \mathbf{e}_k \quad (\text{B.72})$$

$$P_{Noise} = N_0 \sum_{l_1=0}^{L-1} \mathbf{e}_k^H E \left\{ \left[\hat{\mathbf{H}}_{eff,l_1}^{(g)} \right]^H \left[\mathbf{S}^{(g)} \right]^H \mathbf{S}^{(g)} \hat{\mathbf{H}}_{eff,l_1}^{(g)} \right\} \mathbf{e}_k \quad (\text{B.73})$$

$$P_{SICEE} = P_{S^+} + P_S - P_{CC} \quad (\text{B.74})$$

$$P_{ISI} = P_{IU} - P_{S^+} \quad (\text{B.75})$$

$$P_{MUI} = P_{IG} - P_{IU} \quad (\text{B.76})$$

$$P_{IN} = P_S + P_{IG} + P_{IGI} + P_{Noise} - P_{CC} \quad (\text{B.77})$$

$$P_{ALL} = P_{IG} + P_{IGI} + P_{Noise} \quad (\text{B.78})$$

B.3 Derivation of Analytical Results for Probabilistic Terms

Let

- \mathbf{A} , \mathbf{B} , \mathbf{C} and \mathbf{D} be circularly symmetric complex normal random matrices of size $D \times K$ to represent the effective channel matrices,
- \mathbf{E} be a deterministic matrix of size $K \times K$ and diagonal as $\mathbf{E} = \text{diag} \left[\{e_k\}_{k=1}^K \right]$,
- \mathbf{F} be a deterministic matrix of size $D \times D$,
- $(\mathbf{X})_{ij}$ be the entry in the i^{th} row and j^{th} column of the matrix \mathbf{X} ,
- \mathbf{x}^k be the k^{th} column of the matrix \mathbf{X} as $\mathbf{X} = [\mathbf{x}^1, \mathbf{x}^2, \dots, \mathbf{x}^K]$,
- \mathbf{x}^k have $(\mathbf{X})_{ik}$ in its i^{th} entry as $\mathbf{x}^k = [(\mathbf{X})_{1k}, (\mathbf{X})_{2k}, \dots, (\mathbf{X})_{Dk}]^T$ and
- $\mathbf{R}_{x,y}^{k,l} \triangleq E \left\{ \mathbf{x}^k [\mathbf{y}^l]^H \right\}$.

Then, there are two types of expectation terms in the expressions in Section B.2.1. The first type is $\mathbf{e}_k^H E \left\{ \mathbf{A}^H \mathbf{F} \mathbf{B} \right\} \mathbf{e}_k$, which is seen in the noise power expression. The second type is $\mathbf{e}_k^H E \left\{ \mathbf{A}^H \mathbf{B} \mathbf{E} \mathbf{C}^H \mathbf{D} \right\} \mathbf{e}_k$, where \mathbf{A} , \mathbf{B} , \mathbf{C} and \mathbf{D} are effective channel matrices differing according to their delay, group or whether they are true matrices or estimates. In following subsections, the analytic solutions of expectations will be expressed in terms of some covariance matrices, which will be found later.

B.3.1 Expectation Type 1

$$\mathbf{e}_k^H E \left\{ \mathbf{A}^H \mathbf{F} \mathbf{B} \right\} \mathbf{e}_k = \sum_{m=1}^D \sum_{n=1}^D E \left\{ (\mathbf{A})_{mk}^* \mathbf{F}_{mn} (\mathbf{B})_{nk} \right\} \quad (\text{B.79})$$

$$= \sum_{m=1}^D \sum_{n=1}^D E \left\{ (\mathbf{A})_{mk}^* (\mathbf{B})_{nk} \right\} \mathbf{F}_{mn} \quad (\text{B.80})$$

$$= \sum_{m=1}^D \sum_{n=1}^D \left(\mathbf{R}_{b,a}^{k,k} \right)_{nm} \mathbf{F}_{mn} \quad (\text{B.81})$$

$$= \sum_{n=1}^D \left(\mathbf{R}_{b,a}^{k,k} \mathbf{F} \right)_{nn} \quad (\text{B.82})$$

$$= \text{tr} \left(\mathbf{R}_{b,a}^{k,k} \mathbf{F} \right) \quad (\text{B.83})$$

$$\boxed{\mathbf{e}_k^H E \{ \mathbf{A}^H \mathbf{F} \mathbf{B} \} \mathbf{e}_k = \text{tr} \left(\mathbf{R}_{b,a}^{k,k} \mathbf{F} \right)} \quad (\text{B.84})$$

B.3.2 Expectation Type 2

$$\begin{aligned} & \mathbf{e}_k^H E \{ \mathbf{A}^H \mathbf{B} \mathbf{E} \mathbf{C}^H \mathbf{D} \} \mathbf{e}_k \\ &= \sum_{m=1}^D \sum_{n=1}^K \sum_{p=1}^K \sum_{r=1}^D E \left\{ (\mathbf{A})_{mk}^* (\mathbf{B})_{mn} (\mathbf{E})_{np} (\mathbf{C})_{rp}^* (\mathbf{D})_{rk} \right\} \end{aligned} \quad (\text{B.85})$$

$$= \sum_{m=1}^D \sum_{n=1}^K \sum_{p=1}^K \sum_{r=1}^D (\mathbf{E})_{np} E \left\{ (\mathbf{A})_{mk}^* (\mathbf{B})_{mn} (\mathbf{C})_{rp}^* (\mathbf{D})_{rk} \right\} \quad (\text{B.86})$$

$$= \sum_{m=1}^D \sum_{n=1}^K \sum_{p=1}^K \sum_{r=1}^D (e_n \delta_{np}) E \left\{ (\mathbf{A})_{mk}^* (\mathbf{B})_{mn} (\mathbf{C})_{rp}^* (\mathbf{D})_{rk} \right\} \quad (\text{B.87})$$

$$= \sum_{m=1}^D \sum_{n=1}^K \sum_{r=1}^D e_n E \left\{ (\mathbf{A})_{mk}^* (\mathbf{B})_{mn} (\mathbf{C})_{rn}^* (\mathbf{D})_{rk} \right\} \quad (\text{B.88})$$

In the expectation term $E \{ (\mathbf{A})_{mk}^* (\mathbf{B})_{mn} (\mathbf{C})_{rn}^* (\mathbf{D})_{rk} \}$, there is the product of 4 circularly symmetric complex normal random variables. They are known to be zero mean, but there might be correlation between them. In this case, the expectation of the product is known to be

$$E \{ abcd \} = E \{ ab \} E \{ cd \} + E \{ ac \} E \{ bd \} + E \{ ad \} E \{ bc \} \quad (\text{B.89})$$

where a , b , c and d are circularly symmetric complex normal and zero mean random variables. Then, the equation

$$\begin{aligned} E \{ (\mathbf{A})_{mk}^* (\mathbf{B})_{mn} (\mathbf{C})_{rn}^* (\mathbf{D})_{rk} \} &= E \{ (\mathbf{B})_{mn} (\mathbf{A})_{mk}^* \} E \{ (\mathbf{D})_{rk} (\mathbf{C})_{rn}^* \} \\ &\quad + E \{ (\mathbf{D})_{rk} (\mathbf{A})_{mk}^* \} E \{ (\mathbf{B})_{mn} (\mathbf{C})_{rn}^* \} \end{aligned} \quad (\text{B.90})$$

is substituted in the related place. The one term including the pairwise correlation of the conjugates and 'non-conjugates' is omitted, because phase of a single random variable is uniform, and it continues to be uniform after these type of multiplications, which makes the product zero-mean.

$$\begin{aligned}
& \mathbf{e}_k^H E \{ \mathbf{A}^H \mathbf{B} \mathbf{E} \mathbf{C}^H \mathbf{D} \} \mathbf{e}_k \\
&= \sum_{m=1}^D \sum_{n=1}^K \sum_{r=1}^D e_n [E \{ (\mathbf{B})_{mn} (\mathbf{A})_{mk}^* \} E \{ (\mathbf{D})_{rk} (\mathbf{C})_{rn}^* \} \\
&\quad + E \{ (\mathbf{D})_{rk} (\mathbf{A})_{mk}^* \} E \{ (\mathbf{B})_{mn} (\mathbf{C})_{rn}^* \}] \tag{B.91}
\end{aligned}$$

$$= \sum_{m=1}^D \sum_{n=1}^K \sum_{r=1}^D e_n \left[\left(\mathbf{R}_{b,a}^{n,k} \right)_{mm} \left(\mathbf{R}_{d,c}^{k,n} \right)_{rr} + \left(\mathbf{R}_{d,a}^{k,k} \right)_{rm} \left(\mathbf{R}_{b,c}^{n,n} \right)_{mr} \right] \tag{B.92}$$

$$= \sum_{n=1}^K \sum_{r=1}^D e_n \left[\text{tr} \left(\mathbf{R}_{b,a}^{n,k} \right) \left(\mathbf{R}_{d,c}^{k,n} \right)_{rr} + \left(\mathbf{R}_{d,a}^{k,k} \mathbf{R}_{b,c}^{n,n} \right)_{rr} \right] \tag{B.93}$$

$$= \sum_{n=1}^K e_n \left[\text{tr} \left(\mathbf{R}_{b,a}^{n,k} \right) \text{tr} \left(\mathbf{R}_{d,c}^{k,n} \right) + \text{tr} \left(\mathbf{R}_{d,a}^{k,k} \mathbf{R}_{b,c}^{n,n} \right) \right] \tag{B.94}$$

If $\mathbf{E} = \mathbf{E}_{kk}$, then $e_n = \delta_{nk}$.

$$\boxed{ \mathbf{e}_k^H E \{ \mathbf{A}^H \mathbf{B} \mathbf{E}_{kk} \mathbf{C}^H \mathbf{D} \} \mathbf{e}_k = \left[\text{tr} \left(\mathbf{R}_{b,a}^{k,k} \right) \text{tr} \left(\mathbf{R}_{d,c}^{k,k} \right) + \text{tr} \left(\mathbf{R}_{d,a}^{k,k} \mathbf{R}_{b,c}^{k,k} \right) \right] } \tag{B.95}$$

If $\mathbf{E} = \mathbf{I}_K$, then $e_n = 1$ for $n = 1, 2, \dots, K$.

$$\boxed{ \mathbf{e}_k^H E \{ \mathbf{A}^H \mathbf{B} \mathbf{C}^H \mathbf{D} \} \mathbf{e}_k = \sum_{k'=1}^K \left[\text{tr} \left(\mathbf{R}_{b,a}^{k',k} \right) \text{tr} \left(\mathbf{R}_{d,c}^{k,k'} \right) + \text{tr} \left(\mathbf{R}_{d,a}^{k,k} \mathbf{R}_{b,c}^{k',k'} \right) \right] } \tag{B.96}$$

B.4 Implementation of Analytical Results

The covariance matrices in previously found analytical expressions will correspond to the matrices defined below. Whenever they are needed, they will be used.

$$E \left\{ \mathbf{h}_{eff,l}^{(g_k)} \left[\mathbf{h}_{eff,l'}^{(g_{k'})} \right]^H \right\} = \mathbf{R}_{eff,l}^{(g)} \delta_{gg'} \delta_{kk'} \delta_{ll'} \quad (\text{B.97})$$

$$\Phi_{ll'}^{(g_k:g_{k'})} \triangleq E \left\{ \hat{\mathbf{h}}_{eff,l}^{(g_k)} \left[\hat{\mathbf{h}}_{eff,l'}^{(g_{k'})} \right]^H \right\} \quad (\text{B.98})$$

$$\Psi_{ll'}^{(g_k:g_{k'})} \triangleq E \left\{ \hat{\mathbf{h}}_{eff,l}^{(g_k)} \left[\mathbf{h}_{eff,l'}^{(g_{k'})} \right]^H \right\} \quad (\text{B.99})$$

$$\mathbf{R}_{eff,sum}^{(g)} \triangleq \sum_{l=0}^{L-1} \mathbf{R}_{eff,l}^{(g)} \quad (\text{B.100})$$

$$\Phi_{sum}^{(g_k)} \triangleq \sum_{l=0}^{L-1} \Phi_{ll}^{(g_k)(g_k)} \quad (\text{B.101})$$

$$\Psi_{sum}^{(g_k)} \triangleq \sum_{l=0}^{L-1} \Psi_{ll}^{(g_k)(g_k)} \quad (\text{B.102})$$

Rewrite the P_S expression in Section B.2.1.

$$P_S = E_s^{(g)} \sum_{l_1=0}^{L-1} \sum_{l_2=0}^{L-1} \mathbf{e}_k^H E \left\{ \left[\hat{\mathbf{H}}_{eff,l_1}^{(g)} \right]^H \hat{\mathbf{H}}_{eff,l_1}^{(g)} \mathbf{E}_{kk} \left[\hat{\mathbf{H}}_{eff,l_2}^{(g)} \right]^H \hat{\mathbf{H}}_{eff,l_2}^{(g)} \right\} \mathbf{e}_k \quad (\text{B.103})$$

It includes an expectation term which is in the form of Type 2. The matrix in the middle is \mathbf{E}_{kk} , so the expression in (B.95) will be used. As an example, take the third matrix appearing in the right hand side of (B.95), which is $\mathbf{R}_{d,a}^{k,k}$. Subscripts denote the matrices, and superscripts denote the columns of these matrices. The first subscript is d , which points the fourth random matrix in (B.103), and the first superscript is k , which points the k^{th} column of it. The fourth random matrix is $\hat{\mathbf{H}}_{eff,l_2}^{(g)}$ and its k^{th} column is $\hat{\mathbf{h}}_{eff,l_2}^{(g_k)}$. Similarly, the second subscript a and the second superscript k point the vector $\hat{\mathbf{h}}_{eff,l_1}^{(g_k)}$. So, a matrix which is equal to $E \left\{ \hat{\mathbf{h}}_{eff,l_2}^{(g_k)} \left[\hat{\mathbf{h}}_{eff,l_1}^{(g_k)} \right]^H \right\}$ should be substituted in the place of $\mathbf{R}_{d,a}^{k,k}$. This matrix is found to be $\Phi_{l_2 l_1}^{(g_k:g_k)}$ from the definitions above, and it is placed. The procedure continues similarly.

$$P_S = E_s^{(g)} \sum_{l_1=0}^{L-1} \sum_{l_2=0}^{L-1} \mathbf{e}_k^H E \left\{ \left[\hat{\mathbf{H}}_{eff,l_1}^{(g)} \right]^H \hat{\mathbf{H}}_{eff,l_1}^{(g)} \mathbf{E}_{kk} \left[\hat{\mathbf{H}}_{eff,l_2}^{(g)} \right]^H \hat{\mathbf{H}}_{eff,l_2}^{(g)} \right\} \mathbf{e}_k \quad (\text{B.104})$$

$$= E_s^{(g)} \sum_{l_1=0}^{L-1} \sum_{l_2=0}^{L-1} \left[\text{tr} \left(\Phi_{l_1 l_1}^{(g_k, g_k)} \right) \text{tr} \left(\Phi_{l_2 l_2}^{(g_k, g_k)} \right) + \text{tr} \left(\Phi_{l_2 l_1}^{(g_k, g_k)} \Phi_{l_1 l_2}^{(g_k, g_k)} \right) \right] \quad (\text{B.105})$$

$$= E_s^{(g)} \left[\sum_{l_1=0}^{L-1} \text{tr} \left(\Phi_{l_1 l_1}^{(g_k, g_k)} \right) \sum_{l_2=0}^{L-1} \text{tr} \left(\Phi_{l_2 l_2}^{(g_k, g_k)} \right) + \sum_{l_1=0}^{L-1} \sum_{l_2=0}^{L-1} \text{tr} \left(\Phi_{l_2 l_1}^{(g_k, g_k)} \Phi_{l_1 l_2}^{(g_k, g_k)} \right) \right] \quad (\text{B.106})$$

$$= E_s^{(g)} \left[\text{tr} \left(\sum_{l_1=0}^{L-1} \Phi_{l_1 l_1}^{(g_k, g_k)} \right)^2 + \sum_{l_1=0}^{L-1} \sum_{l_2=0}^{L-1} \text{tr} \left(\Phi_{l_2 l_1}^{(g_k, g_k)} \Phi_{l_1 l_2}^{(g_k, g_k)} \right) \right] \quad (\text{B.107})$$

$$= E_s^{(g)} \left[\text{tr} \left(\Phi_{sum}^{(g_k)} \right)^2 + \sum_{l_1=0}^{L-1} \sum_{l_2=0}^{L-1} \text{tr} \left(\Phi_{l_2 l_1}^{(g_k, g_k)} \Phi_{l_1 l_2}^{(g_k, g_k)} \right) \right] \quad (\text{B.108})$$

$$P_{S^+} = E_s^{(g)} \sum_{l_1=0}^{L-1} \sum_{l_2=0}^{L-1} \mathbf{e}_k^H E \left\{ \left[\hat{\mathbf{H}}_{eff, l_1}^{(g)} \right]^H \mathbf{H}_{eff, l_1}^{(g)} \mathbf{E}_{kk} \left[\mathbf{H}_{eff, l_2}^{(g)} \right]^H \hat{\mathbf{H}}_{eff, l_2}^{(g)} \right\} \mathbf{e}_k \quad (\text{B.109})$$

$$= E_s^{(g)} \sum_{l_1=0}^{L-1} \sum_{l_2=0}^{L-1} \left[\text{tr} \left(\left[\Psi_{l_1 l_1}^{(g_k, g_k)} \right]^H \right) \text{tr} \left(\Psi_{l_2 l_2}^{(g_k, g_k)} \right) + \text{tr} \left(\Phi_{l_2 l_1}^{(g_k)(g_k)} \left(\delta_{l_1 l_2} \mathbf{R}_{eff, l_1}^{(g)} \right) \right) \right] \quad (\text{B.110})$$

$$= E_s^{(g)} \left[\text{tr} \left(\sum_{l_1=0}^{L-1} \Psi_{l_1 l_1}^{(g_k, g_k)} \right)^* \text{tr} \left(\sum_{l_2=0}^{L-1} \Psi_{l_2 l_2}^{(g_k, g_k)} \right) + \sum_{l_1=0}^{L-1} \text{tr} \left(\Phi_{l_1 l_1}^{(g_k, g_k)} \mathbf{R}_{eff, l_1}^{(g)} \right) \right] \quad (\text{B.111})$$

$$= E_s^{(g)} \left[\left| \text{tr} \left(\sum_{l_1=0}^{L-1} \Psi_{l_1 l_1}^{(g_k, g_k)} \right) \right|^2 + \sum_{l_1=0}^{L-1} \text{tr} \left(\Phi_{l_1 l_1}^{(g_k, g_k)} \mathbf{R}_{eff, l_1}^{(g)} \right) \right] \quad (\text{B.112})$$

$$= E_s^{(g)} \left[\left| \text{tr} \left(\Psi_{sum}^{(g_k)} \right) \right|^2 + \sum_{l=0}^{L-1} \text{tr} \left(\Phi_{ll}^{(g_k, g_k)} \mathbf{R}_{eff, l}^{(g)} \right) \right] \quad (\text{B.113})$$

$$P_{CC} = 2E_s^{(g)} \text{Re} \left\{ \sum_{l_1=0}^{L-1} \sum_{l_2=0}^{L-1} \mathbf{e}_k^H E \left\{ \left[\hat{\mathbf{H}}_{eff, l_1}^{(g)} \right]^H \mathbf{H}_{eff, l_1}^{(g)} \mathbf{E}_{kk} \left[\hat{\mathbf{H}}_{eff, l_2}^{(g)} \right]^H \hat{\mathbf{H}}_{eff, l_2}^{(g)} \right\} \mathbf{e}_k \right\} \quad (\text{B.114})$$

$$= 2E_s^{(g)} \text{Re} \left\{ \sum_{l_1=0}^{L-1} \sum_{l_2=0}^{L-1} \left[\text{tr} \left(\left[\Psi_{l_1 l_1}^{(g_k, g_k)} \right]^H \right) \text{tr} \left(\Phi_{l_2 l_2}^{(g_k, g_k)} \right) + \text{tr} \left(\Phi_{l_2 l_1}^{(g_k, g_k)} \left[\Psi_{l_2 l_1}^{(g_k, g_k)} \right]^H \right) \right] \right\} \quad (\text{B.115})$$

$$\begin{aligned}
&= 2E_s^{(g)} \text{Re} \left\{ \text{tr} \left(\sum_{l_1=0}^{L-1} \Psi_{l_1 l_1}^{(g_k, g_k)} \right)^* \text{tr} \left(\sum_{l_2=0}^{L-1} \Phi_{l_2 l_2}^{(g_k, g_k)} \right) \right. \\
&\quad \left. + \sum_{l_1=0}^{L-1} \sum_{l_2=0}^{L-1} \text{tr} \left(\Phi_{l_2 l_1}^{(g_k, g_k)} \left[\Psi_{l_2 l_1}^{(g_k, g_k)} \right]^H \right) \right\} \quad (\text{B.116})
\end{aligned}$$

$$\begin{aligned}
&= 2E_s^{(g)} \text{Re} \left\{ \text{tr} \left(\Psi_{sum}^{(g_k)} \right)^* \text{tr} \left(\Phi_{sum}^{(g_k)} \right) + \sum_{l_1=0}^{L-1} \sum_{l_2=0}^{L-1} \text{tr} \left(\Phi_{l_2 l_1}^{(g_k, g_k)} \left[\Psi_{l_2 l_1}^{(g_k, g_k)} \right]^H \right) \right\} \\
&\quad (\text{B.117})
\end{aligned}$$

$$\begin{aligned}
P_{IU} &= \sum_{l=-(L-1)}^{L-1} \sum_{l_1=0}^{L-1} \sum_{l_2=0}^{L-1} \mathbf{e}_k^H E \left\{ \left[\hat{\mathbf{H}}_{eff, l_1}^{(g)} \right]^H \mathbf{H}_{eff, l+l_1}^{(g)} \mathbf{E}_{kk} \right. \\
&\quad \left. \left[\mathbf{H}_{eff, l+l_2}^{(g)} \right]^H \hat{\mathbf{H}}_{eff, l_2}^{(g)} \right\} \mathbf{e}_k E_s^{(g)} \quad (\text{B.118})
\end{aligned}$$

$$\begin{aligned}
&= E_s^{(g)} \sum_{l=-(L-1)}^{L-1} \sum_{l_1=0}^{L-1} \sum_{l_2=0}^{L-1} \left[\text{tr} \left(\left[\Psi_{l_1, l+l_1}^{(g_k, g_k)} \right]^H \right) \text{tr} \left(\Psi_{l_2, l+l_2}^{(g_k, g_k)} \right) \right. \\
&\quad \left. + \text{tr} \left(\Phi_{l_2, l_1}^{(g_k, g_k)} \left(\delta_{l_1 l_2} \mathbf{R}_{eff, l+l_1}^{(g)} \right) \right) \right] \quad (\text{B.119})
\end{aligned}$$

$$\begin{aligned}
&= E_s^{(g)} \left[\sum_{l=-(L-1)}^{L-1} \text{tr} \left(\sum_{l_1=0}^{L-1} \Psi_{l_1, l+l_1}^{(g_k, g_k)} \right)^* \text{tr} \left(\sum_{l_2=0}^{L-1} \Psi_{l_2, l+l_2}^{(g_k, g_k)} \right) \right. \\
&\quad \left. + \sum_{l=-(L-1)}^{L-1} \sum_{l_1=0}^{L-1} \text{tr} \left(\Phi_{l_1, l_1}^{(g_k, g_k)} \mathbf{R}_{eff, l+l_1}^{(g)} \right) \right] \quad (\text{B.120})
\end{aligned}$$

$$\begin{aligned}
&= E_s^{(g)} \left[\sum_{l=-(L-1)}^{L-1} \left| \text{tr} \left(\sum_{l_1=0}^{L-1} \Psi_{l_1, l+l_1}^{(g_k, g_k)} \right) \right|^2 + \sum_{l_1=0}^{L-1} \text{tr} \left(\Phi_{l_1, l_1}^{(g_k, g_k)} \sum_{l=-(L-1)}^{L-1} \mathbf{R}_{eff, l+l_1}^{(g)} \right) \right] \\
&\quad (\text{B.121})
\end{aligned}$$

$$\begin{aligned}
&= E_s^{(g)} \left[\sum_{l=-(L-1)}^{L-1} \left| \text{tr} \left(\sum_{l_1=0}^{L-1} \Psi_{l_1, l+l_1}^{(g_k, g_k)} \right) \right|^2 + \text{tr} \left(\sum_{l_1=0}^{L-1} \Phi_{l_1, l_1}^{(g_k, g_k)} \sum_{l_2=0}^{L-1} \mathbf{R}_{eff, l_2}^{(g)} \right) \right] \\
&\quad (\text{B.122})
\end{aligned}$$

$$\begin{aligned}
&= E_s^{(g)} \left[\sum_{l=-(L-1)}^{L-1} \left| \text{tr} \left(\sum_{l_1=0}^{L-1} \Psi_{l_1, l+l_1}^{(g_k, g_k)} \right) \right|^2 + \text{tr} \left(\Phi_{sum}^{(g_k)} \mathbf{R}_{eff, sum}^{(g)} \right) \right] \\
&\quad (\text{B.123})
\end{aligned}$$

$$\begin{aligned}
P_{IG} &= \sum_{l=-(L-1)}^{L-1} \sum_{l_1=0}^{L-1} \sum_{l_2=0}^{L-1} \mathbf{e}_k^H E \left\{ \left[\hat{\mathbf{H}}_{eff, l_1}^{(g)} \right]^H \mathbf{H}_{eff, l+l_1}^{(g)} \left[\mathbf{H}_{eff, l+l_2}^{(g)} \right]^H \hat{\mathbf{H}}_{eff, l_2}^{(g)} \right\} \mathbf{e}_k E_s^{(g)} \\
&\quad (\text{B.124})
\end{aligned}$$

$$\begin{aligned}
&= E_s^{(g)} \sum_{l=-(L-1)}^{L-1} \sum_{l_1=0}^{L-1} \sum_{l_2=0}^{L-1} \sum_{k'=1}^K \left[\text{tr} \left(\left[\Psi_{l_1, l+l_1}^{(g_k, g_{k'})} \right]^H \right) \text{tr} \left(\Psi_{l_2, l+l_2}^{(g_k, g_{k'})} \right) \right. \\
&\quad \left. + \text{tr} \left(\Phi_{l_2, l_1}^{(g_k, g_k)} \left(\delta_{l_1 l_2} \mathbf{R}_{eff, l+l_1}^{(g)} \right) \right) \right] \tag{B.125}
\end{aligned}$$

$$\begin{aligned}
&= E_s^{(g)} \left[\sum_{l=-(L-1)}^{L-1} \sum_{k'=1}^K \text{tr} \left(\sum_{l_1=0}^{L-1} \Psi_{l_1, l+l_1}^{(g_k, g_{k'})} \right)^* \text{tr} \left(\sum_{l_2=0}^{L-1} \Psi_{l_2, l+l_2}^{(g_k, g_{k'})} \right) \right. \\
&\quad \left. + K_g \sum_{l=-(L-1)}^{L-1} \sum_{l_1=0}^{L-1} \text{tr} \left(\Phi_{l_1, l_1}^{(g_k, g_k)} \mathbf{R}_{eff, l+l_1}^{(g)} \right) \right] \tag{B.126}
\end{aligned}$$

$$\begin{aligned}
&= E_s^{(g)} \left[\sum_{k'=1}^K \sum_{l=-(L-1)}^{L-1} \left| \text{tr} \left(\sum_{l_1=0}^{L-1} \Psi_{l_1, l+l_1}^{(g_k, g_{k'})} \right) \right|^2 + K_g \text{tr} \left(\sum_{l_1=0}^{L-1} \Phi_{l_1, l_1}^{(g_k, g_k)} \sum_{l_2=0}^{L-1} \mathbf{R}_{eff, l_2}^{(g)} \right) \right] \tag{B.127}
\end{aligned}$$

$$\begin{aligned}
&= E_s^{(g)} \left[\sum_{k'=1}^K \sum_{l=-(L-1)}^{L-1} \left| \text{tr} \left(\sum_{l_1=0}^{L-1} \Psi_{l_1, l+l_1}^{(g_k, g_{k'})} \right) \right|^2 + K_g \text{tr} \left(\Phi_{sum}^{(g_k)} \mathbf{R}_{eff, sum}^{(g)} \right) \right] \tag{B.128}
\end{aligned}$$

$$\begin{aligned}
P_{IGI} &= \sum_{g' \neq g} E_s^{(g')} \sum_{l=-(L-1)}^{L-1} \sum_{l_1=0}^{L-1} \sum_{l_2=0}^{L-1} \mathbf{e}_k^H E \left\{ \left[\hat{\mathbf{H}}_{eff, l_1}^{(g)} \right]^H \mathbf{H}_{eff, l+l_1}^{(g')} \right. \\
&\quad \left. \left[\mathbf{H}_{eff, l+l_2}^{(g')} \right]^H \hat{\mathbf{H}}_{eff, l_2}^{(g)} \right\} \mathbf{e}_k \tag{B.129}
\end{aligned}$$

$$\begin{aligned}
&= \sum_{g' \neq g} E_s^{(g')} \sum_{l=-(L-1)}^{L-1} \sum_{l_1=0}^{L-1} \sum_{l_2=0}^{L-1} \sum_{k'=1}^K \left[\text{tr} \left(\left[\Psi_{l_1, l+l_1}^{(g_k, g_{k'})} \right]^H \right) \text{tr} \left(\Psi_{l_2, l+l_2}^{(g_k, g_{k'})} \right) \right. \\
&\quad \left. + \text{tr} \left(\Phi_{l_2, l_1}^{(g_k, g_k)} \left(\delta_{l_1 l_2} \mathbf{R}_{eff, l+l_1}^{(g')} \right) \right) \right] \tag{B.130}
\end{aligned}$$

$$\begin{aligned}
&= \sum_{g' \neq g} E_s^{(g')} \left[\sum_{l=-(L-1)}^{L-1} \sum_{k'=1}^K \text{tr} \left(\sum_{l_1=0}^{L-1} \Psi_{l_1, l+l_1}^{(g_k, g_{k'})} \right)^* \text{tr} \left(\sum_{l_2=0}^{L-1} \Psi_{l_2, l+l_2}^{(g_k, g_{k'})} \right) \right. \\
&\quad \left. + \sum_{l=-(L-1)}^{L-1} \sum_{l_1=0}^{L-1} \sum_{k'=1}^K \text{tr} \left(\Phi_{l_1, l_1}^{(g_k, g_k)} \mathbf{R}_{eff, l+l_1}^{(g')} \right) \right] \tag{B.131}
\end{aligned}$$

$$\begin{aligned}
&= \sum_{g' \neq g} E_s^{(g')} \left[\sum_{k'=1}^K \sum_{l=-(L-1)}^{L-1} \left| \text{tr} \left(\sum_{l_1=0}^{L-1} \Psi_{l_1, l+l_1}^{(g_k, g_{k'})} \right) \right|^2 \right. \\
&\quad \left. + K_{g'} \text{tr} \left(\sum_{l_1=0}^{L-1} \Phi_{l_1, l_1}^{(g_k, g_k)} \sum_{l_2=0}^{L-1} \mathbf{R}_{eff, l_2}^{(g')} \right) \right] \tag{B.132}
\end{aligned}$$

$$= \sum_{g' \neq g} E_s^{(g')} \left[\sum_{k'=1}^K \sum_{l=-(L-1)}^{L-1} \left| \text{tr} \left(\sum_{l_1=0}^{L-1} \Psi_{l_1, l+l_1}^{(g_k, g'_{k'})} \right) \right|^2 + K_{g'} \text{tr} \left(\Phi_{sum}^{(g_k)} \mathbf{R}_{eff, sum}^{(g')} \right) \right] \quad (\text{B.133})$$

$$P_{Noise} = N_0 \sum_{l_1=0}^{L-1} \mathbf{e}_k^H E \left\{ \left[\hat{\mathbf{H}}_{eff, l_1}^{(g)} \right]^H [\mathbf{S}^{(g)}]^H \mathbf{S}^{(g)} \hat{\mathbf{H}}_{eff, l_1}^{(g)} \right\} \mathbf{e}_k \quad (\text{B.134})$$

$$= N_0 \sum_{l=0}^{L-1} \text{tr} \left(\Phi_{l, l}^{(g_k, g_k)} [\mathbf{S}^{(g)}]^H \mathbf{S}^{(g)} \right) \quad (\text{B.135})$$

$$= N_0 \text{tr} \left(\sum_{l=0}^{L-1} \Phi_{l, l}^{(g_k, g_k)} [\mathbf{S}^{(g)}]^H \mathbf{S}^{(g)} \right) \quad (\text{B.136})$$

$$= N_0 \text{tr} \left(\Phi_{sum}^{(g_k)} [\mathbf{S}^{(g)}]^H \mathbf{S}^{(g)} \right) \quad (\text{B.137})$$

B.4.1 Summary

$$P_S = E_s^{(g)} \left[\text{tr} \left(\Phi_{sum}^{(g_k)} \right)^2 + \sum_{l_1=0}^{L-1} \sum_{l_2=0}^{L-1} \text{tr} \left(\Phi_{l_2 l_1}^{(g_k, g_k)} \Phi_{l_1 l_2}^{(g_k, g_k)} \right) \right] \quad (\text{B.138})$$

$$P_{S^+} = E_s^{(g)} \left[\left| \text{tr} \left(\Psi_{sum}^{(g_k)} \right) \right|^2 + \sum_{l=0}^{L-1} \text{tr} \left(\Phi_{ll}^{(g_k, g_k)} \mathbf{R}_{eff, l}^{(g)} \right) \right] \quad (\text{B.139})$$

$$P_{CC} = 2E_s^{(g)} \text{Re} \left\{ \text{tr} \left(\Psi_{sum}^{(g_k)} \right)^* \text{tr} \left(\Phi_{sum}^{(g_k)} \right) + \sum_{l_1=0}^{L-1} \sum_{l_2=0}^{L-1} \text{tr} \left(\Phi_{l_2 l_1}^{(g_k, g_k)} \left[\Psi_{l_2 l_1}^{(g_k, g_k)} \right]^H \right) \right\} \quad (\text{B.140})$$

$$P_{IU} = E_s^{(g)} \left[\sum_{l=-(L-1)}^{L-1} \left| \text{tr} \left(\sum_{l_1=0}^{L-1} \Psi_{l_1, l+l_1}^{(g_k, g_k)} \right) \right|^2 + \text{tr} \left(\Phi_{sum}^{(g_k)} \mathbf{R}_{eff, sum}^{(g)} \right) \right] \quad (\text{B.141})$$

$$P_{IG} = E_s^{(g)} \left[\sum_{k'=1}^K \sum_{l=-(L-1)}^{L-1} \left| \text{tr} \left(\sum_{l_1=0}^{L-1} \Psi_{l_1, l+l_1}^{(g_k, g_{k'})} \right) \right|^2 + K_g \text{tr} \left(\Phi_{sum}^{(g_k)} \mathbf{R}_{eff, sum}^{(g)} \right) \right] \quad (\text{B.142})$$

$$P_{IGI} = \sum_{g' \neq g} E_s^{(g')} \left[\sum_{k'=1}^K \sum_{l=-(L-1)}^{L-1} \left| \text{tr} \left(\sum_{l_1=0}^{L-1} \Psi_{l_1, l+l_1}^{(g_k, g_{k'})} \right) \right|^2 + K_{g'} \text{tr} \left(\Phi_{sum}^{(g_k)} \mathbf{R}_{eff, sum}^{(g')} \right) \right] \quad (\text{B.143})$$

$$P_{Noise} = N_0 \text{tr} \left(\Phi_{sum}^{(g_k)} \left[\mathbf{S}^{(g)} \right]^H \mathbf{S}^{(g)} \right) \quad (\text{B.144})$$

B.5 Perfect Channel Estimation

$$\hat{\mathbf{H}}_{eff,l}^{(g)} = \mathbf{H}_{eff,l}^{(g)} \quad (\text{B.145})$$

$$\Phi_{ll'}^{(g_k)(g_{k'})} = \mathbf{R}_{eff,l}^{(g)} \delta_{ll'} \delta_{kk'} \quad (\text{B.146})$$

$$\Psi_{ll'}^{(g_k)(g_{k'})} = \mathbf{R}_{eff,l}^{(g)} \delta_{ll'} \delta_{kk'} \delta_{gg'} \quad (\text{B.147})$$

$$P_S = E_s^{(g)} \left[\text{tr} \left(\Phi_{sum}^{(g_k)} \right)^2 + \sum_{l_1=0}^{L-1} \sum_{l_2=0}^{L-1} \text{tr} \left(\Phi_{l_2 l_1}^{(g_k, g_k)} \Phi_{l_1 l_2}^{(g_k, g_k)} \right) \right] \quad (\text{B.148})$$

$$= E_s^{(g)} \left[\text{tr} \left(\mathbf{R}_{eff,sum}^{(g)} \right)^2 + \sum_{l_1=0}^{L-1} \sum_{l_2=0}^{L-1} \text{tr} \left(\left(\delta_{l_1 l_2} \mathbf{R}_{eff,l_1}^{(g)} \right) \left(\delta_{l_1 l_2} \mathbf{R}_{l_1}^{(g)} \right) \right) \right] \quad (\text{B.149})$$

$$= E_s^{(g)} \left[\text{tr} \left(\mathbf{R}_{eff,sum}^{(g)} \right)^2 + \sum_{l=0}^{L-1} \text{tr} \left(\mathbf{R}_{eff,l}^{(g)} \mathbf{R}_{eff,l}^{(g)} \right) \right] \quad (\text{B.150})$$

$$P_{S^+} = E_s^{(g)} \left[\left| \text{tr} \left(\Psi_{sum}^{(g_k)} \right) \right|^2 + \sum_{l=0}^{L-1} \text{tr} \left(\Phi_{ll}^{(g_k, g_k)} \mathbf{R}_{eff,l}^{(g)} \right) \right] \quad (\text{B.151})$$

$$= E_s^{(g)} \left[\text{tr} \left(\mathbf{R}_{eff,sum}^{(g)} \right)^2 + \sum_{l=0}^{L-1} \text{tr} \left(\mathbf{R}_{eff,l}^{(g)} \mathbf{R}_{eff,l}^{(g)} \right) \right] \quad (\text{B.152})$$

$$P_{CC} = 2E_s^{(g)} \text{Re} \left\{ \text{tr} \left(\Psi_{sum}^{(g_k)} \right)^* \text{tr} \left(\Phi_{sum}^{(g_k)} \right) + \sum_{l_1=0}^{L-1} \sum_{l_2=0}^{L-1} \text{tr} \left(\Phi_{l_2 l_1}^{(g_k, g_k)} \left[\Psi_{l_2 l_1}^{(g_k, g_k)} \right]^H \right) \right\} \quad (\text{B.153})$$

$$= 2E_s^{(g)} \text{Re} \left\{ \text{tr} \left(\mathbf{R}_{eff,sum}^{(g)} \right)^2 + \sum_{l=0}^{L-1} \text{tr} \left(\mathbf{R}_{eff,l}^{(g)} \left[\mathbf{R}_{eff,l}^{(g)} \right]^H \right) \right\} \quad (\text{B.154})$$

$$= 2E_s^{(g)} \text{tr} \left(\mathbf{R}_{eff,sum}^{(g)} \right)^2 + \sum_{l=0}^{L-1} \text{tr} \left(\mathbf{R}_{eff,l}^{(g)} \left[\mathbf{R}_{eff,l}^{(g)} \right]^H \right) \quad (\text{B.155})$$

$$P_{IU} = E_s^{(g)} \left[\sum_{l=-(L-1)}^{L-1} \left| \text{tr} \left(\sum_{l_1=0}^{L-1} \Psi_{l_1, l+l_1}^{(g_k, g_k)} \right) \right|^2 + \text{tr} \left(\Phi_{sum}^{(g_k)} \mathbf{R}_{eff,sum}^{(g)} \right) \right] \quad (\text{B.156})$$

$$= E_s^{(g)} \left[\sum_{l=-(L-1)}^{L-1} \left| \text{tr} \left(\sum_{l_1=0}^{L-1} \delta_l \mathbf{R}_{eff,l_1}^{(g)} \right) \right|^2 + \text{tr} \left(\mathbf{R}_{eff,sum}^{(g)} \mathbf{R}_{eff,sum}^{(g)} \right) \right] \quad (\text{B.157})$$

$$= E_s^{(g)} \left[\text{tr} \left(\sum_{l_1=0}^{L-1} \mathbf{R}_{eff,l_1}^{(g)} \right)^2 + \text{tr} \left(\mathbf{R}_{eff,sum}^{(g)} \mathbf{R}_{eff,sum}^{(g)} \right) \right] \quad (\text{B.158})$$

$$= E_s^{(g)} \left[\text{tr} \left(\mathbf{R}_{eff,sum}^{(g)} \right)^2 + \text{tr} \left(\mathbf{R}_{eff,sum}^{(g)} \mathbf{R}_{eff,sum}^{(g)} \right) \right] \quad (\text{B.159})$$

$$P_{IG} = E_s^{(g)} \left[\sum_{k'=1}^K \sum_{l=-(L-1)}^{L-1} \left| \text{tr} \left(\sum_{l_1=0}^{L-1} \Psi_{l_1,l+l_1}^{(g_k,g_{k'})} \right) \right|^2 + K_g \text{tr} \left(\Phi_{sum}^{(g_k)} \mathbf{R}_{eff,sum}^{(g)} \right) \right] \quad (\text{B.160})$$

$$= E_s^{(g)} \left[\sum_{k'=1}^K \sum_{l=-(L-1)}^{L-1} \left| \text{tr} \left(\sum_{l_1=0}^{L-1} \delta_{kk'} \delta_l \mathbf{R}_{eff,l_1}^{(g)} \right) \right|^2 + K_g \text{tr} \left(\mathbf{R}_{eff,sum}^{(g)} \mathbf{R}_{eff,sum}^{(g)} \right) \right] \quad (\text{B.161})$$

$$= E_s^{(g)} \left[\text{tr} \left(\mathbf{R}_{eff,sum}^{(g)} \right)^2 + K_g \text{tr} \left(\mathbf{R}_{eff,sum}^{(g)} \mathbf{R}_{eff,sum}^{(g)} \right) \right] \quad (\text{B.162})$$

$$P_{IGI} = \sum_{g' \neq g} E_s^{(g')} \left[\sum_{k'=1}^K \sum_{l=-(L-1)}^{L-1} \left| \text{tr} \left(\sum_{l_1=0}^{L-1} \Psi_{l_1,l+l_1}^{(g_k,g_{k'})} \right) \right|^2 + K_{g'} \text{tr} \left(\Phi_{sum}^{(g_k)} \mathbf{R}_{eff,sum}^{(g')} \right) \right] \quad (\text{B.163})$$

$$= \sum_{g' \neq g} E_s^{(g')} \left[\sum_{k'=1}^K \sum_{l=-(L-1)}^{L-1} \left| \text{tr} \left(\sum_{l_1=0}^{L-1} \delta_{gg'} \delta_{kk'} \delta_l \mathbf{R}_{eff,l_1}^{(g)} \right) \right|^2 + K_{g'} \text{tr} \left(\mathbf{R}_{eff,sum}^{(g)} \mathbf{R}_{eff,sum}^{(g')} \right) \right] \quad (\text{B.164})$$

$$= \sum_{g' \neq g} E_s^{(g')} \left[\text{tr} \left(\mathbf{R}_{eff,sum}^{(g)} \right)^2 + K_{g'} \text{tr} \left(\mathbf{R}_{eff,sum}^{(g)} \mathbf{R}_{eff,sum}^{(g')} \right) \right] \quad (\text{B.165})$$

$$P_{Noise} = N_0 \text{tr} \left(\Phi_{sum}^{(g_k)} [\mathbf{S}^{(g)}]^H \mathbf{S}^{(g)} \right) \quad (\text{B.166})$$

$$= N_0 \text{tr} \left(\mathbf{R}_{eff,sum}^{(g)} [\mathbf{S}^{(g)}]^H \mathbf{S}^{(g)} \right) \quad (\text{B.167})$$

B.5.1 Summary

$$P_S = E_s^{(g)} \left[\text{tr} \left(\mathbf{R}_{eff,sum}^{(g)} \right)^2 + \sum_{l=0}^{L-1} \text{tr} \left(\mathbf{R}_{eff,l}^{(g)} \mathbf{R}_{eff,l}^{(g)} \right) \right] \quad (\text{B.168})$$

$$P_{S+} = P_S \quad (\text{B.169})$$

$$P_{CC} = 2P_S \quad (\text{B.170})$$

$$P_{SICEE} = P_S + P_{S+} - P_{CC} = 0 \quad (\text{B.171})$$

$$P_{IU} = E_s^{(g)} \left[\text{tr} \left(\mathbf{R}_{eff,sum}^{(g)} \right)^2 + \text{tr} \left(\mathbf{R}_{eff,sum}^{(g)} \mathbf{R}_{eff,sum}^{(g)} \right) \right] \quad (\text{B.172})$$

$$P_{IG} = E_s^{(g)} \left[\text{tr} \left(\mathbf{R}_{eff,sum}^{(g)} \right)^2 + K_g \text{tr} \left(\mathbf{R}_{eff,sum}^{(g)} \mathbf{R}_{eff,sum}^{(g)} \right) \right] \quad (\text{B.173})$$

$$P_{IGI} = \sum_{g' \neq g} E_s^{(g')} \left[\text{tr} \left(\mathbf{R}_{eff,sum}^{(g)} \right)^2 + K_{g'} \text{tr} \left(\mathbf{R}_{eff,sum}^{(g)} \mathbf{R}_{eff,sum}^{(g')} \right) \right] \quad (\text{B.174})$$

$$P_{Noise} = N_0 \text{tr} \left(\mathbf{R}_{eff,sum}^{(g)} [\mathbf{S}^{(g)}]^H \mathbf{S}^{(g)} \right) \quad (\text{B.175})$$

B.6 Estimated Channel

$$\bar{\mathbf{y}}^{(\bar{g})} = \sum_{g=1}^G (\mathbf{X}^{(g)} \otimes \mathbf{I}_{D_{\bar{g}}}) \bar{\mathbf{h}}_{eff}^{(g)} + (\mathbf{I}_T \otimes [\mathbf{S}^{(\bar{g})}]^H) \bar{\mathbf{n}}, \quad (\text{B.176})$$

$$\hat{\mathbf{h}}_{eff}^{(\bar{g})} = \mathbf{Z}^{(\bar{g})} \bar{\mathbf{y}}^{(\bar{g})}, \quad (\text{B.177})$$

$$E \left\{ \bar{\mathbf{h}}_{eff}^{(g)} \left[\bar{\mathbf{h}}_{eff}^{(g')} \right]^H \right\} = \delta_{gg'} \bar{\mathbf{R}}_{eff}^{(g)} \quad (\text{B.178})$$

$$\begin{aligned} \Phi^{(g)} \triangleq E \left\{ \hat{\mathbf{h}}_{eff}^{(g)} \left[\hat{\mathbf{h}}_{eff}^{(g)} \right]^H \right\} &= \mathbf{Z}^{(g)} \left((\mathbf{X}^{(g)} \otimes \mathbf{I}_{D_g}) \bar{\mathbf{R}}_{eff}^{(g)} (\mathbf{X}^{(g)} \otimes \mathbf{I}_{D_g})^H \right. \\ &\quad \left. + \mathbf{I}_T \otimes \left[\sum_{\substack{g'=1 \\ g' \neq g}}^G K_{g'} E_s^{(g')} \sum_{l=0}^{L-1} \mathbf{R}_{eff,l}^{(g')} \right] \right. \\ &\quad \left. + N_0 (\mathbf{I}_T \otimes [\mathbf{S}^{(g)}]^H \mathbf{S}^{(g)}) \right) [\mathbf{Z}^{(g)}]^H \quad (\text{B.179}) \end{aligned}$$

$$\begin{aligned} &= \mathbf{Z}^{(g)} \left((\mathbf{X}^{(g)} \otimes \mathbf{I}_{D_g}) \bar{\mathbf{R}}_{eff}^{(g)} (\mathbf{X}^{(g)} \otimes \mathbf{I}_{D_g})^H \right. \\ &\quad \left. + \mathbf{I}_T \otimes \mathbf{R}_{eff,\eta}^{(\bar{g})} \right) [\mathbf{Z}^{(g)}]^H \quad (\text{B.180}) \end{aligned}$$

$$\Psi^{(g,g')} \triangleq E \left\{ \hat{\mathbf{h}}_{eff}^{(g)} \left[\bar{\mathbf{h}}_{eff}^{(g')} \right]^H \right\} = \delta_{gg'} \mathbf{Z}^{(g)} (\mathbf{X}^{(g')} \otimes \mathbf{I}_{D_{g'}}) \bar{\mathbf{R}}_{eff}^{(g')} \quad (\text{B.181})$$

$$E \left\{ \mathbf{h}_{eff,l_1}^{(g_k)} \left[\mathbf{h}_{eff,l_2}^{(g_{k'})} \right]^H \right\} = \mathbf{R}_{eff,l}^{(g)} \delta_{gg'} \delta_{kk'} \delta_{ll'} \quad (\text{B.182})$$

$$\Phi_{ll'}^{(g_k, g_k)} \triangleq E \left\{ \hat{\mathbf{h}}_{eff,l}^{(g_k)} \left[\hat{\mathbf{h}}_{eff,l'}^{(g_k)} \right]^H \right\} = \Phi_{(x_{k,l}:y_{k,l}; x_{k,l'}:y_{k,l'})}^{(g)} \quad (\text{B.183})$$

$$\Psi_{ll'}^{(g_k, g_{k'})} \triangleq E \left\{ \hat{\mathbf{h}}_{eff,l}^{(g_k)} \left[\mathbf{h}_{eff,l'}^{(g_{k'})} \right]^H \right\} = \Psi_{(x_{k,l}:y_{k,l}; x_{k',l'}:y_{k',l'})}^{(g,g')} \quad (\text{B.184})$$

$$x_{k,l} \triangleq [(k-1)L + l]D_g + 1 \quad (\text{B.185})$$

$$y_{k,l} \triangleq [(k-1)L + l]D_g + D_g \quad (\text{B.186})$$